2023

Design of concrete spheres for energy storage at the ocean bed

An optimisation of the conceptual design

AUTHOR: HERWALD VAN DE VREEDE

WITTEVEEN+BOS | TU DELFT

Design of concrete spheres for energy storage at the ocean bed

An optimisation of the conceptual design

by

H. van de Vreede

To obtain the degree of Master of Science
at the Delft University of Technology,
to be defended publicly on Wednesday March 15, 2023 at 14:00

Student number: 4724100

Thesis committee:

Prof.dr.ir. M.A.N. Hendriks	– Chair
Dr. ing. M.Z. Voorendt	– Daily supervisor TU Delft
A. Van Dalfsen MSc	– Daily supervisor Witteveen+Bos

Preface

Dear reader,

This report is the result of my graduation work, carried out in association with the University of Technology in Delft and Witteveen+Bos. It is performed to finish the master Civil Engineering at the faculty of Civil Engineering and Geosciences. The report provides an investigation into the suitability of concrete spheres used for energy storage at a water depth between 100 to 1500 m. An investigation is made into the ability to print the formwork and it is investigated whether it is possible to use unreinforced concrete for the sphere itself.

For readers who want to know more about offshore energy storage, it is recommended to read Appendix A. For readers who want to know more about development and applications of 3D Concrete Printing (3DCP), it is recommended to read Appendix B. For all readers, it is recommended to read the introduction into this report (Chapter 1), the case that is used (Chapter 3) and the most important conclusions & recommendations (Chapter 7). A discussion of used parameters and calculation methods is given in Chapter 6.

I would like to thank several people for their guidance and support during my graduation project. First of all, I would like to thank my graduation committee. Prof. Dr. Ir. Max Hendriks for his guidance as chair of the committee and his experience with large concrete structures. Dr. ing Mark Voorendt for his guidance as daily supervisor from the university. His help for the approach and setup of the report was very helpful, as well as his constructive feedback. Besides the supervisors from the university, I would like to thank Arjen van Dalfsen MSc for his guidance as supervisor from Witteveen+Bos. His experience was very helpful. I would also like to thank my friends and family for their support during my entire study and especially the graduation period. Last but not least, I would like to thank Marie-Lise for her never ending support and listening ear during my entire study and especially during the graduation period.

H. van de Vreede
Krabbendijke, March 7, 2023

Summary

In the energy sector, a transition is made from fossil fuels to sustainable energies. Due to an irregular supply of these sustainable energies, it often occurs that there is a mismatch between supply and demand. Energy storage is a promising technique to overcome this. Energy can be stored in multiple ways; one of these is Pumped Hydro Energy Storage (PHES), which is a type of gravitational energy storage. In this thesis, the aim is to store gravitational energy in concrete spheres which are placed on the seabed. To be able to use this concept worldwide, a scalable and feasible design is required, preferably with a small carbon footprint.

Therefore, this thesis aims to answer whether the most optimal construction method uses 3D Concrete Printing (3DCP) and if so, what the optimal construction method will be using 3DCP. Based on a specific case, five main construction methods are qualitative investigated, from which two are with 3DCP. These main construction methods are evaluated based on ease of construction, construction time, costs, scalability and achieving watertightness. From this, it followed that a combination of 3DCP and conventional casting is the most promising method and is therefore selected for more in-depth research. In this construction method, the formwork is made with 3DCP and concrete is cast in the formwork. A prefab bottom and top part are required, because the maximum inclination (nowadays) for printing is limited to 45°.

Based on the selected construction method, three different 3DCP-variants are investigated: construction in the dry (1), submerged construction (2) and construction on a pontoon (3). The two main topics that are investigated are the use of 3DCP for the formwork and the suitability of unreinforced concrete for the sphere itself, for each variant. The possible use of 3DCP is verified based on two failure mechanisms: plastic collapse and elastic collapse. The verification of plastic collapse results in minimal free height h_1 of the printed formwork, before the concrete can be cast in the formwork, because otherwise the stress in the lowest layer would be larger than the strength in that layer. The verification of elastic collapse results in a maximum free height h_2 of the printed formwork before the concrete should be cast, because otherwise the formwork will buckle. The suitability of unreinforced concrete is verified based on the tensile strength and tensile stress in the concrete, during construction and during use. In this verification, the shear force is not taken into account.

Both in case of construction in the dry and construction on a pontoon, h_1 is 0.20 m and h_2 is 0.65 m. In case of submerged construction, h_1 is 0.25 m and h_2 is 0.72 m. For each construction method, h_1 is smaller than h_2 which gives for every construction method the opportunity to cast concrete in the formwork. The unreinforced wall thickness should not exceed 2.5 m because it is required that the sphere is buoyant. For this wall thickness, a concrete strength class of C60/75 is required for construction in the dry, submerged construction and construction on a pontoon. The construction time (mainly based on printing time) is at least 31 days for construction in the dry and construction on a pontoon and 24 days in case of submerged construction. An evaluation based on feasibility and reliability, combined with the results above, shows that construction in the dry is the most promising method, although a higher concrete class is required and construction time is lower in case of submerged construction.

An adiabatic calculation is made of the temperature increase of the concrete, based on five different cement compositions: ASTM1 to ASTM5. A temperature gradient over the wall thickness leads to differential shrinkage which leads to tensile stresses. It followed that the tensile stress (14.2 MPa) in the concrete is higher than the tensile strength of unreinforced concrete (1.64 MPa in case of C60/75, α_{ct} = 0.8), for ASTM1 to ASTM5. However, in reality, the temperature increase is semi-adiabatic, resulting in lower tensile stresses. It is therefore highly recommended to further investigate this temperature increase in order to verify the suitability of unreinforced concrete. Measures that could

be taken to lower the temperature differences are: addition of liquid nitrogen or addition of ice instead of water for the concrete mix. Besides that, it is recommended to investigate the possible use of fibre-reinforced concrete, which could significantly increase the tensile strength of concrete.

Abbreviations

BEST	Buoyancy Energy Storage Technology
CC	Contour Crafting
3DCP	3D Concrete Printing
FLASC	Floating Liquid piston Accumulator using Seawater under Compression
IIASA	International Institute for Applied Systems Analysis
LCOS	Levelized Cost Of Storage
LHC	Low Heat Cement
MPHES	Marine Pumped Hydro Energy Storage
MCA	Multi Criteria Analysis
PHES	Pumped Hydro Energy Storage
StEnSea	Stored Energy at Sea

Table of Contents

1. Introduction to offshore energy storage and motivation for this report

The motivation and relevance of offshore energy storage in concrete spheres, the approach and outline of the report are given in this chapter. First the motivation for energy storage is explained (Section 1.1). After that, the relevance of this thesis is given (Section 1.2). From this, the research questions are derived, which are stated in Section 1.3. The approach that is used in this report to answer the research questions is given in Section 1.4. The outline of the report can be found in Section 1.5.

1.1. Motivation and relevancy of (offshore) energy storage

Why is energy storage needed? Why should energy storage in concrete spheres, as a type of offshore energy storage, be developed? This section answers these questions and explains the need for (offshore) energy storage, starting with the energy transition from fossil fuels to more sustainable sources of energy.

From fossil fuels to sustainable energies

Climate change has a large impact on our lives. It is assumed that climate change causes phenomena like longer periods of drought (PBL, 2011) and sea level rise (KNMI, n.d.), which can have a large impact on living circumstances on earth. Climate change is mainly caused by the emission of greenhouse gasses. Greenhouse gasses trap heat in the atmosphere which causes global warming. During the 21st Conference Of Parties in 2015 (COP21) the parties agreed on several measures to limit global warming to 2 ^{o}C and if possible limit it to 1.5 ^{o}C above pre-industrial level (United Nations, 2015). To achieve that goal, the emission of greenhouse gasses should be drastically reduced in the coming years and decades.

The production of energy is mostly based on fossil fuels like coal, oil and gas. In the US in 2019, 74% of the anthropogenic greenhouse gas emissions came from burning fossil fuels (U.S. Energy Information Administration, 2021). The atmospheric concentration and CO_2-emissions increased since the start of the Industrial Revolution, at an even higher rate since 1960. Since the start of the Industrial Revolution, the atmospheric concentration is increased by more than 50% (Lindsey, 2020). Increases of carbon dioxide in the atmosphere are responsible for about two-thirds of the total energy imbalance that leads to global warming. Greenhouse gasses in the atmosphere lead to the enhanced greenhouse effect. This means that less warmth is leaving the atmosphere, due to the increase of greenhouse gasses in the atmosphere (KNMI, 2010). There are different greenhouse gasses and the strength of them differs. Of all the greenhouse gasses emitted by human, CO_2 is the most important one: more than 50% of the enhanced greenhouse effect is caused by CO_2 (Milieu Centraal, n.d.). To lower the emission of greenhouse gasses (and thus CO_2), other energy sources are needed. A few sources of sustainable energy are solar, wind and hydro energy. The amount of energy harvested from sustainable energy sources is rapidly increasing over the last few years (International Energy Agency, 2022).

With this energy transition from fossil fuels to renewable energy, new challenges come up. For example the availability of wind- and solar energy is intermittent. When there is no wind, there is no energy from wind turbines. When it is cloudy, less energy can be generated with solar panels. Besides that, the electricity infrastructure is not ready yet for the energy transition. It occurs that the energy from solar panels cannot be transported to the electricity grid on sunny days or wind energy on windy days (Netbeheer Nederland, n.d.).

The need for energy storage

The transition to sustainable energy resources requires that these resources are reliable. The low reliability of solar and wind energy as described leads to low reliable resources. Therefore, other sustainable resources are needed or the generated energy from wind and solar needs to be stored somehow to stabilize the electric grid. Figure 1-1 gives a visualization of the variability of generated energy and how energy storage can overcome this problem.

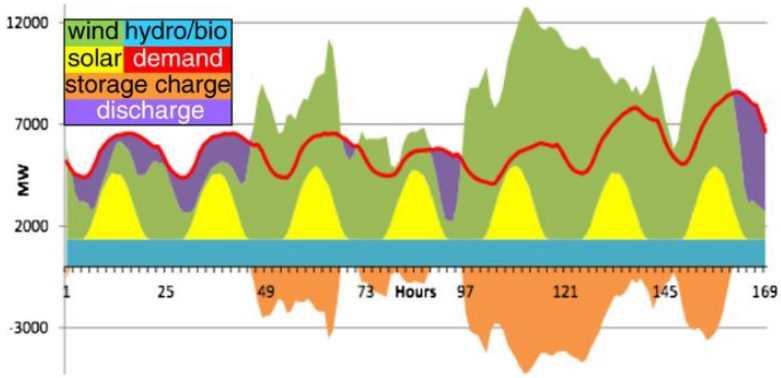

Figure 1-1 Energy storage can solve the mismatch between supply and demand (Hagrey, Köhn, & Rabbel, 2014)

Europe set the goal to become the first climate-neutral continent by 2050. This means that there is no net-CO_2 production. The production of energy from renewable energy sources increased from 2% in 2004 to 15% in 2018 (Pitorac, Vereide, & Lia, 2020). This should increase in the future to become a climate-neutral continent. As a result, the need for energy storage will also increase, as the demand and supply will not always match. Closed loop Pumped Hydro Energy Storage (PHES) is one of the technologies which can be used to increase the energy storage in Europe. For a 100% renewable Europe, the storage need is estimated to range from 80 to 400 TWh with an installed capacity between 500 to 900 GW (Droste-Franke, et al., 2014).

(Pumped Hydro) Energy Storage

The underlying principle of energy storage is conservation of energy. Two main types of energy are distinguished: kinetic energy and potential energy. When the type of energy changes, heat is released, which determines the efficiency of the system. The sum of the two types of energy and the released heat is the first law of thermodynamics and stays constant in a closed system.

Pumped Hydro Energy Storage (PHES) is a form in which water is stored as potential energy. Two reservoirs with different elevation are connected to each other by pipes or channels. The potential energy increases when water is pumped to the upper reservoir and decreases when the water is released to the lower reservoir. PHES accounts for more than 95% of globally installed energy storage (Stocks, Stocks, Lu, Cheng, & Blakers, 2020). The (increase of) potential energy depends on the mass, gravitational constant and the height (difference).

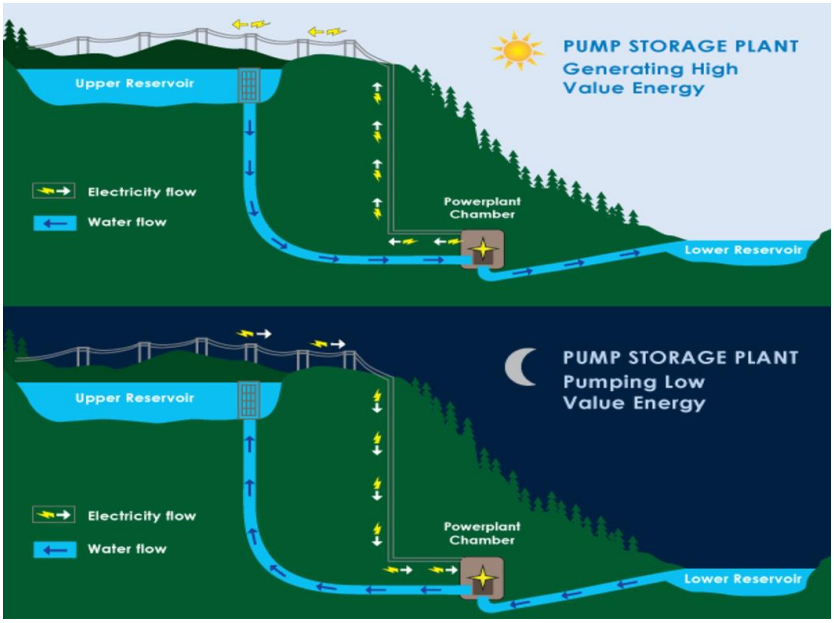

Figure 1-2 Generating energy when the demand is larger than supply and using energy when the demand is lower than supply (Bitew, et al., 2019)

Two principal categories of PHES are distinguished: closed loop and open loop. In the first case there is no (significant) natural inflow to either reservoir, in the second case, in at least one of the reservoirs there is a significant natural inflow. Offshore (Pumped Hydro) Energy Storage is a type of closed loop energy storage. To explain the need for energy storage in concrete spheres, four important other types of energy storage are described. An elaborated version can be found in Appendix A. Only spheres are considered in this report, as this is the most useful shape (depending on depth) (Marrewijk, 2020).

BEST

BEST stands for Buoyancy Energy Storage Technology in which energy is stored using buoyancy. Energy is stored at the seabed with a compressed gas. The system is connected to floating solar panels or wind turbines. When there is a surplus of energy, buoyant tubes are pulled down to the seabed, where they are stored as potential energy (Hunt, et al., 2021). This system could have great potential in storing energy close to the coastline near islands without variation in elevation. The estimated LCOS (Levelized Costs Of Storage) could be reduced to $50/MWh with further optimisation (Blain, 2021).

FLASC

FLASC stands for Floating Liquid piston Accumulator using Seawater under Compression. In this concept, water is pumped into a closed chamber containing pre-charged air (charging mode). When the stored energy is needed, the pressurized water is released through a turbine to generate electricity. The intended depth for this concept is 100-400 m (FLASC, n.d.). The efficiency decreases for larger depth, because the temperature increases for larger air pressure. If this energy is lost to the surroundings, the overall efficiency decreases.

Ocean Grazer

Another type of offshore energy storage is the concept developed by Ocean Grazer. This system consists of two reservoirs, connected with each other by a pump-turbine module. One of the reservoirs is embedded in the seabed, and another flexible one is placed at the seabed. In charging mode, water is pumped from the embedded reservoir to the reservoir on the seabed. The water in the flexible reservoir is pushed back by the hydrostatic pressure into the embedded reservoir (Ocean grazer, n.d.). The efficiency increases for larger depth, but the complexity increases also for larger depth, because it will be more difficult to install the pump-turbine module and the concrete reservoir under the seabed.

Maintenance will also be difficult for larger depth, because the pump-turbine is embedded in the seabed.

Fraunhofer
The concept which is similar to the one that will be optimised in this report is the system developed by Fraunhofer. The aim of this system is to place concrete spheres with 30 m diameter at a depth of 700 m (Geuss, 2017). Several tests were done with a scaled prototype in 2017. A pressure hose was used to avoid cavitation. During these tests, several disadvantages where noticed. The most important one is the fact that the pump was integrated in the system, which made maintenance difficult (Dick, Puchta, & Bard, 2021).

Conclusion
The concrete spheres that will be used for energy storage at sea are needed to store energy at depths between 100 and 1500 m. The other concepts shown above are mainly intended for shallower water depths, as efficiency decreases and complexity increases for larger depth (except the one developed by Fraunhofer). The problems regarding the concrete spheres designed by the Fraunhofer Institute and the aim of connecting multiple spheres to one pump-turbine module in the design of this report show that the design in this report will give an unique option for energy storage at sea.

Within the STORE Consortium, Witteveen+Bos developed together with other parties an innovative energy storage system: the Marine Pumped Hydro-Electric Storage (MPHES). The aim of this project is to use hollow concrete spheres on the ocean bed to store potential energy (RCAM Technologies, n.d.). Energy from wind turbines is stored when the supply of energy exceeds the demand or when the price for electricity is low. The energy is used to pump water out of the spheres. Vice versa, water is let in back via turbines when less energy is generated from the wind turbines than demand or when the price for electricity is high. Combining wind turbines with MPHES makes harvesting energy from wind much more reliable. This report presents a design optimisation of these concrete spheres that are used for energy storage at the ocean bed.

1.2. Problem analysis

Several uncertainties and problems need to be overcome before concrete spheres for energy storage can be deployed. They are explained in this section. The size and weight of the sphere will determine the draft. However, this could be a problem when the desired depth is not available or in case the weight is larger than the buoyancy, which will make it sink. This is explained first. Secondly, it is preferred to use 3D Concrete Printing (3DCP) to lower the carbon footprint, because the aim of 3DCP is to place concrete only where necessary. However, this is an upcoming technology and several aspects regarding strength and stability need to be investigated. Besides that, the spheres should be watertight. However, can watertightness be ensured at large depths?

Investigation of buoyancy and draft
The design of the spheres should enable deployment at depths between 100 and 1500 m. The spheres should withstand a hydrostatic force, which increases to $15*10^3$ kN/m^2 at a depth of 1500 m. Therefore a thick concrete wall is needed to make sure that the sphere will not collapse at large depths. This will increase the weight of the spheres drastically. After the spheres are constructed, they should be transported to the location where they will be deployed. To enable this transport, the buoyancy of the sphere should be such that the sphere will float. This should be investigated.

The use of 3DCP to construct the spheres
The construction industry accounts for 25 – 40% of the world's total carbon emissions. A large amount of these emissions comes from the use of concrete in the construction industry (Renz & Solas, 2016).

Therefore, an innovative solution is to make use of 3DCP. 3DCP has a lot of advantages: concrete is only placed where necessary, all kind of shapes can be made and formwork is often not necessary or can be made much easier (Wolfs, 2019). Therefore, the carbon footprint will be lower in case 3DCP is used.

The potential savings by using 3DCP are high. According to a report from Markets and Markets, 3DCP has the potential to lower construction waste with 30 to 60%, reduce labour costs with 50 to 80% and reduce construction time with 50 to 70% (3Printr, 2016). If the spheres are built with a traditional formwork, the labour costs are high because for every sphere the formwork has to be rebuild which is labour intensive.

It is not possible yet to apply steel rebars as reinforcement in printed concrete as in conventional concrete. Concrete can take significant compressive forces, but the tensile strength is limited. Due to hoop forces in the sphere, it could be that tensile stresses larger than the tensile strength occur in the sphere during the construction phase, which should be investigated.

Although the advantages of 3DCP are promising, there are also numerous topics that are unknown yet. At this stage, 3DCP is mostly used in cases where compression is dominant in the concrete. This is because reinforcement (on large scale) cannot be added while printing. It is unknown whether there will be always compression in the entire sphere.

Cracking and watertightness of the concrete spheres

The forces acting on the sphere can be divided into external and internal loads. External loads are applied during construction (formwork) and during operation. Internal loads may occur due to shrinkage. Due to hardening of the concrete, the concrete will shrink. It is the result of interaction between cement paste and aggregates (Lu, Li, & Huang, 2021). Cement paste does shrink, whereas the aggregates do not shrink and deformation may develop. If the deformation is restrained, tensile forces may develop which cannot be taken by the concrete itself and cracks will occur due to that.

Deformation is also possible under thermal loading. Temperature differences may causes shrinkage or expansion, which may lead to cracks in concrete. While hardening, water and cement react with each other. Since this is an exotherm reaction, heat is released. Generally, if the concrete wall thickness exceeds 0.8 m, the temperature differences are significant over the cross-section (de Vries, 2005). Due to this, cracks may occur. This is an important part of the design of the spheres. These cracks may affect the strength of the concrete.

Moreover, in this case another important problem is the watertightness of the spheres. The hydrostatic pressure will vary between 10^3 kN/m^2 and $15*10^3$ kN/m^2. In case that the spheres are empty, the pressure difference between outside and inside the sphere is high. Therefore, even a small crack through the entire cross section may lead to leakage into the sphere which reduces the efficiency of the energy storage.

Problem statement

Combining the different problems that are stated above, a problem statement is defined. 3DCP is an upcoming technology and has a potential for constructing concrete spheres for energy storage, but numerous topics are unknown. The relevant failure mechanisms of 3DCP are unknown and little research has been done for combining reinforcement and printed concrete to achieve structural concrete which can meet requirements as they are nowadays (Gebhard, Mata-Falcon, Anton, Dillenburger, & Kaufmann, 2021). It is not known whether reinforcement is required and how watertightness can be ensured.

A list of bottlenecks and unknowns is given below. This presents the problem statement.

- It is unknown whether tensile forces will develop in the sphere during construction and during use. This is necessary to verify whether reinforcement should be applied;
- It is unknown if 3DCP can be used to construct the spheres;
- It is unknown what is most important regarding crack formation in the spheres and what the estimated crack width will be;
- It is unknown whether the sphere fulfils the requirements regarding watertightness.

1.3. Goal of the thesis and research questions

The goal of this thesis is to come with an optimisation of the conceptual design of the spheres and how the spheres could be built. To end up with this optimal design, several topics are required to investigate further. It should be investigated how watertightness can be ensured, whether tensile stresses will develop in the sphere or not and whether the preferred construction method makes use of 3DCP.

Combining these topics, the research question is as follows:

> *How does the optimal design of a concrete sphere, that will be used for energy storage at large water depth, look like?*

Several things should be investigated to come up with an optimisation of the design. To make it more organized, the question is divided in several sub-questions:

- *Does the best construction method make use of 3DCP?*

- *How can 3DCP be used in an optimal way to construct the spheres?*

- *Is it possible to construct the spheres with unreinforced concrete?*

1.4. Method used to answer the research question

This thesis aims an optimal design of concrete spheres for energy storage. To be able to come up with an optimisation, several parameters and calculation methods regarding 3DCP and requirements regarding crack width and watertightness should be determined, before the design optimisation can be done. To achieve these requirements and calculation methods, literature will be reviewed. This is step 1 of the approach. In the design of the concrete spheres, a design method will be used which is explained below. This is step 2 of the approach.

Step 1 - Literature study

To answer the research (sub-)question(s), a few important topics will be reviewed in literature. For each topic the relevance is given for the optimisation of the design. The following topics will be reviewed in literature:

- What are the properties of 3DCP and what are possibilities of 3DCP?

The development of strength and stiffness of 3DCP in time will influence the affect the ability to use 3DCP in the design of the spheres. Therefore, these subjects should be investigated. Topics that will be reviewed in literature are the development of 3DCP, strength properties in fresh state, strength properties in hardened stage, bonding between different layers and what influences these properties.

- How can submerged concrete hollow structures be watertight?

Leakage will cause a lower efficiency and therefore leakage should be avoided. Literature will be reviewed how watertightness is achieved for submerged hollow concrete structures. Eurocode 2 gives a rule regarding watertightness; the applicability for this case will be reviewed.

- What are causes for cracks in thick-walled concrete structures?

Cracks through the entire cross-section will cause leakage. Literature will be reviewed regarding different types of shrinkage, especially in case of thick-walled structures. The hardening of concrete in a thick-walled structure causes temperature differences which could lead to thermal cracking. It will be reviewed how large these temperature differences can be and what the influence is on crack formation. This information is needed to come up with measures (if needed) to lower crack width and to improve watertightness.

Step 2 - Design method

In this report, a specific case is used in the design of the spheres. In the design, the engineering design process is used as a basis for the design method used in this report (TeachEngineering, n.d.). The design consists of the following steps:

2.1 The case is analysed;
2.2 From the case analysis, the requirements and boundary conditions are determined;
2.3 The concepts, based on main construction methods, will be developed;
2.4 A qualitative verification is made for the main construction method;
2.5 A selection of main construction method is made based on a Multi Criteria Analysis (MCA);
2.6 Variants are developed, based on the selected main construction method;
2.7 A quantitative verification is made for the variants;
2.8 An evaluation and selection is made based on a Multi Criteria Analysis (MCA);
2.9 The hydration heat is estimated, crack width calculations are performed and watertightness will be verified;

1.5. Outline of the report

- In Chapter 2, the literature review is given. In this chapter, literature is reviewed on the current stage of 3DCP and calculation methods for 3DCP, requirements regarding watertightness and concrete cracking of thick-walled constructions.

- The case that is used in this report is analysed in Chapter 3. The requirements and boundary conditions are determined from this analysis (steps 2.1 and 2.2 of the design method) and several starting points are given.

- In Chapter 4, concepts are developed based on the different (main) construction methods (step 2.3 of the design method). A qualitative verification and selection is made based on main construction methods (step 2.4 & 2.5). After that, 3 3DCP-variants are described, based on the selected main construction method (step 2.6). A quantitative verification is given for the 3DCP-variants (step 2.7) and a choice is made based on evaluation criteria (step 2.8).

- In Chapter 5, calculations are performed regarding hydration heat, (thermal) shrinkage & (thermal) cracking and watertightness, which is step 2.9 of the design process.

- Chapter 6 gives an discussion of choices that have been made during the design and describes limitations of models that are used;

- The report ends in Chapter 7 with answering the research questions and recommendations for further design.

2. Literature research into required parameters and calculation models

In this chapter, several topics are reviewed from literature. The relevance of each section is given at the start of each section. Section 2.1 gives an overview of required parameters and calculation models regarding 3DCP. The characteristic properties regarding strength and stability in fresh and hardened state are described and conflicting requirements are mentioned. Section 2.2 gives an overview of watertightness of submerged concrete structures and how crack width is related to watertightness. Besides that, it is given how the amount of leakage can be calculated. In Section 2.3 several types of shrinkage are described, from which the impact on crack width is described. This information is necessary to carry out steps 2.7 and 2.9 of the design method. At the end of each section, a conclusion is given and how the knowledge is applied during the design.

2.1. Applications and properties of 3DCP

3DCP is an upcoming technique which may have a large impact on the construction sector. Extensive research is done in the past decades and is still needed to overcome some serious challenges regarding the strength development, stability and bonding between different layers, before 3DCP can be widely used in the construction sector. The properties of 3DCP can be roughly divided into properties of the 'fresh' stage and the 'hardened' stage. These properties and especially the development of the strength are important to verify whether it will be possible to construct the spheres with use of 3DCP. An introduction to 3DCP is given in Appendix B, which gives some information about the current applications of 3DCP. The strength development of 3DCP during and shortly after printing are given in Section 2.1.1. Fresh concrete may also collapse due to insufficient stiffness and stability. Therefore, important information about this is also given in Section 2.1.1. Section 2.1.2 describes the properties of printed concrete in the hardened stage. This information is necessary to perform step 2.7 of the design method.

2.1.1. Investigation to properties of fresh printed concrete

The shape of printed concrete is maintained by the gravitational load of the concrete, without the support of a formwork. This should be taken into account when designing the concrete mix, which is an fundamental issue for 3DCP. The concrete should reach the requirements of pumpability, extrudability and buildability. The water/cement ratio should be high enough to reach the pumpability. To fulfil the requirement of extrudability, often the maximum aggregate size is relatively small compared to conventional cast concrete, because most existing printers work with small nozzles; this reduces the strength of the concrete. However, to reach enough strength, the binder content should increase.

Pumpability of 3DCP

Pumpability can be defined 'as the characteristic of the print mix to be workable enough to be mobilized through a pumping system under pressure to the printing head while retaining its initial properties for the entire time' (Zhang, et al., 2021). Higher workability means better pumpability, but lower stiffness. This contradicts with the requirement of stiffness for 3DCP, because the extruded material should remain their shape in absence of a formwork. In the pipe, the mix tends to segregate under high pressures (Choi, Roussel, Kim, & Kim, 2013). Therefore, the mix should be able to resist this segregation.

Extrudability of 3DCP

Extrudability can be defined 'as the ability of the print mix material to be extruded smoothly as a continuous filament exiting the nozzle at the printhead with an unhindered material flow' (Zhang, et al., 2021). This partly coincides with the pumpability. If the mix does not segregate during pumping, the extrudability is higher. At the other side, when the aggregates will accumulate to the centre of the pipe, the mix can be blocked in the end of the pipe or in the nozzle.

Buildability of 3DCP

The buildability can be defined as the ability of the print material to keep its form after extrusion. Printed concrete without any formwork need to have stability from gravity. Therefore, the bonding need to be strong enough, in particular if the layers are printed little sidewards of the previous layer. The strength of the fresh concrete should be high enough to endure the weight of the subsequent layers. The strength of the concrete while printing is therefore higher than the strength of concrete when it is conventionally cast. This also depends on the time between printing two layers above each other and is therefore dependent of the geometry of the structure. For 3D printing, the buildability is a challenging issue, due to conflicting requirements. The viscosity of the mix while pumping should not be too high, whereas for better buildability a higher viscosity is needed.

These three (conflicting) requirements are important for the design of the concrete spheres. Figure 2-1 represents the workability requirements and the rheological requirements. These are important to keep in mind for the construction of the spheres.

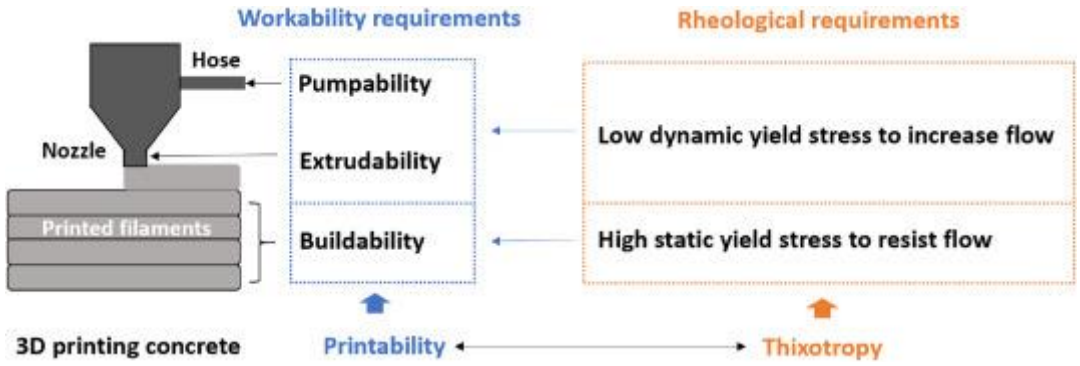

Figure 2-1 Conflicting requirements for 3DCP (Zhang, et al., 2021)

Failure modes of 3DCP

Failure of 3DCP can be caused by two failure modes: plastic failure and elastic failure. In case of plastic failure, the stress in the bottom layer increases due to the increase in weight of the printed layers which are added on top. When the stress in the bottom layer exceeds the strength, the structure will collapse. The second failure mode is elastic failure and depends on the geometry and the slenderness of the structure.

Failure mode 1: plastic failure

Pumpability, extrudability and buildability are also closely related to yield stress (Perrot, Rangeard, & Pierre, 2016). The yield stress can be divided into static yield stress and dynamic yield stress. Static yield stress refers to the stress to make the material flow from a state of rest. If the material is in state of rest and the stress is lower than the yield stress, the material exhibits elastic behaviour. Because layers are printed above each other during the printing process, the compressive stress increases for the lowest layers. If the stress becomes higher than the yield stress, the material will flow and the structure will collapse. The dynamic yield stress is the stress which is needed to keep the state of movement, once the material is moving and is lower than the static yield stress. The ratio of the static

yield stress to the dynamic yield stress can be used as a thixotropy index of the material (Zhang, et al., 2021).

The increase of yield stress depend on re-flocculation and structuration. Re-flocculation is the 'reversible particle flocculation process', which largely occurs shortly after removal of applied energy. In case of 3DCP, this refers to the moment after extrusion. During re-flocculation, the bonding increases and thus the static yield stress increases too.

The structuration rate describes the second part. The time scale of structuration is much longer. The structuration rate mainly describes the early formation of hydration products and is influenced by more factors than the re-flocculation rate. It could be influenced by for example accelerators in the concrete mix and environmental conditions like humidity and temperature (Kruger, Zeranka, & Zijl, 2019).

Below, 3 models are given which describe the static yield stress increase. The third model (from Kruger) makes a distinction between the re-flocculation and the structuration.

Yield stress - Roussel

Roussel developed a model, in which the strength evolution is linear (Roussel, 2006). The development of yield stress according to Roussel is given in Eq. 2.1. He combined the re-flocculation and the structuration in one parameter.

$$\tau_0(t) = \tau_0(0) + A_{thix} \cdot t \tag{2-1}$$

Where:

$\tau_0(t)$ = yield stress [N/mm^2]

$\tau_0(0)$ = initial yield stress, typical value of 4*10^{-3} [N/mm^2] (Jiao, Schryver, Shi, & Schutter, 2021)

A_{thix} = Structuration rate, typical value of 0.5*10^{-6} [N/(mm^2 · s)] (Jiao, Schryver, Shi, & Schutter, 2021)

t = time [s]

Yield stress - Perrot

Perrot made a new model, by proposing an exponential increase of the yield stress (Perrot, Rangeard, & Pierre, 2016). They proposed a model which gives a smooth transition from the linear to the exponential yield stress development, which is given by Eq. 2.5. To verify their theory, they simulated loading on a cylindrical sample (which could be the first layer of a cylinder) by loading this cylindrical sample with increments of 1.5 N, representing new layers printed above. They also showed the effect of the time span between the increments by ranging this from 11 to 60 s. This represents 3D printing of a column with a building rate ranging from 1.1 to 6 m/h. The tests showed that the longer the time span between load increase, the longer it took before the sample collapsed. The development of yield stress is given in Figure 2-2, in which can be seen that the exponential model starts to deviate from the linear model at 30 minutes. The model can be used for layers with a maximum of 6 hours after extrusion.

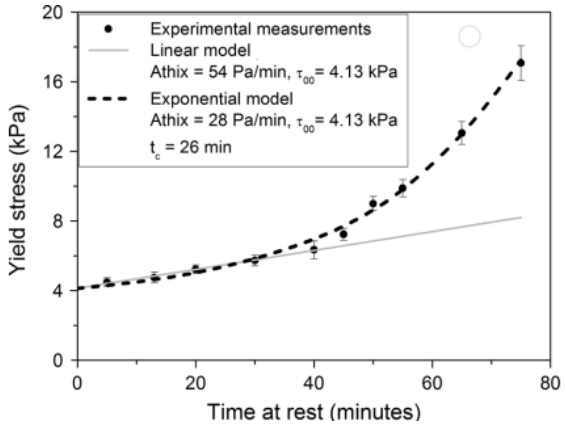

Figure 2-2 Results from research done by Perrot (Perrot, Rangeard, & Pierre, 2016). The exponential model starts to deviate from the linear model at 30 minutes.

The exponential behaviour of the yield stress development is given in Eq. 2.2.

$$\tau_0(t) = A_{thix} \cdot t_c \cdot \left(e^{\frac{t_{rest}}{t_c}} - 1\right) + \tau_{0,0} \tag{2-2}$$

Where:

t_c = characteristic time value to get best fit [s]
t_{rest} = time of concrete at rest [s]

Yield stress - Kruger

In both models, the re-flocculation rate is not clearly defined. To make a clear distinction between the re-flocculation rate and the structuration rate, which have a different time scale, Kruger (Kruger, Zeranka, & Zijl, 2019) developed a new bi-linear model in which both the re-flocculation and the structuration are taken into account. In the research they have done, the main focus was on the re-flocculation. Therefore, the model is mostly based on Roussel's model, because he also used a linear model. The bi-linear model is shown in Figure 2-3.

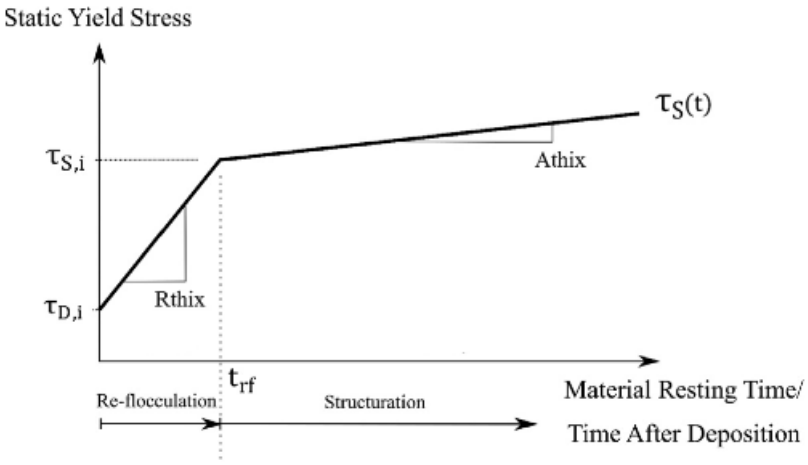

Figure 2-3 Development of static yield stress, with a distinction between re-flocculation and structuration (Kruger, Zeranka, & Zijl, 2019).

The corresponding equations are given in Eq. 2.3, Eq. 2.4 and Eq. 2.5.

$$\tau_s(t) = \tau_{D,i} + R_{thix} \cdot t \quad for\ [t \leq t_{rf}] \tag{2-3}$$

$$t_{rf} = \frac{\tau_{S,i} - \tau_{D,i}}{R_{thix}} \quad (2\text{-}4)$$

$$\tau_s(t) = \tau_{S,i} + A_{thix} \cdot \left(t - t_{rf}\right) \qquad for \quad [t > t_{rf}] \quad (2\text{-}5)$$

Where:

$\tau_s(t)$	= static yield stress	[N/mm^2]
$\tau_{s,i}(t)$	= initial static yield stress	[N/mm^2]
$\tau_{D,i}(t)$	= initial dynamic yield stress	[N/mm^2]
R_{thix}	= re-flocculation rate	[N/(mm^2 · s)]
t_{rf}	= time at which structuration starts	[s]

Yielding of the concrete can be described using the behaviour of soils, as the fresh concrete fails due to sliding of the particles rather than crushing of particles (Hoogeveen, 2020). This criterion is described in Eq 2.6, which makes use of the More-Coulomb criterion.

$$\tau_0(t) > \ c(t) + \sigma_n(t) \cdot tan\,(\varphi) \quad (2\text{-}6)$$

Where:

$c(t)$	= cohesion	[N/mm^2]
σ_n	= normal stress	[N/mm^2]
φ	= friction angle	[degrees]

Failure mode 2: elastic failure

Another failure mode of printed concrete is elastic buckling. The stresses in the concrete depend on the weight of the concrete on top of the layer and the geometry of the structure. For uniaxial behaviour, the stresses are related with the Young's modulus and the uniaxial strain. The lateral contraction is defined with the Poisson's ratio. Therefore, the two properties, which develop with time, which influences the stability of the structure, are the Young's modulus $E(t)$ and the Poisson's ratio $\nu(t)$. These properties both develop with time. It should therefore be ensured that the strength, depending on these two properties, should always be higher than the loads stresses acting on the structure (Wolfs, 2019).

Description of model used to estimate the critical buckling height

Suiker (2018) and Roussel (2018) both developed a model to estimate the critical length at which buckling is expected to occur for a vertical, straight wall. To start with Roussel, one simple equation gives an (underestimated) value of the critical height and is thus conservative. However, the increase of stiffness and strength is not taken into account, as well as the vertical growth velocity of the wall. These aspects do get included in the model of Suiker, which is more comprehensive. The support configuration is taken into account as well in this model. Therefore, the model of Suiker is used in this report to calculate the critical buckling height; the model of Roussel is given in Appendix D.

Suiker starts with the vertical wall growth velocity (Eq. 2.7). This equation can be simplified by modelling it as a continuous growing process, which depends on several printing parameters.

$$\dot{l} = \frac{Q}{v_n \cdot h \cdot T_l} \quad (2\text{-}7)$$

Where:

$\dot{l}$	= vertical wall growth velocity	[m/s]
Q	= discharge of material	[m^3/s]

v_n = horizontal velocity of printer head [m/s]
h = wall thickness [m]
T_l = period of printing one layer [s]

The increase of stiffness is given with the curing rate ξ_E. This curing rate can be determined by measuring the stiffness of the printed concrete at different time steps after the concrete is deposited.

Regarding support conditions at the sides, Suiker makes a distinction between a free wall, simply supported wall and a fully clamped wall.

Case 1: Free wall
In case of a free wall, the critical height can be calculated with the approximation given in Eq. 2.8.

$$\bar{l}_{cr} = \left(\frac{\rho \cdot g \cdot h}{D_0}\right)^{\frac{1}{3}} \cdot l_{cr} \tag{2-8}$$

$$\bar{l}_{cr} = 1.98635 + 0.996 \cdot \left(\bar{\xi}_E^{\,l}\right)^{0.793} \tag{2-9}$$

Where:

$$\bar{\xi}_E^{\,l} = \left(\frac{D_0}{\rho \cdot g \cdot h}\right)^{\frac{1}{3}} \cdot \frac{\xi_E^{\,l}}{l} \tag{2-10}$$

$$D_0 = \frac{E_0 \cdot h^3}{12 \cdot (1-\nu^2)} \tag{2-11}$$

Where:

l_{cr} = critical buckling height [m]
ξ_E = curing rate elastic stiffness [s^{-1}]
D_0 = initial bending stiffness [Nm]
E_0 = initial elastic stiffness [N/m^2]
ν = Poisson's ratio [-]

Case 2: Simply supported or Fully-clamped wall
In case of a simply supported and fully clamped wall, de design graphs of Figure 2-4 need to be used to find the dimensionless critical buckling height, depending on the dimensionless linear curing rate and the dimensionless wall length. The dimensionless wall length can be calculated with Eq. 2.12.

$$\bar{w} = \left(\frac{\rho \cdot g \cdot h}{D_0}\right)^{\frac{1}{3}} \cdot w \tag{2-12}$$

Where:

w = wall length [m]

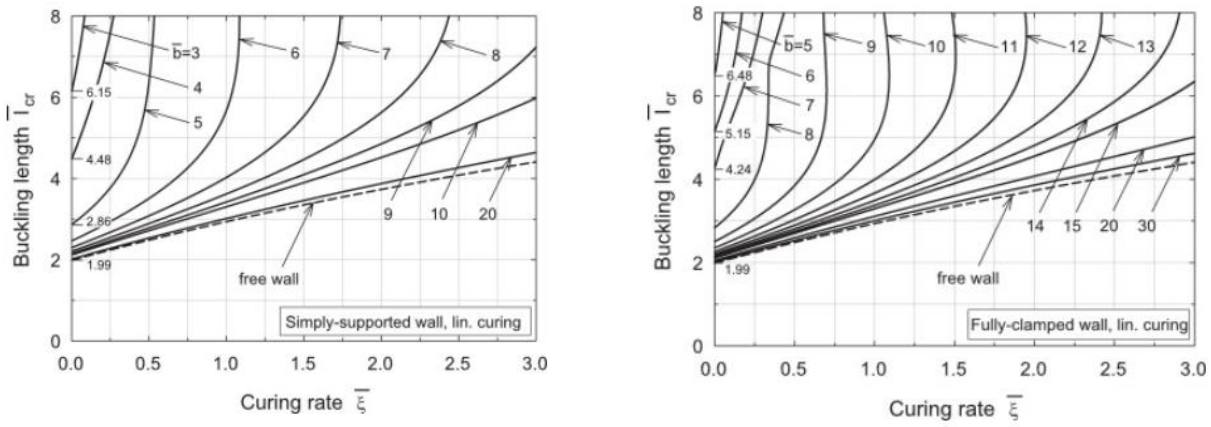

Figure 2-4 Design graphs to obtain the dimensionless critical buckling height in case of simply supported wall and fully-clamped wall (Suiker, 2018)

2.1.2. Properties of hardened printed concrete

The properties of hardened printed concrete are somewhat different than cast concrete. These differences are explained in this section, to understand how the strength and stability relates to conventionally cast concrete.

Mixture composition of 3DCP

Due to the requirements of pumpability, extrudability and pumpability, the mixture composition is different than the mixture composition of conventional concrete. Coarse aggregates are hardly ever used in printed concrete, because they make it less extrudable. However, coarse aggregates are normally added to make the concrete more compact, decrease the need for water and cement and also gives mechanical strength to the concrete (Cemex, n.d.). Thus, to get the same strength, more cement is needed than for conventional concrete. Cement could also be replaced by other binders, to lower the usage of cement, but also to optimise the properties of the fresh and hardened stage of 3DCP (Zhang, et al., 2021).

Interlayer bonding

A structure which is printed consists of several layers of concrete above each other. An important factor of the strength of the structure is the bonding between the layers. This depends on the material composition as well as process parameters (Zhang, et al., 2021). Rheological properties, which depend on the composition of 3DCP, affect the interlayer bond and their strength. Process parameters that influence the bond strength are the time interval between two deposited layers, extrusion pressure, nozzle geometry and ambient condition (Zhang, et al., 2021). A longer time interval leads to less bond strength, for a higher extrusion pressure the concrete is more pressed into the last layer, which result in a higher bond strength and higher humidity also leads to higher bond strength.

Eurocode 2 gives some parameters which influences the bond strength between two layers of concrete that are cast at different time. These parameters are the roughness of the concrete mix, surface roughness coefficients, stress normal to interface and if present, the degree and orientation of reinforcement (EN 1992, 2011). Although these parameters are not sufficient to describe the interlayer bonding, knowledge about these is important.

Regarding the interlayer bonding, Wolfs et al. (2019) did several tests to verify the impact of the layer interval time, covered versus uncovered dehydration and the nozzle height. The strength clearly reduces for larger layer interval time, but it is only a minor drop from an time interval of 15s to 4h. As can be seen in Figure 2-5, the drop of bond strength is larger for the tensile splitting strength than for the flexural tensile strength.

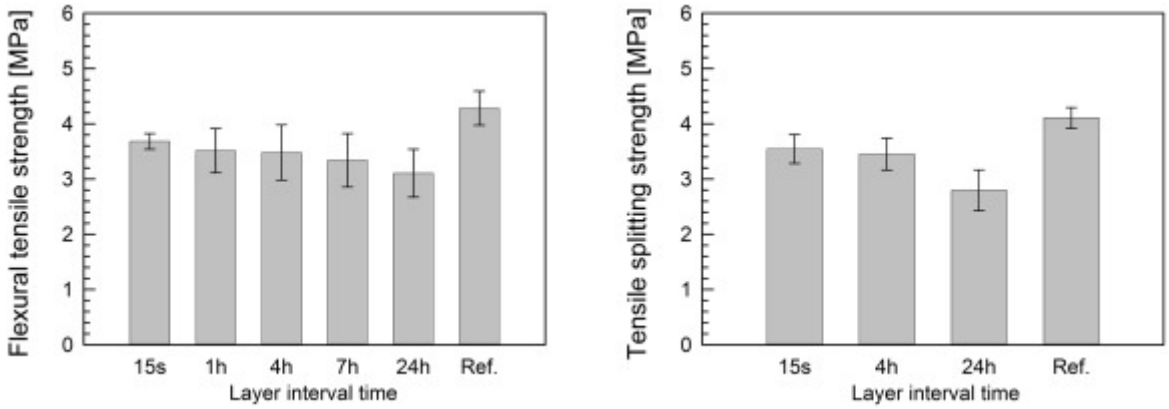

Figure 2-5 results of layer interval time for flexural tensile strength (left) and tensile splitting strength (right). All specimens have been covered for the duration of the time span, with exception of the 15s interval time (Wolfs, Bos, & Salet, 2019).

This reduction of strength should be related with the process parameters used in the research. For example, Kim et al. (2017) reported reductions of 72% with an interval time of 60 min and Panda et al. (2018) indicated a reduction of 75% with 20 min time interval. This clearly shows that the process parameters have a large impact on the bonding between two layers.

A large factor that influences the bond strength is whether dehydration is covered or uncovered. Wolfs et al. (2019) showed that the for a layer interval time of 4h, the decrease in strength for uncovered dehydration is 51% with respect to covered hydration, as shown in Figure 2-6. In case of a layer interval time of 24h, this drop is 26%. Although it was surprisingly that the drop was lower for the longer layer interval time, it is clearly shown that the strength significantly reduces for uncovered dehydration.

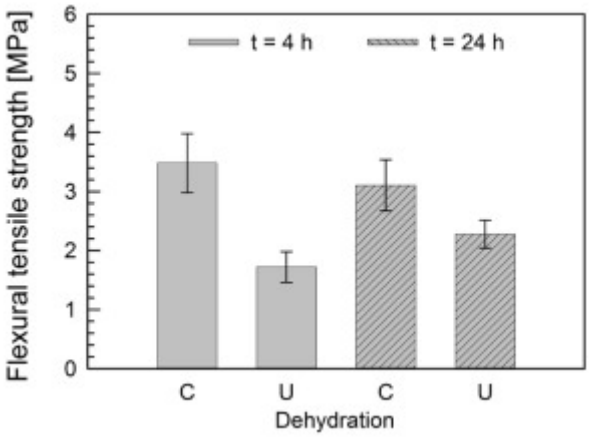

Figure 2-6 difference in strength for covered and uncovered dehydration (Wolfs, Bos, & Salet, 2019).

Durability of 3DCP

Besides the interlayer bonding, the fact that a structure consists of layers above each other makes it also more sensitive for water that penetrates in the concrete. This can severely reduce the durability and may affect its strength. Another challenge regarding durability of printed concrete is the combination of high cement content and absence of a formwork. Due to the higher amount of cement and no or low amount of (coarse) aggregates, plastic shrinkage increases and more cracks will develop due to drying shrinkage (Zhang, et al., 2021). As 3DCP is a relative new construction method, the long-term durability is still under research. Therefore 3DCP will not be used in this case for elements which have a long design life time.

2.1.3. Concluding remarks regarding 3DCP

3DCP is an promising technology to use in the construction sector. 3DCP can be used to build constructions of all kind of shapes and has therefore potential to be used during construction of the concrete spheres. The properties in fresh state regarding strength and stability are most important to keep in mind during the design of the spheres, as they will determine whether the structure will collapse or not.

A distinction can be made between plastic failure and elastic collapse. Plastic failure occurs when the yield stress is lower than the yield strength. 3 models are available to describe the strength development, depending on the initial yield strength, structuration rate and re-flocculation rate. The model which can be used best for the design depends on the timescale. For an increasing timescale, the sequence is Kruger (seconds to minutes), Roussel (minutes) and Perrot (hours).

Regarding elastic failure, Suiker (2018) gives an estimation of the height at which buckling is expected to occur. A distinction is made between a free wall, simply supported and fully-clamped wall. The results will be accurate at the middle of the sphere, where the wall can be assumed vertical over a certain height. For an increasing angle, bending becomes more important than buckling.

The properties of 3DCP are determined by the mix composition and the climate conditions after the concrete is printed. Covered dehydration gives a significant higher strength than uncovered dehydration, which is therefore an important design aspect. Besides that, the layer interval time will determine the bonding between different layers. A smaller interval time leads to higher bond strength which increases tensile strength. However, a longer interval time gives the lower layers more strength, which decreases the change that the printed concrete will collapse in fresh state. This should also be taken into account during the development of concepts (step 3 of the design).

2.2. Literature review into requirements to achieve required watertightness

Leakage should be avoided, as this could affect for example safety or, in the case of the spheres, it affects the efficiency. Therefore, watertightness of submerged hollow concrete hollow structures is important. Leakage can be through the porous concrete wall, through cracks and through joints, whereas the ratio of these three is $10^0 : 10^4 : 10^{10}$ (Breugel, Veen, Walraven, & Braam, 1996). Leakage through a concrete wall depends on the thickness of the wall, the pressure difference between outside and inside of the structure and the crack width. Eurocode 2 combines these components.

Estimation of leakage using Darcy moisture flow

The amount of leakage through a uncracked concrete wall can be estimated with the Darcy moisture flow, given in Eq. 2.13. The leakage depends on the area, pressure difference, dynamic viscosity, thickness of the member and the permeability of the concrete.

$$Q = \left(\frac{A \cdot \Delta p}{\eta \cdot D}\right) \cdot \kappa \tag{2-13}$$

Where:

Q	= leakage through concrete	[m^3/s]
A	= area through which leakage occurs	[m^2]
Δp	= pressure difference	[Pa]
η	= dynamic viscosity of fluid	[$N \cdot s/m^2$]
D	= thickness of the member	[m]
κ	= intrinsic permeability	[m^2]

The amount of leakage through a cracked concrete wall can also be calculated with the Darcy moisture flow, given in Eq. 2.14. The leakage depends on the surface roughness, crack width, pressure difference, dynamic viscosity, thickness of the member and the length of the crack width.

$$Q = \alpha \cdot \left(\frac{w^3 \cdot \Delta p}{\eta \cdot D}\right) \cdot L \tag{2-14}$$

Where:

α	= roughness factor	[-]
w	= crack width	[m]
L	= length of the crack	[m]

Using Eq 2.13 and Eq. 2.14, the leakage in uncracked and cracked stage can be estimated. The leakage through the uncracked sphere, with the dimensions of the sphere in this specific case, is in the order of 0.025 m^3/hr and the leakage through the cracked sphere, assuming 1 crack through the whole cross-section every m^2, is in the order of 80 m^3/hr. The entire calculations can be found in Appendix F.

Requirements regarding watertightness according to Eurocode 2

Leakage should be limited to a small amount. This is because the amount of leakage negatively influences the efficiency of the entire system. Therefore, the watertightness of the spheres should be in Tightness Class 1, according to Eurocode 2-3 (Eurocode 2, 2006), Table 2-1. For this particular Class, cracks through the full thickness of the cross section should be limited to w_{k1}. This crack width requirement depends on the ratio of hydrostatic pressure, h_d, and the wall thickness d. If $h_d/d < 5$, $w_{k1} = 0.2$, while for $h_d/d > 35$, $w_{k1} = 0.05$. between these ratios, linear interpolation may be used. In the case that is used in this report, the ratio is 1000/2.5 = 400. This is far out of the range and it could be questioned whether the criterion of 0.05 mm is applicable.

Table 2-1 Tightness Classes (EN 1992-3)

Tightness Class	Requirements for leakage
0	Some degree of leakage acceptable, or leakage of liquids irrelevant.
1	Leakage to be limited to a small amount. Some surface staining or damp patches acceptable.
2	Leakage to be minimal. Appearance not to be impaired by staining.
3	No leakage permitted

The maximum crack width is based on experiments done by Lohmeijer regarding self-healing of the concrete under hydrostatic pressure (Breugel, Veen, Walraven, & Braam, 1996). The results are given in Figure 2-7.

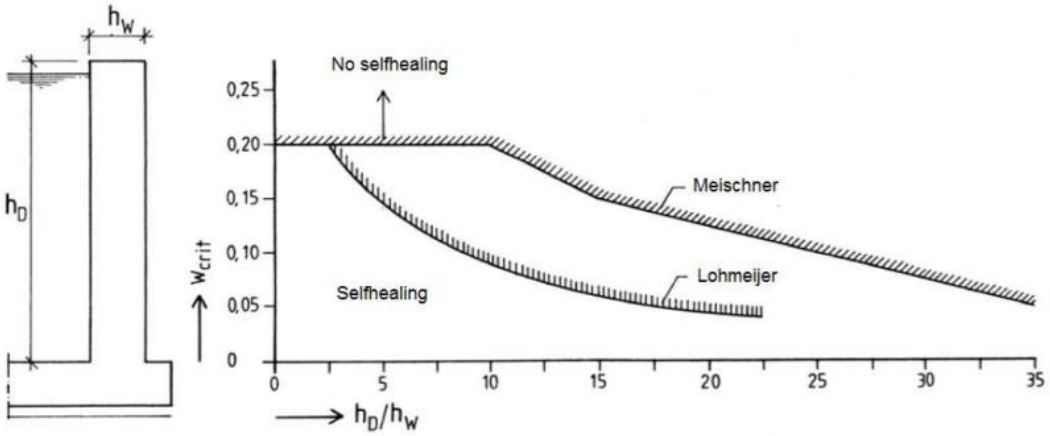

Figure 2-7 Critical crack width for which self-healing can be assumed, depending on the ratio of depth and thickness (Breugel, Veen, Walraven, & Braam, 1996)

Lohmeijer based the criterion on observations in the field, whereas the results of Meischner come from tests done in a laboratory. This could explain why the criterion of Meischner results in a larger allowable critical crack width, as environmental conditions could negatively affect the observations of Lohmeijer in the field. If cracks occur through the entire cross-section and if they are smaller than the critical crack width, the cracks will disappear through self-healing. Prerequisites for this are (Breugel, Veen, Walraven, & Braam, 1996):

- Stable crack width (no temperature differences)
- Low flow velocity through crack
- The fluid should not be leaching

Combining this, a structure will be watertight when (Breugel, Veen, Walraven, & Braam, 1996):

- There are no cracks
- Cracks occur, but not through the entire cross section. The compression zone should be larger than the smallest of 50 mm and 0.2*element thickness.
- Cracks occur through the entire cross section, but are smaller than the critical crack width given in Figure 2-7.

Conclusion regarding requirements to achieve the desired watertightness
The spheres are classified in Leakage Class 1. The maximum crack width therefore should be lower than 0.05 mm. This rule is based on experiments from Lohmeijer. Self-healing will occur for lower crack width, if enough cement is added to the concrete mixture. The criterion of 0.05 mm will be used for this case, as the results of Lohmeijer asymptoticly tends to 0.05 mm for an increasing ratio of depth over thickness.

Besides that, the ratio of leakage through the concrete wall, through cracks and through joints is 10^0 : 10^4 : 10^{10} (Breugel, Veen, Walraven, & Braam, 1996). Therefore, joints should be avoided as much as possible, and special attention should be given to the joints which are necessary. This will be used in step 3 of the design, where the concepts will be developed. Crack width calculations and leakage calculations are performed during step 4 of the design method.

2.3. Literature review into required models to calculate shrinkage

Cracks in concrete occur when the tensile stress becomes higher than the tensile strength. Cracks should be avoided in this case, as it will reduce strength and, more important, could affect

watertightness. The tensile strength develops with time, as well as the compressive strength. Shrinkage and loads are two main causes for tensile stresses in the concrete, which may cause cracking. The relevant types of shrinkage are described in this section, to understand which factors contribute to shrinkage. If the shrinkage could be minimized, crack width can also be minimized. The loads are described in Chapter 3.

2.3.1. Types of shrinkage

In this paragraph, four types of shrinkage are described, with a formulation how they can be estimated/calculated. As the wall-thickness of the spheres is large, much hydration heat will be released. This may become a problem, when the temperature difference between the edge and the centre of the concrete wall will cause differential shrinkage, causing thermal cracking. Therefore, this is extensively explained.

Plastic shrinkage

Volumetric changes or differential settlement of the plastic concrete (not yet hardened) may cause stresses higher than the tensile strength, resulting in cracks. Changes in volume often occurs when water is rapidly lost from the fresh concrete. This could be due to suction of old concrete underneath or evaporation of surface water, which is most common (Larosche, 2009). Aggregates and cement has a higher density than water, which causes bleeding: the water goes up and aggregates and cement goes down. If the bleeding rate is smaller than the evaporation rate, the concrete surface dries and shrinks. The amount of evaporation depends on several parameters. Higher temperatures, low humidity and high wind speed causes more evaporation. The rate of evaporation can be estimated with the nomograph given in Figure 2-8, depending on the three mentioned aspects.

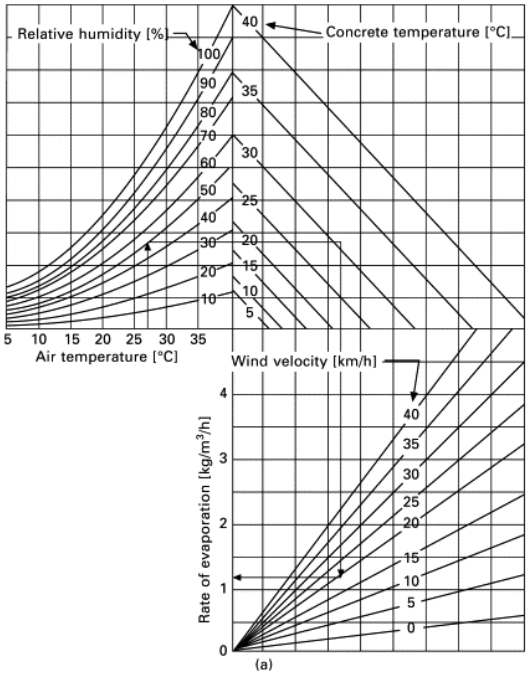

Figure 2-8 Nomograph for estimating amount of evaporation (Larosche, 2009)

Higher evaporation rate than bleeding rate causes tensile stresses at the surface which lead to cracking. The cracks have a short length and occur in an irregular pattern (Larosche, 2009). Whereas the evaporation is related to ambient conditions, the relative amount of water in the concrete mix also determines the amount of evaporation. To avoid cracking from plastic shrinkage, the mix should designed such that the w/c ratio is as high as possible and ambient conditions should be kept such that

the evaporation is low. Another option could be to revibrate the concrete after cracks have formed, but before initial set (time at which concrete starts to lose plasticity) (Day & Clarke, 2003).

Drying shrinkage

After the concrete has hardened, the volume reduction that occurs due to loss of water is known as drying shrinkage. This water is stored in the capillary pores of the hardened concrete and evaporates when the concrete is exposed to relative low humidity. The loss of moisture results in a volume reduction which lead to tensile stresses if this volume reduction is restrained. If this is unrestrained, the volume can freely contract and no cracks will occur (Larosche, 2009).

Plastic shrinkage (not yet hardened concrete) and drying shrinkage are influenced by mostly the same factors. The tensile stresses that occur due to drying shrinkage are influenced by the rate of shrinkage, degree of restraint, amount of creep and modulus of elasticity (Larosche, 2009). Shrinkage of the cement paste is primarily responsible for drying shrinkage. Therefore, to reduce drying shrinkage, the cement volume should be reduced or replaced with another binder and conditions should be kept such that evaporation is minimized.

Autogenous shrinkage

The autogenous shrinkage is a chemical shrinkage and occurs when the concrete hardens (and no water is added). In the hydration process, the volume of the reacting constituents (water and cement) is higher than the volume of the hydrated product. Especially concrete with a relatively low w/c ratio of (w/c < 0.4) the concrete is susceptible to autogenous shrinkage (Larosche, 2009).

Drying shrinkage and autogenous shrinkage are both described in Eurocode 2 (EN 1992, 2011). These two components both depend on time: drying shrinkage develops slowly and ranges from days to months, whereas autogenous shrinkage is linearly linked to the hardening of the concrete, which is mostly in the first days. The total shrinkage is given in Eq. 2.15 to Eq. 2.21.

$$\varepsilon_{cs} = \varepsilon_{cd} + \varepsilon_{ca} \tag{2-15}$$

$$\varepsilon_{cd} = \beta_{ds}(t, t_s) \cdot k_h \cdot \varepsilon_{cd,0} \tag{2-16}$$

Table 2-2 Value for k_h depending on the fictitious thickness of the cross-section

h_0	k_h
100	1,0
200	0,85
300	0,75
≥ 500	0,70

Where the fictitious thickness equals:

$$h_0 = 2 \cdot \frac{A_c}{u} \tag{2-17}$$

$$\beta_{ds}(t, t_s) = \frac{t - t_s}{(t - t_s) + 0.04 \cdot \sqrt{h_0^3}} \tag{2-18}$$

The autogenous shrinkage:

$$\varepsilon_{ca}(t) = \beta_{as}(t) \cdot \varepsilon_{ca}(\infty) \tag{2-19}$$

with:

$$\varepsilon_{ca}(\infty) = 2.5 \cdot (f_{ck} - 10) \cdot 10^{-6} \quad (2\text{-}20)$$

and:

$$\beta_{as}(t) = 1 - exp(-0.2 \cdot t^{0.5}) \quad (2\text{-}21)$$

Where:

ε_{cs}	= total shrinkage	[-]
ε_{cd}	= drying shrinkage	[-]
$\varepsilon_{cd,0}$	= initial drying shrinkage	[-]
ε_{ca}	= autogenous shrinkage	[-]
β_{ds}	= factor for drying shrinkage	[-]
β_{as}	= factor for autogenous shrinkage	[-]
A_c	= area of the cross section	[mm^2]
u	= perimeter of the cross section	[mm]
t_s	= time when drying shrinkage starts	[s]
h_0	= fictitious thickness of cross section	[mm]
f_{ck}	= characteristic compressive strength	[N/mm^2]

Thermal shrinkage

Thermal shrinkage can play a significant role in thick-walled concrete. Due to the hydration process, the temperature can go up to 70 ^{o}C or 80 ^{o}C, whereas a temperature difference of 20 ^{o}C is used as a limit to avoid large thermal cracking (Structural Guide, n.d.). If the exterior of the concrete is not insulated, large temperature differences may occur, which can lead to cracking. As the thickness of the spheres is calculated at order of magnitude of 2.5 m in early design stage, thermal shrinkage can be significant in this case, and it is therefore important to know how temperature increases and how temperature (differences) can be minimized.

The hydration heat can be large, especially in thick-walled concrete. For thick-walled concrete, the exterior will cool earlier than the interior. This can lead to relative large temperature differences. This non-uniform cooling will cause differential shrinkage and internal tensile stresses may develop which causes cracking (Larosche, 2009). The rate at which the heat is generated and the peak temperature both depends on the type and amount of the cement, the initial temperature, type of the formwork and the geometry of the structure (Day & Clarke, 2003).

The production of heat in the concrete highly depends on the degree of hydration. The hydration process can be divided into three different parts (Breugel, Veen, Walraven, & Braam, 1996):

- Dormant period: when cement comes into contact with water, a thin layer is formed at the surface of the cement. This thin layer causes hydration to slow down, so there is hardly any hydration.
- Acceleration period: at the end of the dormant period, the acceleration period starts. In a relative short time, most of the hydration products are formed. Most of the heat is released during this period.
- Deceleration period: this period is the last period. As most of the hydration products are formed during the acceleration period, the hydration rate decreases, as well as the heat release.

Regarding the heat production and maximum temperature inside the concrete, the second period is most important. If this period is longer, the hydration is spread out over a longer period of time, resulting in a lower maximum temperature. The temperature difference then will be lower which gives lower thermal stresses.

Another important aspect is the time when the acceleration period starts. The dormant period can be influenced by adding accelerators or decelerators to decrease respectively increase the dormant period (Breugel, Veen, Walraven, & Braam, 1996). For a shorter dormant period, the maximum temperature is sooner reached, which leads to lower temperature difference between the exterior and interior concrete, provided that the heat release at the exterior is the same as for a longer dormant period. This results in lower thermal stresses.

Adiabatic temperature increase of concrete

The amount of heat that is released depends on the degree of hydration. In this report, it is assumed that the temperature increase is adiabatic. The semi-adiabatic formulation is given in Appendix E. The degree of hydration can be obtained by dividing the amount of hydrated cement by the original amount of cement, Eq. 2.22 (Breugel, Veen, Walraven, & Braam, 1996).

$$\alpha_h(t) = \frac{V_{ce}(0) - V_{ce}(t)}{V_{ce}(0)} \tag{2-22}$$

Where:

α_h	= degree of hydration	[-]
$V_{ce}(0)$	= initial volume cement	[m^3]
$V_{ce}(t)$	= volume of cement at time t	[m^3]

As the amount of hydrated cement is approximately equal to the amount of heat that is released, the degree of hydration can also be given as in Eq. 2.23 (Breugel, Veen, Walraven, & Braam, 1996).

$$\alpha_h(t) = \frac{Q(t)}{Q_{max}} \tag{2-23}$$

Where:

Q	= amount of heat released	[J]
Q_{max}	= maximum heat released	[J]

The heat that is released near the outside can be released into the air but the heat that is released in the core of the member results in warming of the concrete. Therefore, if the member becomes thicker, the maximum temperature will also increase, as the distance to the outside is larger and thus less heat is released into the air. The temperature increase, which can be considered adiabatic when no heat is released into the air, at time t, depends on the amount of cement in the concrete, the specific mass, specific heat and the hydration rate at time t, as given in Eq. 2.24 (according to Van Breugel (1996)).

$$\Delta T_a(t) = \frac{a_h(t) \cdot C \cdot Q_{max}}{\rho_c \cdot c_c} \tag{2-24}$$

Where:

$\Delta T_a(t)$	= adiabatic temperature increase	[K]
C	= cement content per unit volume	[kg/m^3]
ρ_c	= specific mass of concrete	[kg/m^3]
c_c	= specific heat of concrete	[J/(kg · K)]

With this formula, the temperature in adiabatic conditions can be formulated as in Eq. 2.25.

$$T_a(t) = T_R + \Delta T_a(t) = T_R + \frac{C \cdot Q_{max}}{\rho_c \cdot c_c} \cdot a_h(t) \tag{2-25}$$

Where:

T_r = surrounding temperature [K]

Q_{max} is the maximum amount of energy that is released when the cement hydrates. In reality however, not all the cement will hydrate (Breugel, Veen, Walraven, & Braam, 1996) & (Martinelli, Koenders, & Caggiano, 2013). This is related to the degree of hydration and given in Eq. 2.26.

$$Q^*_{max} = Q_{max} \cdot \left[\lim_{t\to\infty} \alpha_h(t)\right] = Q_{max} \cdot \alpha_{h,max} \tag{2-26}$$

Where:

Q^*_{max} = maximum amount of released energy [J]
$\alpha_{h,max}$ = maximum degree of hydration [-]

Based on results of experimental testing on hardening concrete samples, in adiabatic conditions, two possible analytical expressions were given to approximate the time evolution of the hydration heat $Q_a(t)$ (Breugel, 1991):

$$Q_a(t) = Q^*_{max} \cdot (1 - e^{-r \cdot t}) \tag{2-27}$$

$$Q_a(t) = Q^*_{max} \cdot e^{-\left(\frac{\tau}{t}\right)^{\beta}} \tag{2-28}$$

Where:

$r, \tau \text{ and } \beta$ = parameters introduced to control the shape of the heat evolution [-]

Estimation of hydration heat

An estimation of the temperature increase can be made with the heat that is released during hydration. The heat that is released depend on the constituent. Different cement types have a different composition of constituents. OPC (Ordinary Portland Cement) consists for more than 95% of clinker. The main components of Portland clinker are tricalcium silicate (C_3S), dicalcium silicate (C_2S), tricalcium aluminates (C_3A) and calcium ferro-aluminate (C_4AF). These components react at a different timescale, as shown in Figure 2-9. CEM III-B is another type of cement. In this type of cement, the amount of clinker is lowered and replaced by furnace slag. The composition of this cement type results in less heat production during hydration, and is therefore often used for large concrete structures. Because the rate of hydration also depends on temperature, the early age strength is lower.

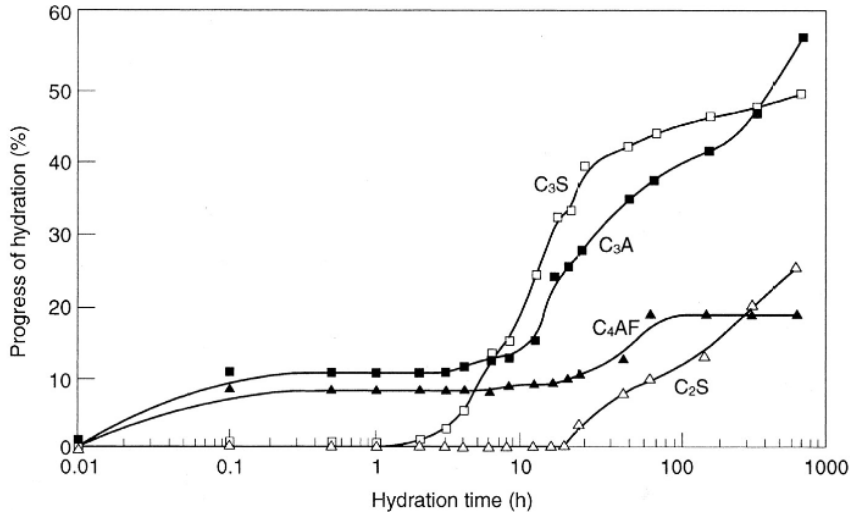

Figure 2-9 Hydration kinetics of ordinary Portland cement (Hewlett & Liska, 2017)

The heat of hydration of the constituents determine the increase of temperature in the concrete. The timescale at which the temperature increase is most important depends on the hydration rate and thus on the cement type. The heat of hydration of the main four constituents of Portland clinker is given in Table 2-3.

Table 2-3 Heat of hydration of four Bogues Compounds (Civil Giant, n.d.)

Constituent	Heat of hydration [J/g]
C_3S	500
C_2S	260
C_3A	865
C_4AF	420

With the rate of hydration and the heat of hydration of different constituents, a given w/c ratio and composition of cement type, the heat of hydration can be calculated with time. With the specific heat of concrete (typical 900 J/(kg*^{o}C)), the temperature increase at time t can be calculated.

2.3.2. Options to minimize crack width due to thermal shrinkage

Several options are applied in practice to lower thermal shrinkage and crack width due to shrinkage. Some of these are given below.

Adjust mix composition

The hydration heat comes from the exothermal reaction between cement and water. The most straight-forward way to lower the hydration heat is to use as little cement as possible to reach the design strength. This will give the lowest possible amount of hydration heat and the lowest temperature differences. Other binders could be used to reach the binder content that is needed.

The mix could also be adjusted by using Low Heat Cement (LHC), which is a type of Portland cement, instead of Ordinary Portland Cement (OPC). As the name says, low heat is generated during the chemical reaction, which lowers the temperature differences. This is achieved by replacing $Ca_3Al_2O_6$ (tricalcium aluminate), which releases most of the heat, by Ca_2SiO_4 (dicalcium silicate). As a result, the temperature difference can be 20 ^{o}C to 30 ^{o}C smaller. This type of cement is developed in US during 1930 to construct large gravity dams (Parmar, n.d.). A disadvantage is that the hydration process is relatively slow, which leads to a slower strength development (Wang, Yang, Zhou, Chen, & Tang, 2018). Blast furnace cement would also be an option. In this type of cement, part of the OPC is replaced by blast furnace slag, which lowers the hydration heat. This is also more eco-friendly, as the slag is reused.

Use of insulation

Thermal cracking occurs due to differential shrinkage, which is due to different temperatures. If this temperature gradient is decreased, differential shrinkage is lower and cracks will be limited. This can be achieved by insulating the exterior of the concrete. Better insulation then leads to lower temperature differences, as the heat is held in the concrete and will not be released. The insulation is related to the thermal conductivity: a lower thermal conductivity means better insulation.

A disadvantage of insulation is that the insulation should remain until the temperature differences between the core and the outside of the concrete are lowered again, otherwise cracking will still occur when the insulation is removed by a thermal shock due to the ambient temperatures (Gajda & Nasvik, 2017).

Cooling of the concrete

- Cooling with ice

The temperature of the concrete can be cooled in two ways: pre-cooling and post-cooling. Cooling with ice is a form of pre-cooling. Water can be replaced by ice to reduce the initial temperature of the concrete. This makes that the maximum temperature due to hydration heat will also be lower (Lagundžija & Thiam, 2017).

- Cooling with nitrogen

Pre-cooling can also be done by adding liquid nitrogen to the concrete mix, just before the concrete is cast. This lowers the initial temperature and thereby also the maximum temperature in the concrete. Pre-cooling with nitrogen is used during construction of the Calandtunnel in The Netherlands. Measurements showed that the initial temperature and the maximum temperature were both 10 ^{o}C lower than in case no nitrogen was used. This shows the potential of liquid nitrogen.

A important disadvantage of cooling with nitrogen is the safety during construction. As the temperature of liquid nitrogen is -196 ^{o}C, special equipment is needed. Prolonged exposure to skin may cause severe injuries. This makes it an expensive solution, but it could be a good solution. Another point of attention is that nitrogen may lead to local freezing of the concrete, pausing the hydration process (Juenger, Hema, & Solt, 2007)

- Cooling with cooling pipes in the concrete

The temperature inside the concrete can also be reduced with post-cooling. A technique that is widely used is cooling with pipes that are integrated in the structure, Figure 2-10. Cold water flows through these pipes, by which the concrete is cooled. Topics that should be considered regarding post-cooling are the pipe material, spacing between pipes, temperature of cooling water, convective heat transfer coefficient and flow rate of water (Tasri & Susilawati, 2019).

Figure 2-10 White cooling pipes are installed between the reinforcement to lower the maximum temperature (Kalhara, 2021)

Although pipe cooling could be an adequate solution to control the temperature of the concrete, there are some disadvantages. It is important to keep in mind that the temperature of the water is much lower than the temperature of the concrete around the pipes. This temperature difference may cause local cracking of the concrete around the pipes (Qiu & Zhang, 2017).

Dense pattern of reinforcement

Cracks develop due to low tensile strength of the concrete. If a (dense) pattern of reinforcement is applied, the tensile stresses are taken by the steel. The pattern of reinforcement leads to more cracks, resulting in a smaller crack width.

2.3.3. Concluding remarks

The relevant types of shrinkage are: plastic shrinkage, drying shrinkage, autogenous shrinkage and thermal shrinkage. The most important one for the concrete spheres will be thermal shrinkage, as it is a thick walled structure. The other types are less relevant, because if they lead to cracking, cracks occur at the surface. This will hardly affect the strength and durability, in case no reinforcement is applied. Therefore, they will be neglected in this design optimisation.

Thermal differences may cause differential shrinkage, which can lead to cracks. The maximum temperature difference is reached later for thicker walls and will also be higher. If cracks larger than the critical crack width develop through the entire cross-section, leakage will occur, which decreases the efficiency. The mix composition is an important factor for the number of cracks and the crack width. The measures given to lower the thermal differences will be taken into account during the during step 2.9 of the design.

An estimation of the temperature at time t can be made with the hydration kinetics of the four main constituents of cement. The constituents all have a different hydration rate in time which results in different temperature development for different cement compositions. The temperature that is calculated is in the case of a fully adiabatic process. The temperature will be lower for a semi-adiabatic process, but this calculation is outside the scope of this report.

3. Case analysis and requirements & boundary conditions for the design

In this report, a specific case is used to be able to make a quantitative verification of construction methods. The case is described in Section 3.1. From this, the boundary conditions and requirements are derived. Besides that, the starting points for the design are determined. These topics are given in Section 3.2.

3.1. Case analysis

The aim of the energy storage in the concrete spheres is to provide a long duration energy storage solution to balance the supply and demand of energy. In the North of Isle of Lewis (Scotland), a new wind farm is proposed. Because the aim of the Marine Pumped Hydro Energy Storage is to smoothen the energy supply, this location is chosen as a case for this thesis.

Location of proposed offshore energy storage

The location of the proposed wind farm is about 30 km North of Isle of Lewis. The energy that is stored and generated depends on the depth at which the spheres are placed. A larger depth means larger potential energy. This potential energy, together with the construction costs, installation costs, operation costs and demolition costs are expressed with the Levelized Cost Of Storage. These costs become lower when the depth at which the spheres are placed, increases. The efficiency of the pump/turbine module increases for an increasing depth and the storage capacity increases also for an increasing depth. For this case a depth of 1000 m is chosen because this is near the location of the wind turbines (Figure 3-1). The conceptual design with indicative dimensions is given in Figure 3-2. The pedestal connects the sphere to the foundation.

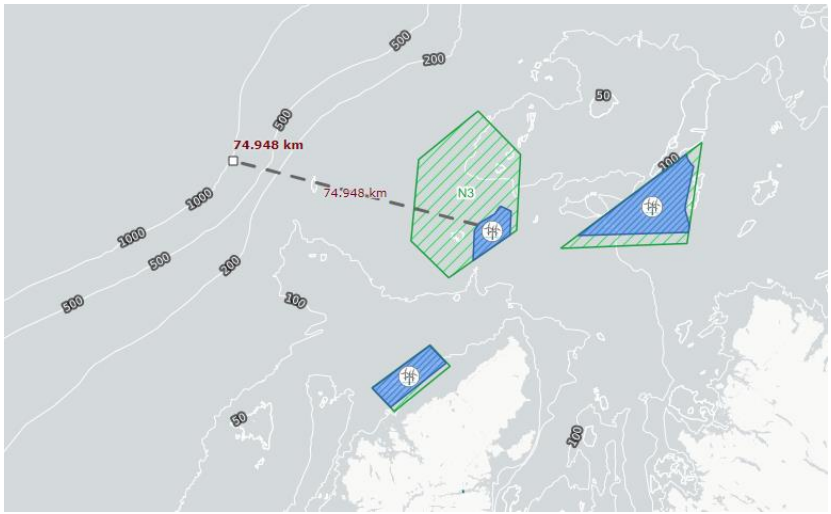

Figure 3-1 Location of wind farm (N3) and distance to 1000 m depth (A. van Dalfsen, personal communication, April 19, 2022)

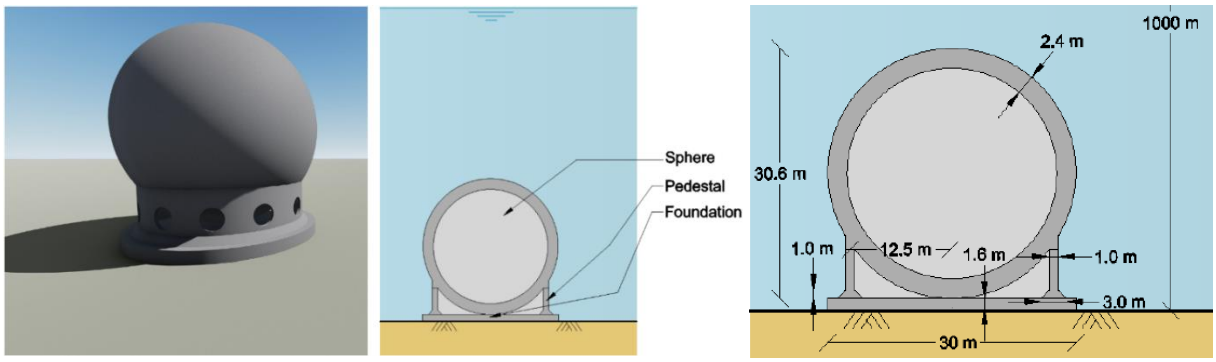

Figure 3-2 Main dimensions of the concept design (A. van Dalfsen, personal communication, April 19, 2022)

Storage capacity

The storage capacity depends on the depth and the size of the spheres. For this case, the intended depth is 1000 m and the intended storage capacity equals 20 MWh. With an expected overall efficiency of 0.8, the inner diameter of the spheres is 25.6 m.

Maintenance

Maintenance is expensive at large depth and should therefore be avoided as much as possible. The concrete components will be designed for 50 years without maintenance.

3.2. Determination of requirements, boundary conditions and starting points for the design

In this specific case, the design is verified based on buildability, crack width and watertightness. The requirements which follow from these design aspects depend on several parameters, which could be different for several cases. For a smaller storage capacity, the spheres could be constructed easier, because a printer with less capacity is needed for example. For a different ratio of depth and thickness, the critical crack width could be different. If a thinner wall is needed, thermal cracking due to hydration will be less critical. The influence of these parameters are described in Chapter 6.

In this section the requirements, boundary conditions and starting points are described. They follow from the case description in Section 3.1. The requirements regarding all phases (construction, transport, installation and use phase) are given in Section 3.2.1. The boundary conditions are given in Section 3.2.2 and the starting points are given in Section 3.2.3.

3.2.1. Requirements for the design

The design of the sphere is based on several requirements. The requirements are related to the construction phase, transport phase, installation phase and use phase. An suitable solution for the end of life is preferred to be found too. The requirements are divided into structural requirements and functional requirements.

Structural requirements

- Consequence Class 2 (CC2). Damage to the system or collapse of the system would have significant economic damage, whereas danger for humans is limited (EN 1990, 2019);
- Exposure classes XC4 and XS3. Class XC4 because the inside of the sphere is alternating wet and dry; carbonation could lead to corrosion. Class XS3 (corrosion due to chlorides) because the system is alternating wet and dry. This influences the construction class. Regarding class XC4, the construction class can be lowered with one for concrete classes higher than C40/50. Regarding class XS3, the construction class can be lowered with one for concrete classes higher

than C45/55. The starting class for structures is S4 (EN 1992, 2011). The minimum concrete strength class for exposure classes XC4 and XS3 is C35/45;
- The sphere should meet the requirements of watertightness class 1;

Functional requirements
To derive the functional requirements, a functional analysis is made which is given in Figure 3-3.

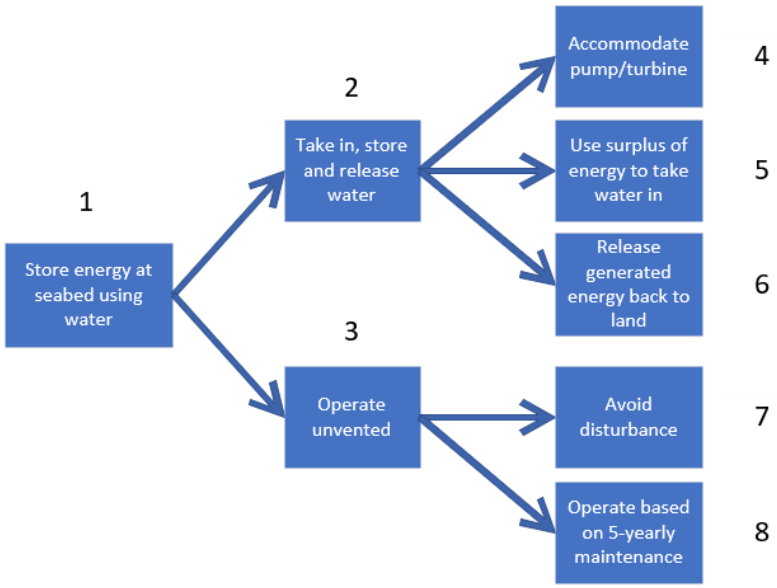

Figure 3-3 Function analysis for energy storage

The requirements below follow from the functional analysis.
- The carbon footprint should be as low as possible; at least lower than the revenue of lifetime. Energy storage is needed for the energy transition which is needed to lower the anthropogenic emissions of CO_2 (explained in Section 1.1); this requirement is based on function 1;
- The system should be suitable for depths between 100 - 1500 m. The aim is to use the system at more locations where depth could be different than in this case. This is based on function 1 & 2;
- The system should be suitable for seawater (salt) without need for extensive maintenance. This is based on function 7 and 8;
- Design life of concrete components: 50 years. The Levelized Costs Of Storage become lower when the storage system is deployed for a longer period and if little maintenance is required. This is based on function 3 & 8;
- The buoyancy of the structure should be larger than the weight of the structure resulting in a floating structure. This enables towing of the structure.

Besides the structural and functional requirements, it is also preferred to have a modular design.

3.2.2. Boundary conditions for the design
Boundary conditions in this case describe shipping and the environmental conditions such as waves and currents. They are given in this section.

Temperature, salinity and density of seawater
The density of seawater is higher than the density of clear water and depends on the temperature and the salinity. These two parameters change in depth and depend on the latitude. The pycnocline, which is defined by the thermocline (transition from warm water at the surface to cold water at deep water)

and halocline (transition in salinity from the surface water to deep water) differs per latitude, which is depicted in Figure 3-4. This is therefore important to keep in mind during design for other locations. The project location in this case is at 60 ^{o}N where there is no pycnocline. Therefore, the density (1030 kg/m^3) and temperature (3 – 4 ^{o}C) are constant over depth.

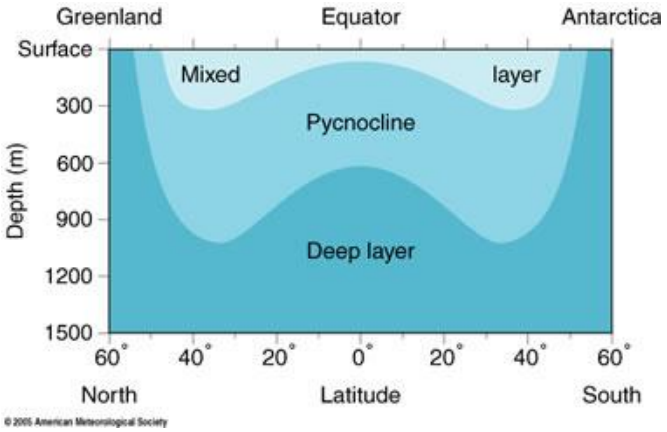

Figure 3-4 The pycnocline depends on the latitude. Above 50 ^{o}N and below 50 ^{o}S there is hardly any pycnocline (Oceanmotion, n.d.).

Waves and currents

Transport of the spheres will be done in calm seas. Waves during transport are therefore neglected for the design. The impact of waves during use phase depends on the wavelength. Waves will not initiate any motion near the bottom when the depth is larger than half of the wavelength (Water Encyclopedia, n.d.). The ocean tide and tsunamis have a wavelength that are larger than the depth in this case. It should be kept in mind for other cases, especially in shallower water, that waves could have an impact on the system at the seabed. For this specific case, tsunamis are neglected. For a 1/50 year current (tidal and ocean current) at seabed level, a current of 1 m/s shall be applied (A. van Dalfsen, personal communication, April 19, 2022).

Shipping

At the location where the spheres will be deployed, there is little shipping (MarineScotland, n.d.). When the spheres are installed at the sea bed, shipping may be possible at that location. There will be no influence of shipping on the system at the seabed. The risk of vessels that may sink and attack the spheres is accepted.

Ecology

Marine life at large depth is largely unknown, because it is difficult to investigate at large depth. Sunlight is an important factor for marine life. Until a depth of 200 m, photosynthesis takes place, which enables marine life. Sunlight could penetrate until 1000 m, but the amount is small. For this specific location, the marine life should be investigated with an Remotely Operated Vehicle (ROV) to be able to estimate the impact of the spheres on the marine life. This is beyond the scope of this report.

3.2.3. Starting points for the design

In this section, the most important starting points are given.

- The shape that will be considered in this report is a sphere. Depending on the depth, wave influence and the dimensions of the structure, the optimal shape can be estimated (Marrewijk, 2020), which is a sphere in this particular case;
- Buildability depends on the maximum printing angle. Experiments show that, in case accelerators are added at the nozzle, hardening is accelerated and the maximum printing angle

can go up to 45^{o} (S. Wu, personal communication, October 31, 2022). This is therefore used as a starting point;
- The maximum interlayer time is set to 20 minutes, according to experiments (S. Wu, personal communication, October 31, 2022);
- The following print parameters are used:
    - Layer thickness = 1 cm
    - Layer width = 10 cm
    - Maximum print rate = 5-8 l/min
- The ratio between the tensile strength and compressive strength of 3DCP is related to the ratio of the tensile strength and compressive strength of conventional concrete, which is approximately 1/15. Therefore, a factor 1/15 is added to the compressive strength development to get the tensile strength development.
- Regarding cast concrete, five cement types will be considered in the design regarding hydration heat: ASTM type 1 to type 5. This is to verify the impact of different cement types on the temperature differences in the concrete, which may lead to thermal cracking, reducing watertightness.
- In case the wall of the sphere is constructed with unreinforced concrete, the design compressive strength and design tensile strength are lowered with a factor 0.8 (= α_{cc}), due to less ductile behaviour.

4. Overview and selection of sphere concepts based on construction method

The construction method is an important factor for the design of the spheres. For example, in case the sphere is made of prefab elements, reinforcement can be added easily. In case of a fully printed sphere, reinforcement cannot be applied with current techniques. Besides that, the spheres should be watertight to ensure the desired efficiency. For example, in case the sphere is made monolithically, the sphere is less sensitive to leakage, although it costs more labour to construct a formwork for the sphere.

Therefore, in this chapter, the optimal design is described, based on the most suitable construction method, which is step 3 of the design process. First, an overview of optional construction methods is given in Section 4.1. A qualitative comparison is made in Section 4.2, based on the requirements given in Section 3.2. The design, based on the construction method with the highest potential (based on the score on the requirements) is optimised in Section 4.3.

4.1. Overview of sphere concepts

The construction process is an important factor determining whether the design could be used for energy storage at numerous places in the world. Measures to achieve watertightness and reducing (thermal) cracking are important topics which will influence the design. It is assumed that the concepts which are described in this section satisfies structural requirements. In Section 4.2 a selection is made based on the evaluation criteria mentioned below.

Evaluation criteria regarding construction

A thickness of 2.4 m is foreseen in the conceptual design, resulting in an outer diameter of 30.6 m (A. van Dalfsen, personal communication, April 19, 2020), which is used as an starting point. The solution for construction should be safe and feasible. A list of evaluation criteria follow from construction possibilities, which are listed below.

- The structure should be easy buildable;
- The construction time should be kept as low as possible;
- The costs should be kept as low as possible;
- The design should be scalable;
- Watertightness should be achieved easily.

1: 3DCP + cast in place

A promising variant is to use 3D Concrete Printing (3DCP) in combination with conventional cast concrete. 3DCP will be used to construct a formwork and in this formwork, the concrete is cast. The formwork will consist of an outer and inner shell, in between which the concrete is cast, see Figure 4-1. The construction process consists of the following steps (A. van Dalfsen, personal communication, April 19, 2022):

- Building and installation of temporary concrete factory on site;
- Building and installation of 3D concrete printer in a dry dock;
- Printing outer and inner shell;

- After a small time step, simultaneously casting concrete in between the outer and inner shell. The time step is needed for the printed concrete to gain strength;
- The bottom and top element could be made as follows:
    - Printed bottom and top element. A supporting structure is needed for these element, due to a large cantilever;
    - Construct bottom and top element with cast in place concrete. In this case, a formwork is needed for the bottom and top element;
    - Prefab bottom and top element, which will be placed with a crane.
- Inundation of dry dock and transport of spheres to installation site.

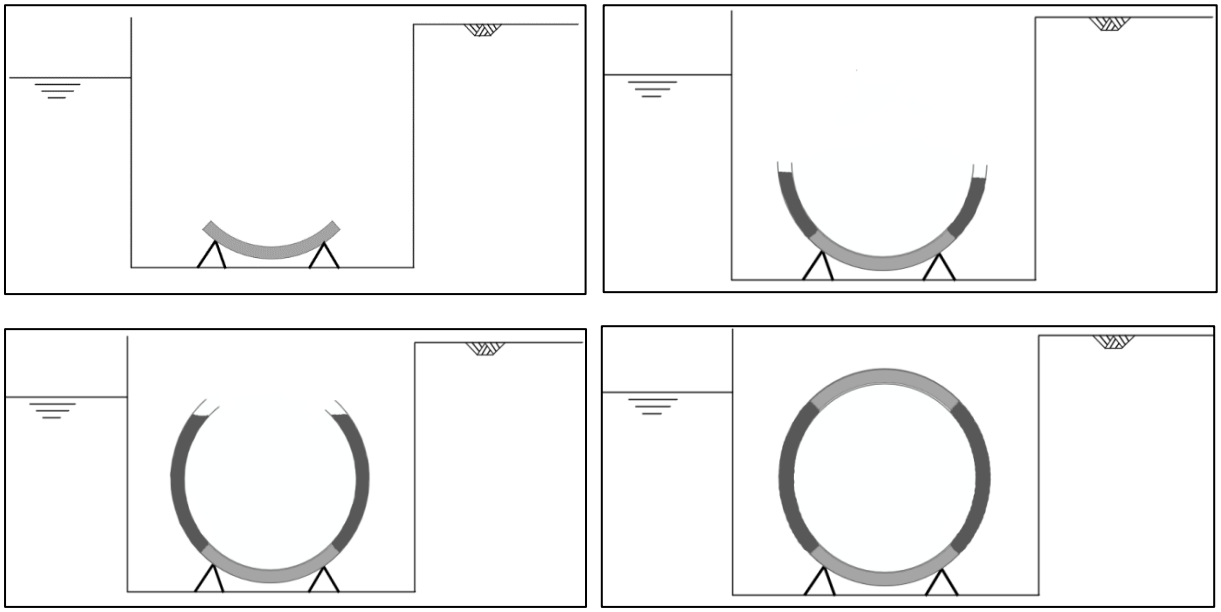

Figure 4-1 Printing outer and inner shell and casting of concrete (2D view). The bottom and top element can be made with prefab elements (light grey).

2: Fully printed sphere

Another variant which makes use of 3DCP is a fully printed hollow sphere, see Figure 4-2. In this variant, buckling will be less critical, as the width of the printed layers equals the thickness of the sphere. Plastic failure will also be less critical, as the printing time per layer increases, for an equal rate of extruded concrete. On the other hand, to reach the desired bond strength, the printing time per layer could be critical. The construction process consists of the following steps (A. van Dalfsen, personal communication, April 19, 2022):

- Building and installation of temporary concrete factory on site;
- Building and installation of 3D concrete printer(s) in a dry dock;
- Printing the sphere;
- The bottom and top element could be made as follows:
    - Printed bottom and top element. A supporting structure is needed for these elements, due to a large cantilever;
    - Construct bottom and top element with cast in place concrete. In this case, a formwork is needed for the bottom and top element;
    - Prefab bottom and top element, which will be placed with a crane.
- Inundation of dry dock and transport of spheres to installation site.

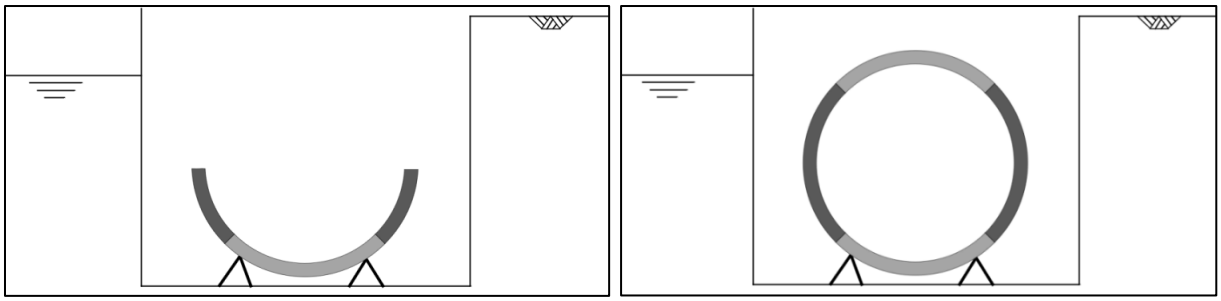

Figure 4-2 The full cross section of the sphere is printed. Prefab elements (light grey) are used for the bottom and top as this cannot be printed without formwork, due to a large cantilever.

Although the emphasis is on construction with 3DCP, several other construction processes are considered as well.

3: Slip/jump forming concrete

Slip forming construction is a construction method in which the concrete is continuously poured in a continuously moving formwork, see Figure 4-3. One of the advantages is that the structure can be made without seams, which increases watertightness (Section 2.2). There is no need to build a formwork for the entire sphere, as the formwork is continuously moving. However, the cross section of the sphere changes in vertical direction, so the formwork should also be changing with height. The speed at which the formwork moves depends on the strength development of the concrete. High initial strength is required for this type of construction.

A slightly different form is jump forming construction. In this case, the formwork moves in steps and the concrete is poured in steps as well. This enables the concrete to gain enough strength. When the strength is sufficient, the formwork is replaced ('jumped') to a higher level, where the next part of the structure is poured. Special attention should be given to the seams, because they are prone for leakage.

The construction process consists of the following steps (A. van Dalfsen, personal communication, April 19, 2022):

- Building and installation of temporary concrete factory on site;
- Construction of formwork to start construction in a dry dock;
    - For slip forming: the formwork should be made such that the shape of the formwork can be adapted continuously, as the cross section of the sphere changes in vertical direction;
    - For jump forming: the formwork should be made such that the shape can be adapted easily, so the formwork will fit for each vertical level of the sphere.
- Casting of concrete and simultaneously (slip forming) or in steps (jump forming) placing and adapting formwork for a higher level;
- To finish construction, a prefabricated element is mounted on top;
- Inundation of dry dock and transportation of spheres to installation site.

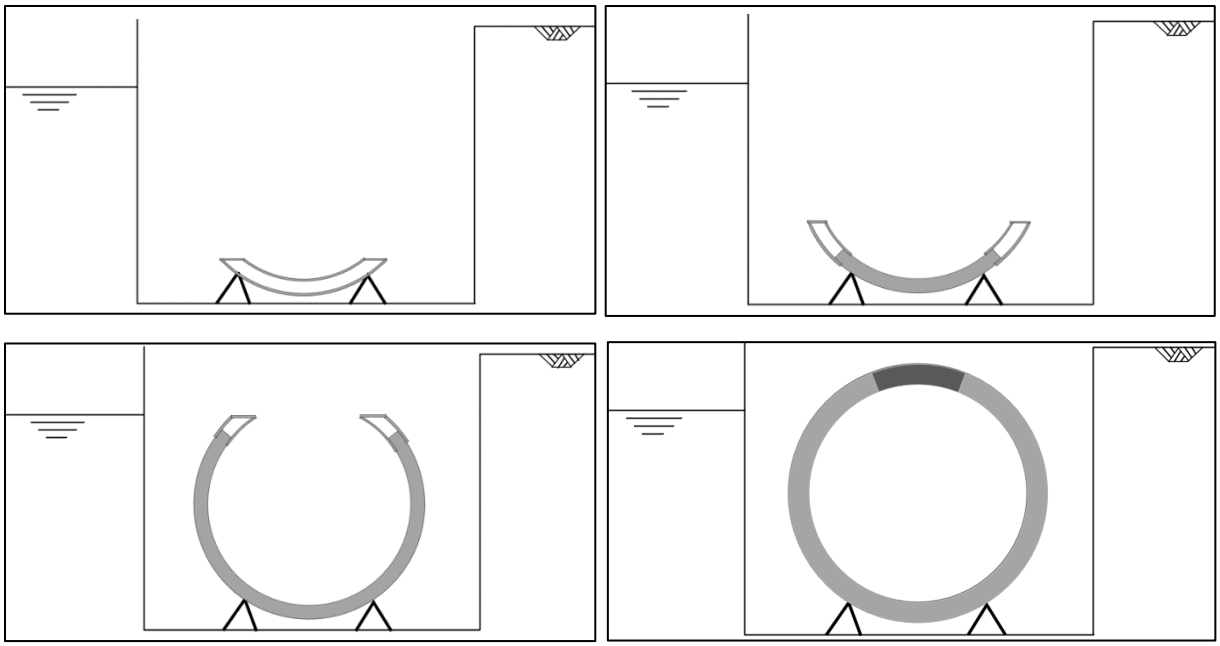

Figure 4-3 Construction sequence in case of slip or jump forming concrete.

4: Conventional casting

Conventional casting is a proven construction method. It is used for all kind of structures, although it is more challenging for structures with a complex geometry. This method allows to integrate reinforcement as well. When a formwork is made for the entire sphere and the concrete is cast in one go, there will be no seams, which positively affects watertightness. The construction process consists of the following steps (Figure 4-4):

- Building and installation of temporary concrete factory on site;
- Construction of formwork in a dry dock;
- Casting of concrete;
- The interior formwork should be removed before casting of the concrete is finished, otherwise this cannot be removed anymore;
- To finish the construction, a prefab element on top is applied.
- Inundation of dry dock and transport of spheres to installation site.

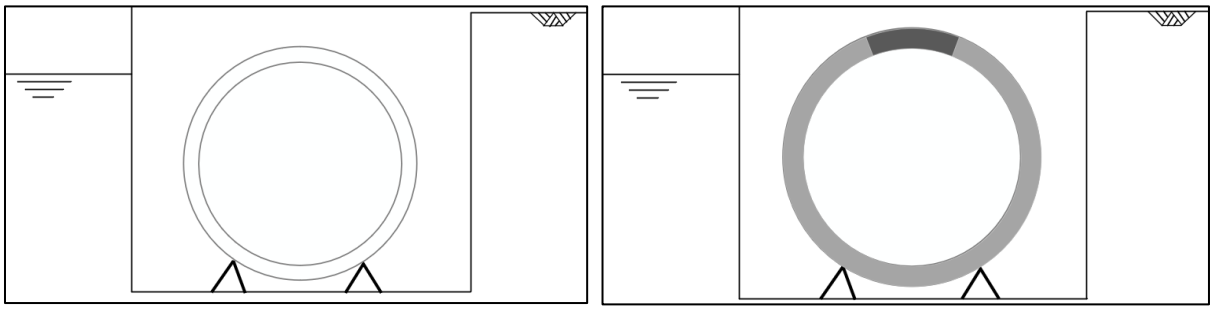

Figure 4-4 Construction sequence in case of conventional casting. First, a formwork is made, then the concrete is poured. A prefab element is placed on top.

5: Prefab

Another variant for construction is prefab, see Figure 4-5. Several prefabricated elements will be made in a factory, which are assembled using prestressing cables. The seams should be carefully injected, as the seams are prone for leakage. A formwork is necessary when assembling the prefab elements. For

tensioning the cables and injection of the seams labour is needed. The construction process consists of the following steps (A. van Dalfsen, personal communication, April 19, 2022):

- Construction of prefabricated elements;
- Transport of prefabricated elements;
- Construction of formwork in a dry dock;
- Assembling of prefabricated elements;
- Tensioning the cables;
- Injection of the seams;
- Inundation of dry dock and transport of spheres to installation site.

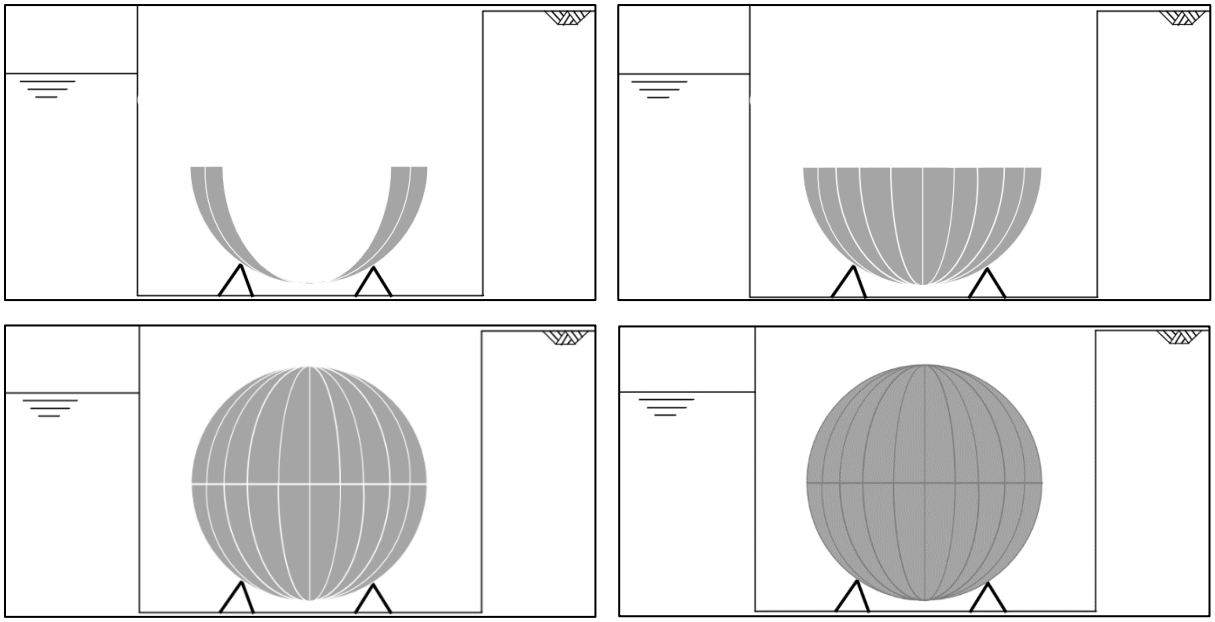

Figure 4-5 Construction sequence in case of prefab construction. The elements are assembled in a dry dock and at the end the seams are injected.

4.2. Selection based on main construction method criteria

A qualitative selection is made based on the evaluation criteria regarding construction, mentioned in Section 4.1. The different construction methods will be reviewed regarding these evaluation criteria:

- Ease of construction;
- Construction time;
- Construction costs;
- Scalability of the design;
- Ease of achieving watertightness.

1: 3DCP + cast in place

The aim of 3DCP in this construction method is to act as a formwork, so the formwork does not need to be built before, which saves money and labour. Printing the formwork and casting the concrete in between the printed shells simultaneously decreases the construction time. Moreover, the construction of the spheres is an continuous process, so there will be no seams. This affects watertightness positively. Besides that, the design is easily scalable. Special attention should be given to the bottom and top elements, in case they are made with prefab elements. The surface of these elements should be rough to reach an optimal bonding with the cast concrete.

2: Fully printed sphere

In case of a fully printed sphere, there is no need for any formwork. The top and bottom part will be made differently, as this the angle will be too large for printing. For this construction method, several nozzles and pumps are needed, otherwise construction time will be long. If one pump would be used with capacity of 0.5 m^3/h, the printing time would be 500 days. When more pumps and nozzles are applied, construction time can be decreased. The advantage of this method is that the spheres can be constructed with 3DCP only, besides the bottom and top part. Therefore, there will be no joints in the structure, improving watertightness. The design is also scalable.

3: Slip/jump forming concrete
The advantage of slip or jump forming concrete is that the formwork is not made for the entire sphere. This reduces costs for constructing the formwork. However, the formwork should be made such that the shape could be adapted easily, as the formwork moves continuously (slip forming) or in steps (jump forming). As a result, the complexity of the formwork increases. In case of slip forming, there are no seams which positively affect watertightness. In case of jump forming, there will be seams between the different segments, making it prone to leakage. The design is also less scalable with this construction method.

4: Conventional casting
In case of conventional casting, a formwork is made for the entire sphere. Therefore, costs are high due to labour and material for the formwork. The formwork can be reused for spheres with exactly same dimensions but not for other dimensions. Construction time decreases when the formwork is made for each sphere. However, costs will increase in that case, due to labour and materials. An advantage is that there will be no seams, which positively affect watertightness.

5: Prefab
In case of prefabricated elements, concrete quality can be ensured. Besides that, thermal shrinkage is less important and can be controlled better, although the other types of shrinkage become more important in this case. Regarding thermal shrinkage, the maximum temperature will be lower as more heat is released to the environment because the surface/volume ratio is larger. Besides that, a less complex formwork is required.

A disadvantage of this construction method is the scalability. In case the dimensions of the sphere are changed for different locations, the formwork for the precast elements should be adjusted too, which is an time consuming process and labour intensive (A. van Dalfsen, personal communication, April 19, 2022). Besides that, the amount of seams will negatively affect watertightness and extensive labour is needed to inject all the seams to reach Leakage Class 1.

Conclusion
The score of the different requirements regarding construction for each construction method is given in Table 4-1.

Table 4-1 Trade-off matrix regarding construction methods. Scores regarding ease of construction, construction time and costs are based on personal communication (A. van Dalfsen, personal communication, April 19, 2022).

	3DCP + cast in place	Fully printed	Slip/jump forming	Conventional casting	prefab
Ease of construction	+	+	-	-	+
Construction time	+	-	+	+	+
Costs	+	+	-	-	+
Scalability	++	++	-	--	-
Watertightness	++	+	+	+	-

It can be concluded that, based on a qualitative comparison, that 3DCP + cast in place has the highest potential to come to an optimal and scalable design. Therefore, this construction method is used as a starting point for Section 4.3.

4.3. Investigation into the most suitable 3DCP method

In Section 4.2 it is concluded that 3DCP + cast in place has the highest potential to come to an optimal and scalable design. This construction method is further described in this section. 3 different sub-variants are described: construction in a dry-dock, submerged construction and construction on a pontoon. The 3 3DCP-variants are described in Section 4.3.1. The verification is made in Section 4.3.2, 4.3.3 and 4.3.4 for variant 1, 2 and 3 respectively.

4.3.1. 3 different 3DCP-construction methods

The first sub-variant is the basis for the other two sub-variants. Quality can be ensured best in case of construction in the dry, so this is the first variant. The second variant is submerged construction. The main difference between the first and second one is the submerged weight. It will be investigated what influence this has on the stresses and stability. The third variant describes construction on a pontoon. During construction, the sphere will sink due the weight. This third variant will be investigated because the hydrostatic pressure at the outside has a positive effect on the stresses in the sphere. This is until the sphere is constructed halfway, because from then on both the hydrostatic pressure and the own weight are directed inwards.

Construction in the dry

3DCP will be used to construct a formwork and in this formwork, the concrete is cast, see Figure 4-6. The formwork will consist of an outer and inner shell, in between which the concrete is cast. The construction process consists of the following steps (A. van Dalfsen, personal communication, April 19, 2022):

- Building and installation of temporary concrete factory on site;
- Building and installation of 3D concrete printer in a dry dock;
- Printing outer and inner shell;
- After a small time step, simultaneously casting concrete in between the outer and inner shell. The time step is needed for the printed concrete to gain strength;
- The bottom and top element could be made as follows:
    - Printed bottom and top element. A supporting structure is needed for these element, due to a large cantilever;
    - Construct bottom and top element with cast in place concrete. In this case, a formwork is needed for the bottom and top element;
    - Prefab bottom and top element, which will be placed with a crane;
- Inundation of dry dock and transport of spheres to installation site.

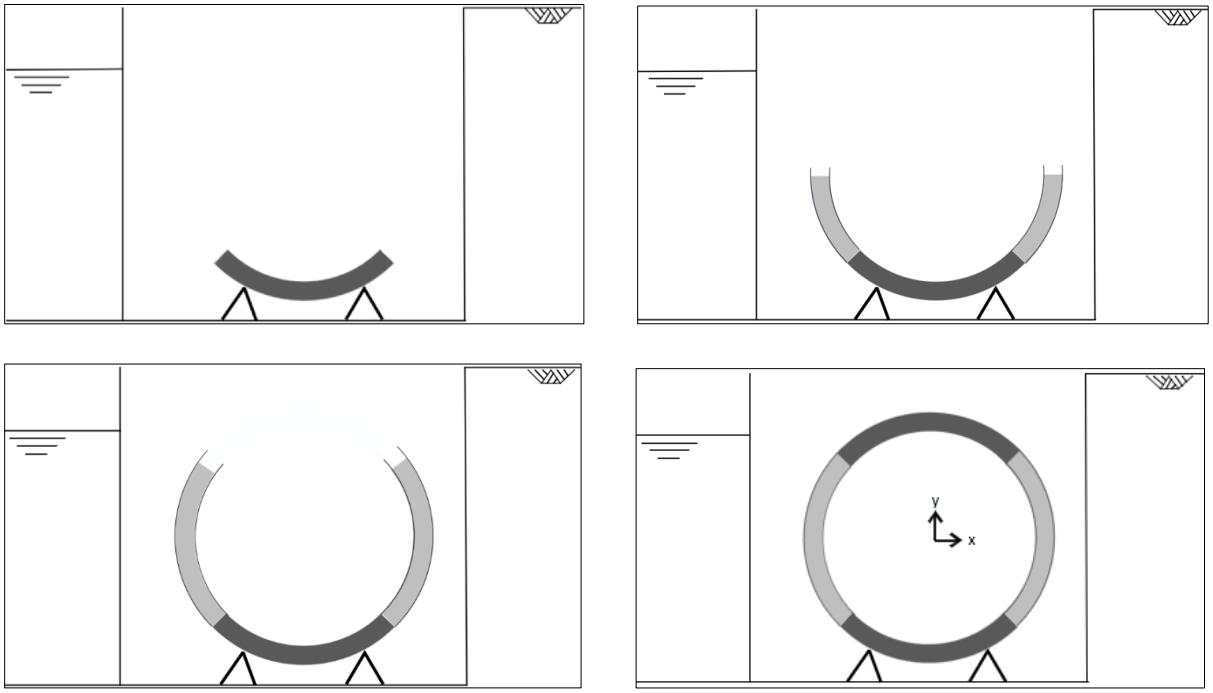

Figure 4-6 Printing outer and inner shell and casting of concrete (2D view). The bottom and top element can be made with prefab elements (dark grey).

Submerged construction

An important challenge of 3DCP is the contradiction between the requirements for pumpability and buildability. A lower viscosity is needed for pumpability, whereas a higher viscosity is needed for buildability. A solution for this is submerged concrete printing, see Figure 4-7. The submerged weight is significantly lower, which increases buildability (A. van Dalfsen, personal communication, April 19, 2022). The increase of buildability depends on the development of the yield stress for submerged printed concrete and the submerged weight. The construction process consists of the following steps:

- Building and installation of temporary concrete factory on site;
- Building and installation of 3D concrete printer;
- Flooding of a dry dock. Printing at sea or in a bay will be more difficult, because continuous supply of fresh concrete is required;
- Printing outer and inner shell;
- After a small time step, simultaneously casting concrete in between the outer and inner shell. The time step is needed for the printed concrete to gain strength;
- The bottom and top part could be smaller, because the maximum angle that can be printed submerged is larger and could be made as follows:
    - Printed bottom and top parts. A supporting structure is needed for these parts, due to a large cantilever;
    - Construct bottom and top part with cast in place concrete. In this case, a formwork is needed for the bottom and top part;
    - Prefab bottom and top part, which will be placed with a crane.
- Transport of spheres to installation site.

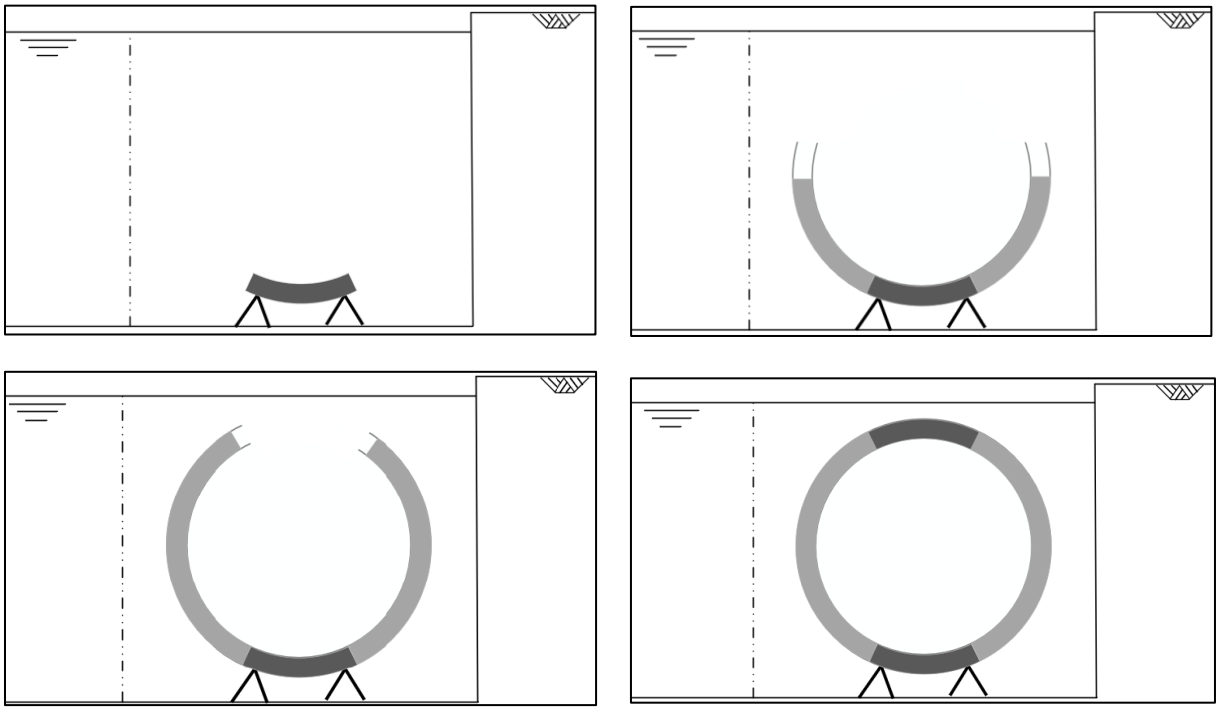

Figure 4-7 Printing outer and inner shell and casting of concrete (2D view), submerged. The bottom and top element can be made with prefab elements (dark grey).

Construction on a pontoon

The advantage of this third variant is that printing and casting can be done on a pontoon 'in the dry'. This pontoon should be designed such that printing and casting is always emerged and on the other hand, that as much as possible of the structure is submerged due to the weight, see Figure 4-8. This will give more stability to the structure. The construction process consists of the following steps:

- Building and installation of temporary concrete factory on site;
- Building and installation of 3D concrete printer;
- Flooding of a dry dock and installation of a pontoon in the flooded dock. Construction at sea is more difficult because continuous supply of concrete is required;
- An inner and outer shell are printed on a pontoon;
- After a small time step, simultaneously casting concrete in between the outer and inner shell. The time step is needed for the printed concrete to gain strength;
- To keep printing and casting in the dry and simultaneously as much as possible of the structure submerged, it is preferred to be able to change the buoyancy manually during construction.
- The bottom and top part could be made as follows:
    - Printed bottom and top parts. A supporting structure is needed for these parts, due to a large cantilever;
    - Construct bottom and top part with cast in place concrete. In this case, a formwork is needed for the bottom and top part;
    - Prefab bottom and top part, which will be placed with a crane.
- Transport of spheres to installation site.

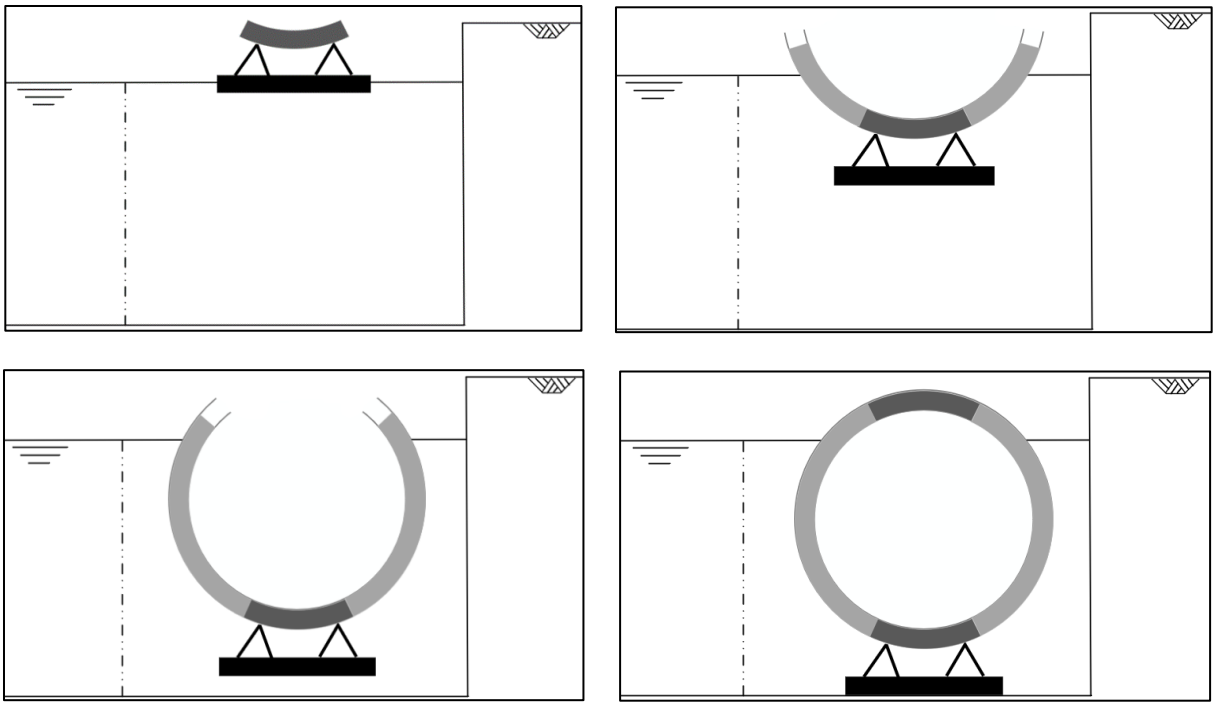

Figure 4-8 Printing outer and inner shell and casting of concrete (2D view) on a pontoon. The bottom and top element can be made with prefab elements (dark grey).

Evaluation criterion regarding construction with 3DCP

The 3 different 3DCP-variants will be verified in Section 4.3.2, 4.3.3 and 4.3.4. After that, the different 3DCP-construction methods will be evaluated based on 5 different evaluation criteria to make the choice for the preferred 3DCP-construction method. The evaluation criteria are:

- Feasibility of construction method;
- Reliability of construction method;
- Required concrete class;
- Time span for casting concrete;
- Construction time.

4.3.2. Verification of 3DCP + cast in place

Regarding 3DCP, two important failure mechanisms are described in Section 2.1 and will be investigated in this section for the sphere: plastic collapse (strength verification) and elastic buckling (stability verification). These failure mechanisms are depicted in Figure 4-9. H_1 is the height at which the printed concrete collapses and h_2 is the height at which the printed concrete buckles.

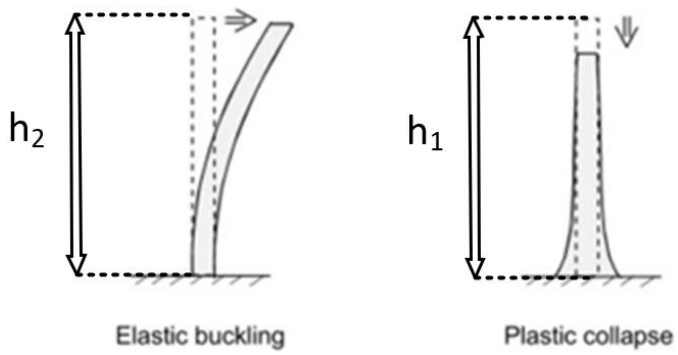

Figure 4-9 Failure mechanisms of fresh 3DCP (Suiker, 2018).

When the concrete is cast in between the printed formwork, the stress will increase in the formwork. Then, the lowest layer should carry the load of the formwork and the load of the cast concrete. Therefore, until the printed formwork is bonded to the cast concrete in the formwork, the lowest layer should be strong enough to carry the load of the formwork and the cast concrete. This is represented in Figure 4-10. This determines the minimal time span (t_1) between the onset of printing and onset of casting. The stress in the formwork due to the cast concrete is calculated with RFEM.

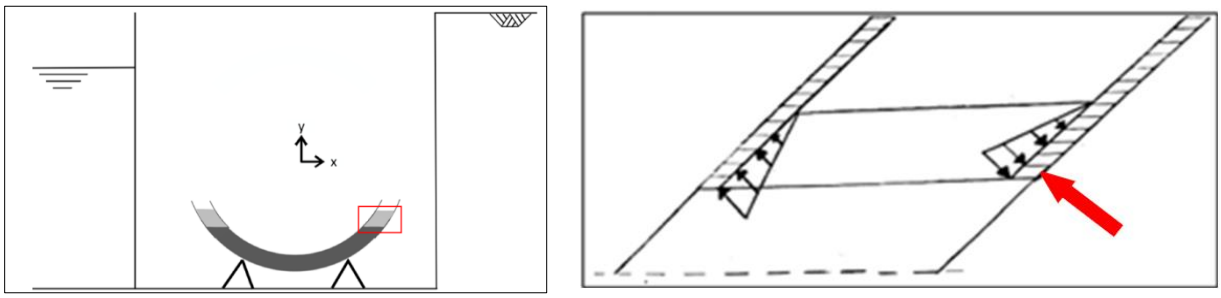

Figure 4-10 Load on the formwork due to the cast concrete.

The stresses in the lowest layer are the result from the loads shown in Figure 4-11. F_g is due to the self-weight of the layers on top, M_g is due to the eccentricity of the layers on top and M_c is due to the load of the cast concrete.

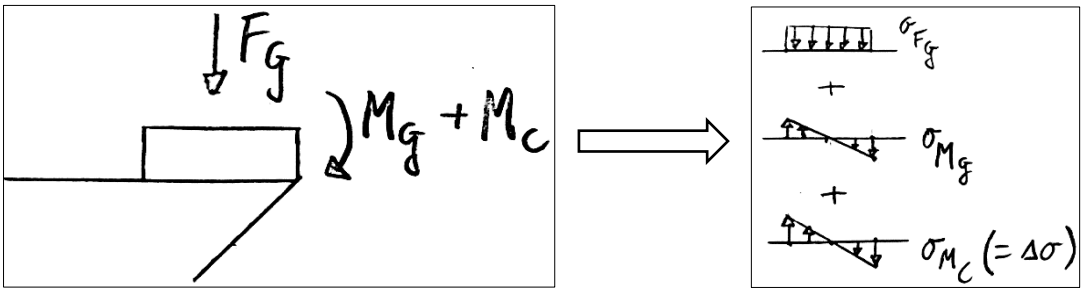

Figure 4-11 Representation of vertical stresses in lowest printed layer.

Elastic buckling occurs when the free height of the printed formwork becomes larger than the buckling height (h_2, Figure 4-12). To prevent the formwork from buckling, the concrete should be cast in between the formwork before the free height of the formwork reaches the buckling height. Combining these two criteria (strength and stability) give two values of height (h_1 and h_2) in between the concrete can be cast. The height of the formwork depends on time and thus these two criteria give a certain timespan in which the concrete can be safely cast (t_1 and t_2). It is important to mention that the principle of the upper part of Figure 4-12 is the same for compression and tension. Thus, it is a combination of tensile stress, tensile strength and where $\Delta\sigma$ is a tensile stress or a combination of compressive stress, compressive strength and where $\Delta\sigma$ is a compressive stress.

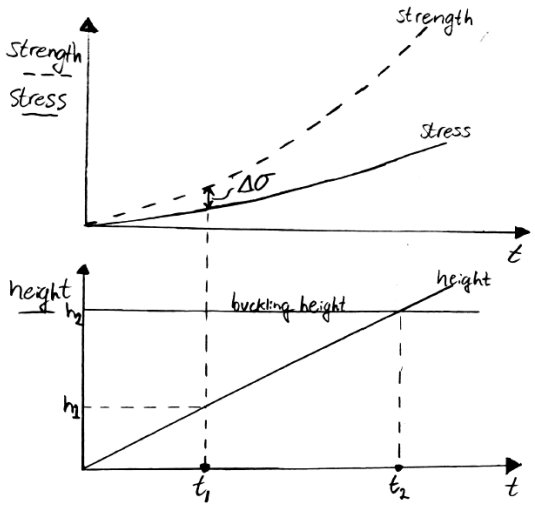

Figure 4-12 Development of strength and vertical stress (due to self-weight) in lowest layer. ⊿σ determines when the concrete can be cast. This coincides with t_1 and h_1. When the height of the formwork becomes larger than h_2, the formwork will buckle (at time = t_2).

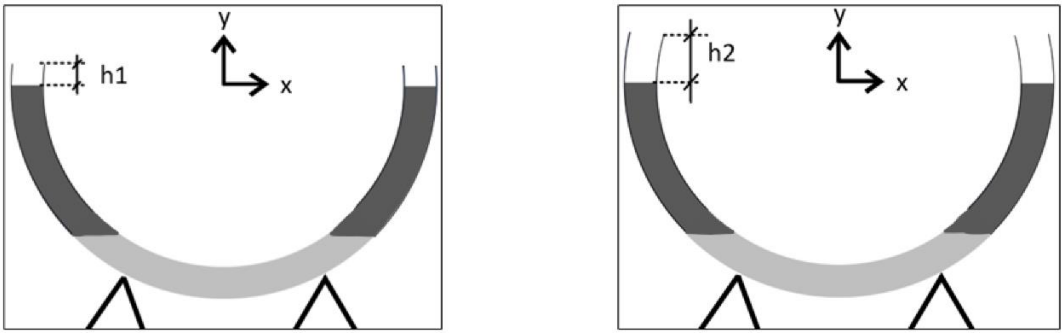

Figure 4-13 The height of the formwork should be at least h_1 (regarding strength) and at most h_2 (regarding stability) when the concrete is cast in between.

Determination of minimal height h1

In this part, the strength and stress for the critical layer, which is the first layer, are shown. This is the upper part of Figure 4-12. In case of plastic collapse, the stress in the lowest layer is higher than the strength of the material. In Section 2.1, three models are given to calculate the strength development. A thickness of 1 cm and width of 10 cm is used for the printed layers. For conventional 3D concrete printers, a maximum print rate of 5-8 l/min is used. Then, at the onset of printing, the interlayer time ranges from 8 minutes to 13 minutes. Perrot showed that the strength increase is exponentially from approximately 30 minutes. Because the strength of the lowest layer is verified when multiple layers are added on top, the timescale of the model of Perrot fits best.

The stress can be divided into normal stress due to the weight of the layers on top and bending stresses, due to the eccentricity of the layers on top, in case the layers are inclined. This is represented in Figure 4-14. The normal stress $\sigma_{i,1}$ and bending stress $\sigma_{i,2}$ in layer i are given in Eq. 4.1 and Eq. 4.2 respectively, in case 1 m length is used.

$$\sigma_{i,1} = \frac{F}{A} = \frac{(h \cdot b \cdot 1) \cdot \rho \cdot g}{b * 1} \tag{4-1}$$

$$\sigma_{i,2} = \frac{M}{W} = \frac{F \cdot a}{\frac{1}{6} \cdot 1 \cdot b^2} \tag{4-2}$$

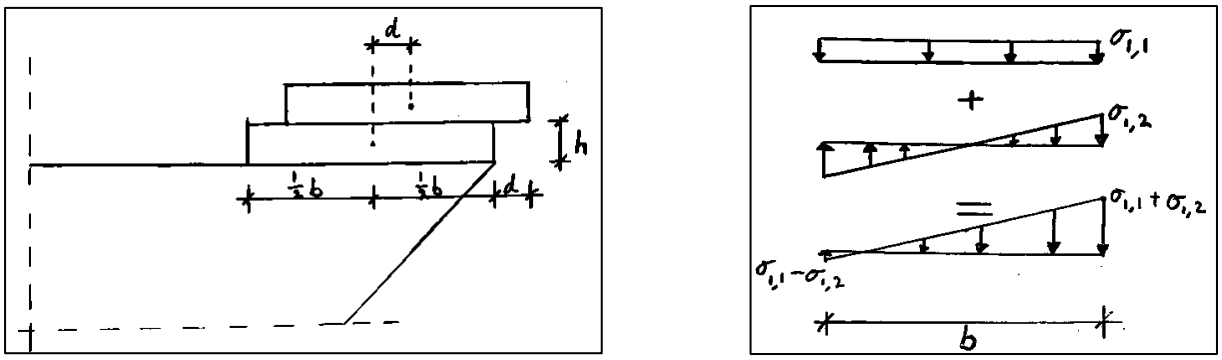

Figure 4-14 First printed layers of concrete at the prefab element (left) and stresses in lowest printed layer due to a layer on top.

The calculation of stresses in the lowest layer is shown in Appendix G. For each layer that is added on top of the first layer, the normal stress due to weight and bending stress due to the eccentricity of the layer on top is calculated. The results for the lowest layer are shown in Figure 4-15. Each green and red dot represents an added layer on top. A factor 1/15 is added to the compressive strength development of 3DCP to get the tensile strength development (stated in Section 3.2.3). The following parameters are used:

b	$= layer\ width$	$= 0.1$	[m]
h	$= layer\ thickness$	$= 0.01$	[m]
d_{max}	$= maximum\ cantilever$	$= 0.01$	[m]
ρ	$= density$	$= 2200$	[kg/m^3]
g	$= gravity\ constant$	$= 9.81$	[m/s^2]

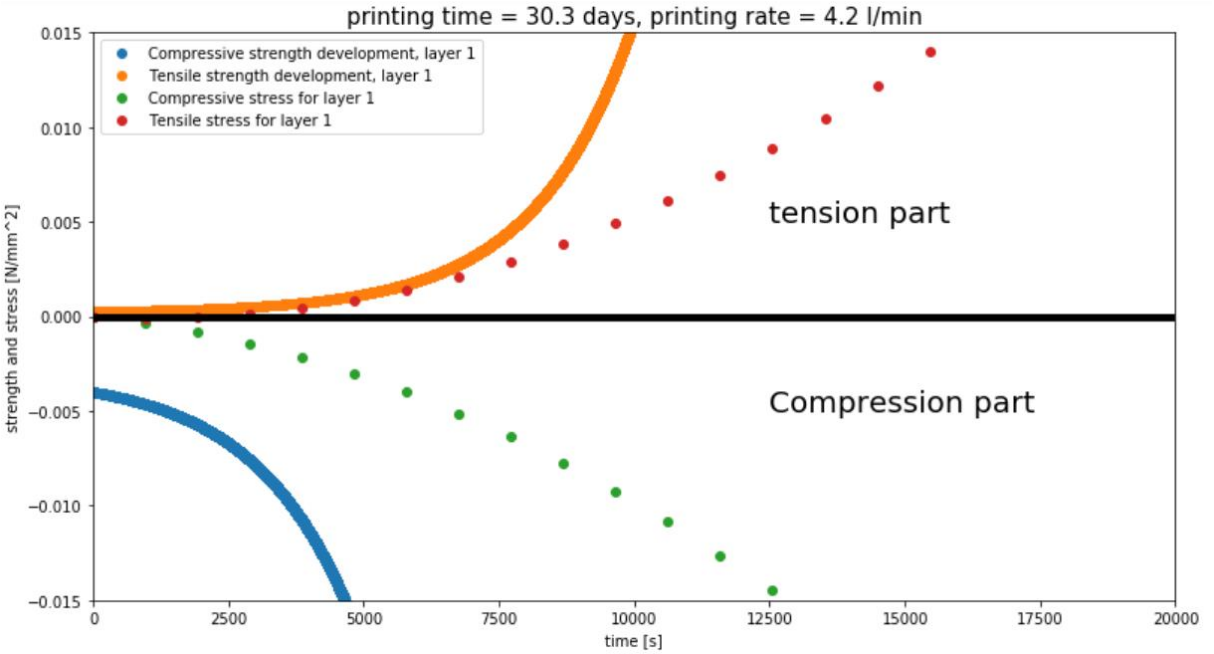

Figure 4-15 Development of stress and strength of lowest layer for construction in the dry. Each dot represents an added layer on top.

The tensile stress should always be smaller than the tensile strength and the compressive stress should always be larger than the compressive strength. The stress increase (both tensile and compressive) depend on the print rate. From an iterative process, it follows that the maximum printing rate, with the chosen dimensions, is 4.2 l/min.

Verification of concrete pressure on printed formwork

The cast concrete will lead to a lateral pressure onto the formwork. Therefore, the printed formwork should have gained enough strength before the concrete can be cast. This lateral pressure depends on the height of the cast concrete, vertical growth rate and consistency class. The construction time is such that the concrete cast at the bottom will have gained certain strength level, which reduces the pressure of the concrete on the formwork. The distribution of fresh concrete pressure over the height of the formwork is given in Figure 4-16 (NEN 8670, 2021).

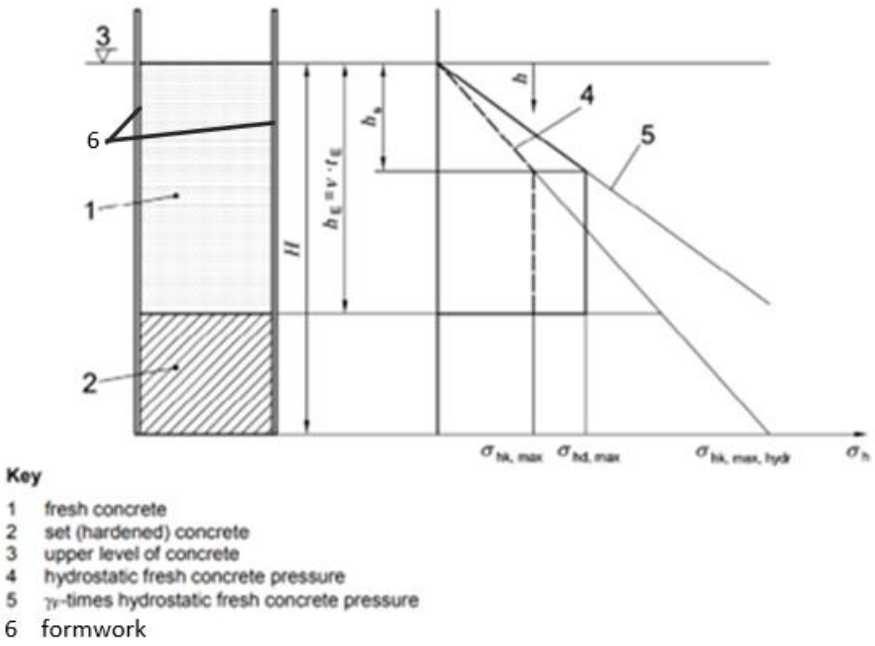

Figure 4-16 Distribution of fresh lateral concrete pressure over the height of the formwork (NEN 8670, 2021)

The pressure distribution for fresh concrete for this specific case is shown in Figure 4-17.

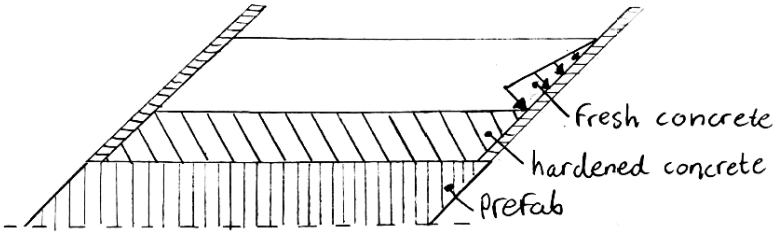

Figure 4-17 Concrete pressure of fresh concrete onto the formwork. The concrete between the prefab element and fresh concrete is yet hardened.

The maximum pressure $\sigma_{hk,max}$ can be calculated with Table 4-2 and Table 4-3 (NEN 8670, 2021).

Table 4-2 Characteristic value of maximum lateral concrete pressure (NEN 8670, 2021)

1	Consistency class	Maximum lateral fresh concrete pressure when placed in opposite direction to the rise in level (from above) $\sigma_{hk,max}$ kN/m^2
2	F1	$(5 \cdot v + 21) \cdot KI \geq 25$
3	F2	$(10 \cdot v + 19) \cdot KI \geq 25$
4	F3	$(14 \cdot v + 18) \cdot KI \geq 25$
5	F4	$(17 \cdot v + 17) \cdot KI \geq 25$
6	F5	$25 + 30 \cdot v \cdot KI \geq 30$
7	F6	$25 + 38 \cdot v \cdot KI \geq 30$
8	SCC	$25 + 33 \cdot v \cdot KI \geq 30$

Table 4-3 Factor KI, depending on setting behaviour (NEN 8670, 2021)

1	Consistency class	Factors KI			
2		End of setting t_E = 5 h	End of setting t_E = 10 h	End of setting t_E = 20 h	General [b]
3	F1 [a]	1,0	1,15	1,45	1 + 0,03 · (t_E – 5)
4	F2 [a]	1,0	1,25	1,80	1 + 0,053 · (t_E – 5)
5	F3 [a]	1,0	1,40	2,15	1 + 0,077 · (t_E – 5)
6	F4 [a]	1,0	1,70	3,10	1 + 0,14 · (t_E – 5)
7	F5, F6, SCC	1,0	2,00	4,00	t_E / 5

[a] Applies for concreting sections of a height H up to 10 m.
[b] Applies for 5 h ≤ t_E ≤ 20 h; t_E in h.

Where:

v = rate of placement (vertical) [m/h]

The consistency classes are classified between dry (F1) and very liquid (F6). SCC (Self Compacting Concrete) depends on several other parameters. To be on the save side, the most liquid concrete mix is assumed (F6), together with a setting time of 20 hours. The maximum vertical rate of placement depends on the vertical velocity of the printed formwork and is at the onset of casting. In case of a construction time of 30.3 days, the maximum rate of placement at the onset of casting is 0.018 m/h. Then, the maximum lateral pressure equals:

$$\max [25 + 38 \cdot \nu \cdot \mathrm{KI} \,; 30] = \max[\, 25 + 38 \cdot 0.018 \cdot 4 \,; 30] \; = 30 \; \mathrm{kN/m^2}$$

However, in this case, the concrete has reached a height of 0.36 m after 20 hours. This corresponds to a lateral pressure of 9 kN/m^2 in case a hydrostatic pressure gradient is assumed (weight of concrete that is used: 25 kN/m^3). Therefore, the maximum pressure of 30 kN/m^2 is not reached. In Figure 4-16, the lateral pressure goes from $\sigma_{hk,max}$ to zero between the interface of fresh and hardened concrete. This principle is also used to model the lateral pressure for this case. A safety factor γ_F of 1.5 is used for the design pressure. The stresses will be the highest at the onset of printing and casting, where the printed formwork is at an angle of 45 degrees. Per meter width, this results in a characteristic load of 9 kN/m and a design load of 13.5 kN/m (Figure 4-18).

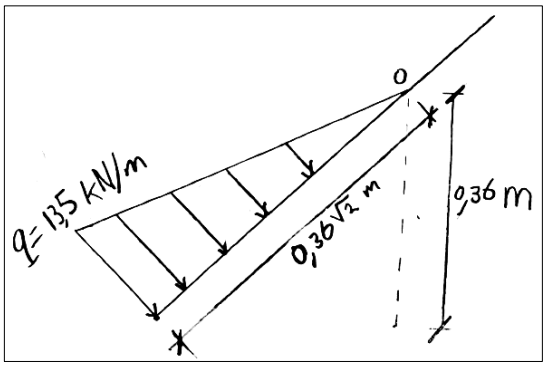

Figure 4-18 Modelling concrete pressure on the formwork.

The stresses in local x-direction (radial) and local y-direction (axial) at both sides of the printed formwork are calculated using RFEM (Figure 4-19).

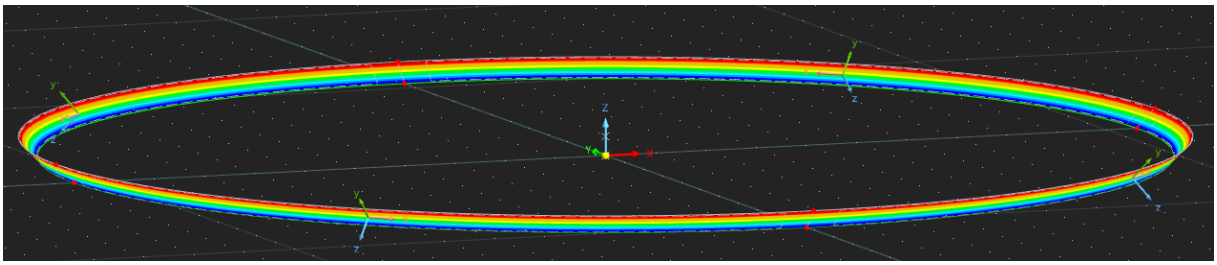

Figure 4-19 graphical result of stresses in local x-direction at positive (local-)z-side and representation of local axis system.

The results of the stresses in x-direction (radial direction) and y-direction (axial direction) are given in Table 4-4. The numbers are given for the positive surface side (positive local z = outside) and negative surface side (negative local z = inside).

Table 4-4 Results of stresses due to concrete pressure on formwork. Positive stresses are tensile stresses, negative stresses are compressive stresses.

Stress type	$\sigma_{x,+}$	$\sigma_{x,-}$	$\sigma_{y,+}$	$\sigma_{y,-}$
Stress [N/mm^2]	$-0.108 < \sigma_{x,+} < 0.916$	$0.101 < \sigma_{x,-} < 1.115$	$-0.018 < \sigma_{y,+} < 0.061$	$-0.092 < \sigma_{y,-} < 0$

The maximum stress that determines the minimum height of the formwork before the concrete can be cast is $\sigma_{x,-}$, which is 1.115 MPa.

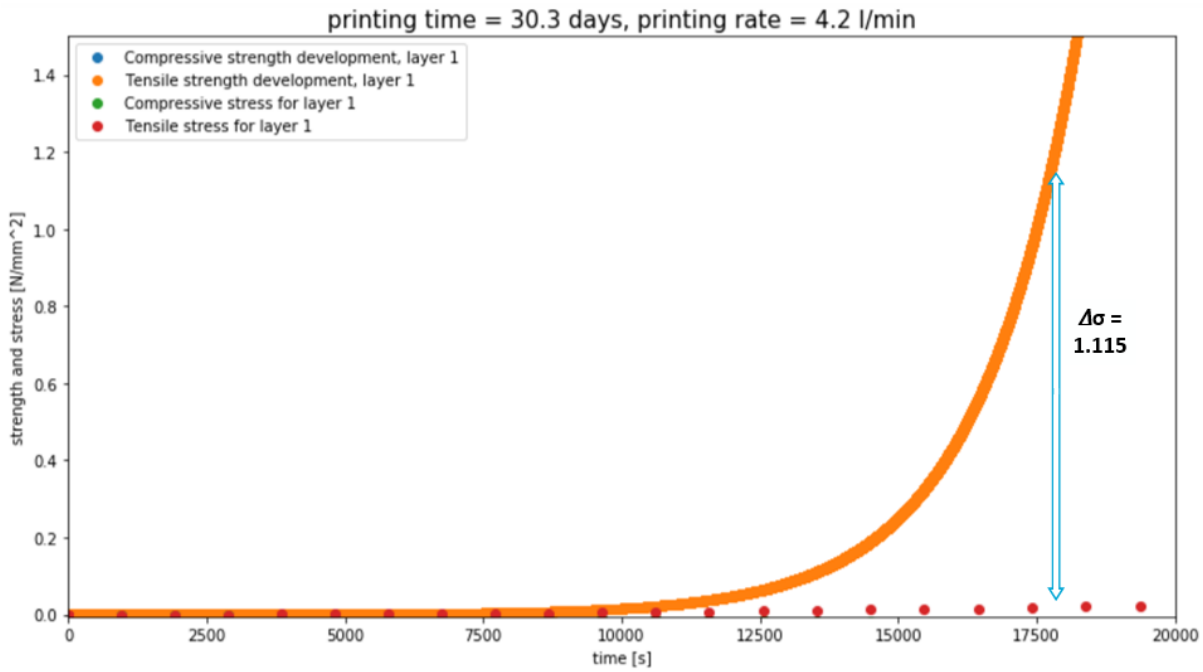

Figure 4-20 Difference between strength and stress required to cast the concrete in the formwork.

The difference between stress and strength is large enough from the 20th printed layer (each dot is one layer). Therefore, the minimum height h_1 of the printed formwork is 0.2 m in case the thickness of a printed layer is 0.01 m.

Determination of buckling height to determine maximum height h2

Elastic buckling is the second failure mode of printed concrete (Figure 4-21). This has to do with the geometry and stability of the structure.

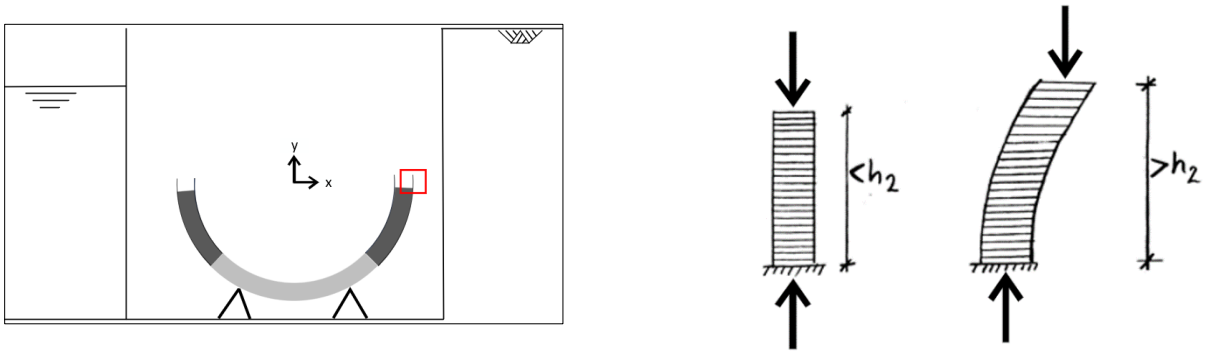

Figure 4-21 Elastic buckling of the printed formwork.

The model that is used to predict the buckling height is the model from Suiker (presented in Section 2.1). The vertical wall growth velocity $\dot{l}$ can be simplified by modelling it as a continuous growing process, which depends on printing parameters (print rate, print velocity, wall width and interlayer time).

$$\dot{l} = \frac{Q}{v_n \cdot b \cdot T_l} \tag{4-3}$$

The increase of stiffness is given with the curing rate ξ_E. This curing rate can be determined by measuring the stiffness of the printed concrete at different time steps after the concrete is deposited. In this report, the initial stiffness and curing rate of stiffness are taken from Figure 4-22, based on experiments by Suiker (2018). From this, the linear relation equals:

$$E = 0.0781 + 0.0012 \cdot t \tag{4-4}$$

Then, the curing rate equals:

$$\xi_E^l = \frac{0.0781}{0.0012} = 0.0154\ \text{min}^{-1} = 2.6 \cdot 10^{-4}\ \text{s}^{-1} \tag{4-5}$$

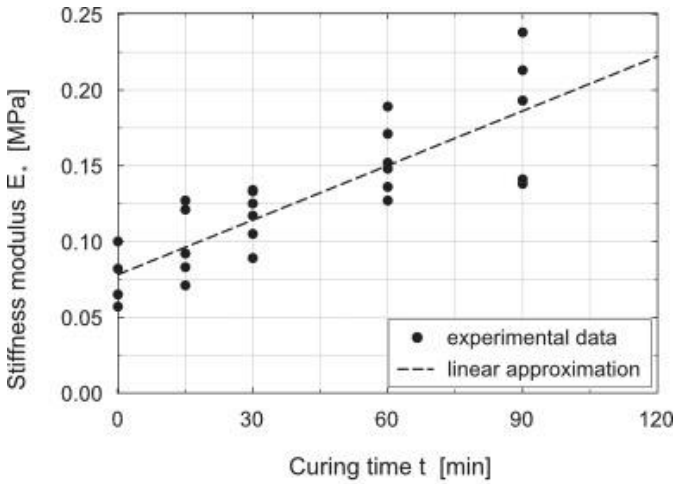

Figure 4-22 Initial stiffness and increase of stiffness for printed concrete, coming from experiments (Suiker, 2018)

Case 1: Free wall

In case of a free (unrestrained at both vertical sides) vertical wall, the critical height can be calculated with the approximation given in Eq. 4.6.

$$\bar{l}_{cr} = \left(\frac{\rho \cdot g \cdot b}{D_0}\right)^{\frac{1}{3}} \cdot l_{cr} \tag{4-6}$$

$$\bar{l}_{cr} = 1.98635 + 0.996 \cdot \left(\bar{\xi}_E^l\right)^{0.793} \tag{4-7}$$

Where:

$$\bar{\xi}_E^l = \left(\frac{D_0}{\rho \cdot g \cdot b}\right)^{\frac{1}{3}} \cdot \frac{\xi_E^l}{l} \tag{4-8}$$

$$D_0 = \frac{E_0 \cdot b^3}{12 \cdot (1 - \nu^2)} \tag{4-9}$$

In case of a vertical wall, the critical buckling height is given in Figure 4-23. The critical buckling height depends on the y-value (axis given in Figure 4-6). The red part is in case of printing under an angle larger than 45 degrees, the green part shows the result for a wall with an angle between 45 and 0 degrees. It should be kept in mind that the wall is only vertical at $y=0$. However, the order of the buckling height at the onset of printing does not differ from a vertical wall. Besides that, bending stresses become more important than buckling when the inclination increases. The calculation is shown in Appendix G and the result is shown in Figure 4-23.

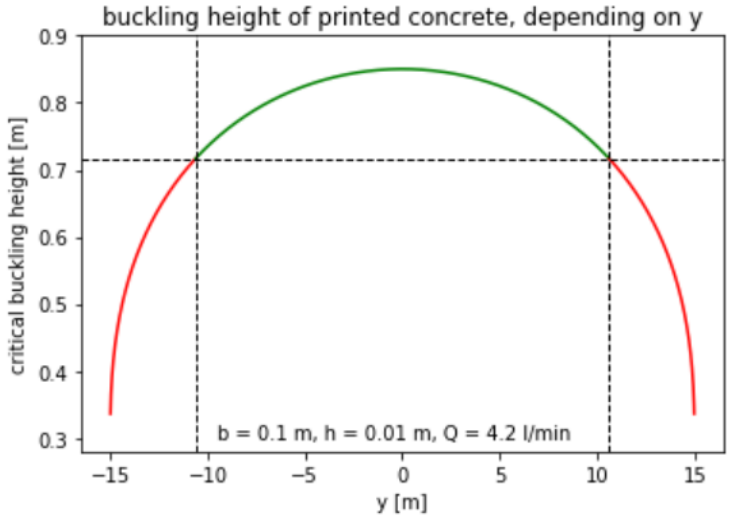

Figure 4-23 Buckling height of printed concrete, in case of vertical printing. The critical buckling height depends on the y-value.

It follows that the buckling height for a free vertical wall, with these parameters, is 0.85 m.

Case 2: Simply supported or Fully-clamped wall

In case of a simply supported and fully clamped wall, design graphs need to be used to find the dimensionless critical height, depending on the dimensionless linear curing rate and the dimensionless wall width. The dimensionless wall width can be calculated with Eq. 4.10.

$$\overline{w} = \left(\frac{\rho \cdot g \cdot b}{D_0}\right)^{\frac{1}{3}} \cdot w \tag{4-10}$$

Where:

w = wall width [m]

Eq. 4-10 is based on a straight vertical wall. In this particular case, the cross-section is a circle and therefore there is no straight wall. Therefore, part of the circle will be assumed to be straight. For small angles, the design graphs cannot be used to determine the buckling height. Due to that, part of the circle will be assumed to be straight with a maximum curvature of 10° (see Figure 4-24). In case of larger angles the wall cannot be assumed straight.

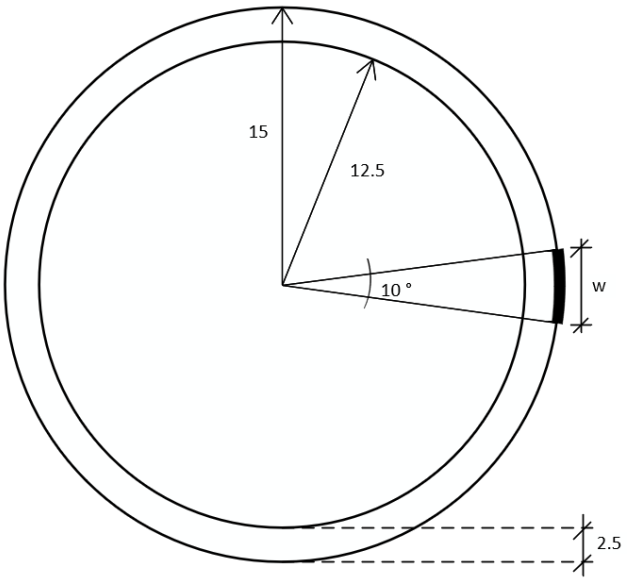

Figure 4-24 Top view of cross-section at y=0. The wall length is chosen such that the curvature is 10°.

The buckling length will be calculated for the two governing situations: at the onset of printing (angle of 45°, case 1) and at $y=0$ (case 2), where the wall is vertical.

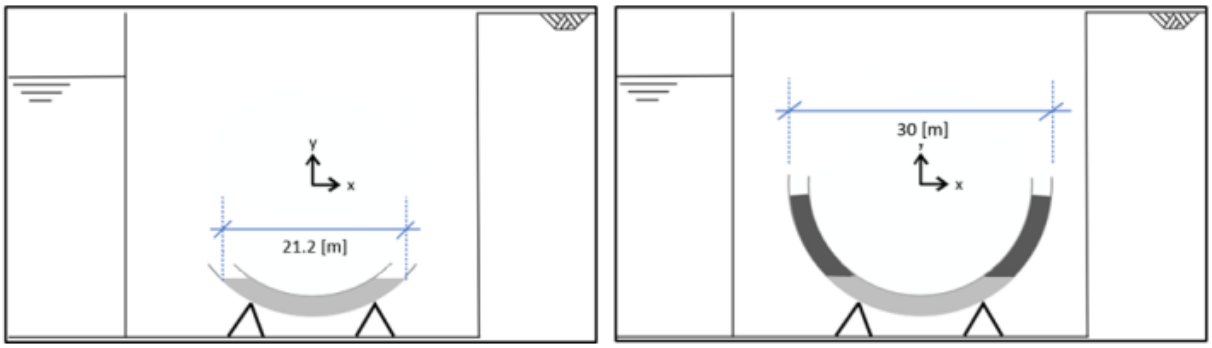

Figure 4-25 The buckling length is calculated for two cases: at the onset of printing (case 1, left) and when printing vertical (case 2, right)

The corresponding parameters for both cases are presented in Table 4-5. In this case, a larger pump rate is used, because the same pump rate as for free buckling results in a normalized curing rate which is outside the range of the design graphs. This is a conservative approach, as this will give a lower buckling height than it will be in reality with a lower print rate.

Table 4-5 parameters for cases, represented in Figure 4-25

Parameter	**Case 1**	**Case 2**
Q [m^3/s]	$1.53*10^{-4}$	$1.53*10^{-4}$
R [m]	10.6	15
b [m]	0.1	0.1
h [m]	0.01	0.01
v_n [m/s] (Q/(b*h))	0.153	0.153
T [s] *((π*2*R)/v_n)*	435	616

The normalized buckling length for case 1 can be found using Figure 4-26.

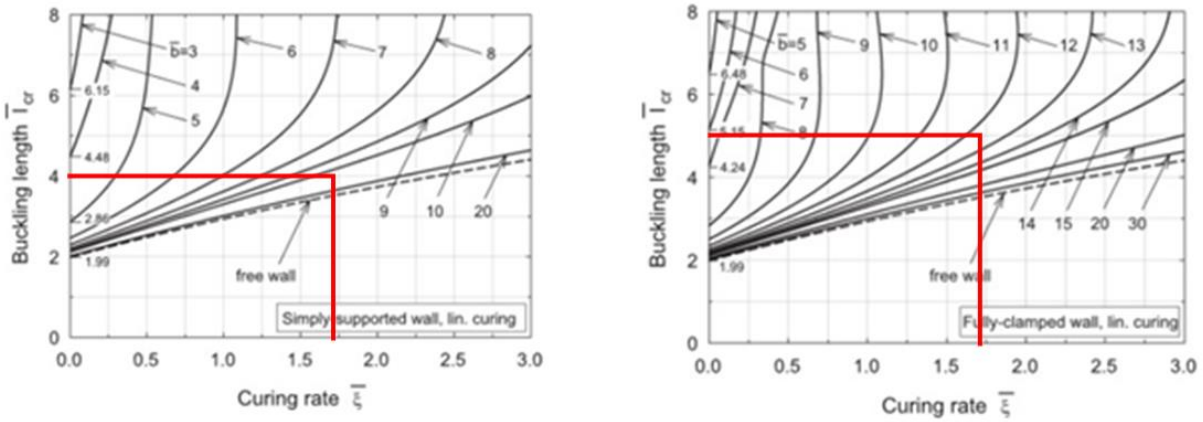

Figure 4-26 The normalized curing rate and normalized width gives the normalized buckling length l_{cr} in case of simply supported wall and fully-clamped wall. The parameters which define the curing rate and normalized width corresponds to the y-value corresponding to an angle of 45 °.

Then, the actual buckling length can be calculated, in case of simply supported and fully-clamped wall:

$$l_{cr,s-s} = \frac{\bar{l}_{cr}}{\left(\frac{\rho \cdot g \cdot b}{D_0}\right)^{\frac{1}{3}}} = \frac{4.0}{\left(\frac{2200 \cdot 9.81 \cdot 0.1}{7.152}\right)^{\frac{1}{3}}} = 0.60 \text{ [m]}$$

$$l_{cr,f-c} = \frac{\bar{l}_{cr}}{\left(\frac{\rho \cdot g \cdot b}{D_0}\right)^{\frac{1}{3}}} = \frac{5.0}{\left(\frac{2200 \cdot 9.81 \cdot 0.1}{7.152}\right)^{\frac{1}{3}}} = 0.75 \text{ [m]}$$

Thus: $0.60 < l_{cr} < 0.75$ [m]

The normalized buckling length for case 2 can be found using Figure 4-27.

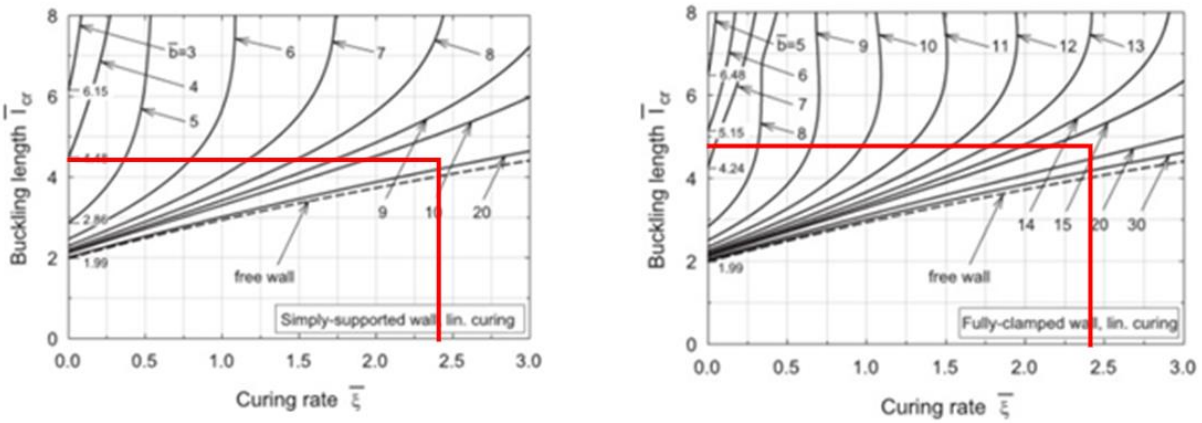

Figure 4-27 The normalized curing rate and normalized width gives the normalized buckling length l_{cr} in case of simply supported wall and fully-clamped wall. The parameters which define the curing rate and normalized width corresponds to the y-value corresponding to an angle of 0 ^{o} (y=0).

Then, the actual buckling length can be calculated, in case of simply supported and fully-clamped wall:

$$l_{cr,s-s} = \frac{\bar{l}_{cr}}{\left(\frac{\rho \cdot g \cdot b}{D_0}\right)^{\frac{1}{3}}} = \frac{4.4}{\left(\frac{2200 \cdot 9.81 \cdot 0.1}{7.152}\right)^{\frac{1}{3}}} = 0.65 \text{ [m]}$$

$$l_{cr,f-c} = \frac{\bar{l}_{cr}}{\left(\frac{\rho \cdot g \cdot b}{D_0}\right)^{\frac{1}{3}}} = \frac{4.7}{\left(\frac{2200 \cdot 9.81 \cdot 0.1}{7.152}\right)^{\frac{1}{3}}} = 0.70 \text{ [m]}$$

Thus: $0.65 < l_{cr} < 0.70$ [m]

Conclusion regarding maximum height h_2

The buckling behaviour of the printed formwork can be modelled best by a wall which is supported at the sides by a rotational stiffness. However, the model does not provide this and therefore, to be on the safe side, the value in case of a simply-supported wall will be used. Then, the maximum free height h_2 of the formwork before the concrete is cast is 0.65 m. The buckling length in case of a vertical wall is used, because this gives the best estimate of what will happen in reality.

Verification of wall thickness and required concrete class based on strength requirement

The concrete which is cast in the formwork should carry the loads in the use phase, but also in the construction phase. The construction time largely depends on the parameters for printing the formwork. The printing time is 30.3 days in case of a print rate of 4.2 l/min. The concrete which is cast first will already have reached significant strength at the end of construction, while the concrete which is cast at the end has no strength. This is used during construction of the spheres: the load on the formwork will become lower with time, because the load of the cast concrete will be taken increasingly by the concrete which is cast before.

The condition in use phase is the same for the three 3DCP-construction variants which are investigated. Therefore, the use phase is modelled first to verify what thickness is required for the use phase. After that, the construction phase is analysed for the three variants, to verify whether a larger thickness is

required to carry the loads during construction. The load condition in use-phase is given in Figure 4-28. The hydrostatic pressure is applied perpendicular to the surface of the sphere.

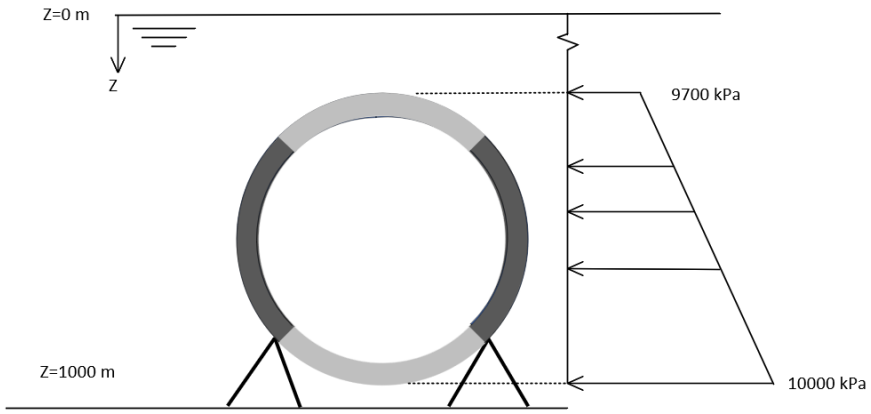

Figure 4-28 A hydrostatic pressure is applied at the outside of the sphere (the pressure is perpendicular to the surface). The support of the pedestal is modelled with a hinged support at an angle of 45°.

It is required that the sphere will float from itself. Therefore, regarding the draft of the sphere, the thickness is limited to a certain value. In case of a sphere with an outer diameter of 30 m and a weight of concrete of 24 kN/m^3, the thickness is limited to 2.5 m. Therefore, a thickness of 2.5 m is used as a starting point. The concrete class which is used depends on the stresses in the sphere, but should be at least C35/45.

The principle stresses σ_x and σ_y are used to verify the required concrete class. $\sigma_{x,+}$ refers to the stress in direction of the local x-axis on the positive surface side, $\sigma_{x,-}$ refers to the stress in direction of the local x-axis on the negative surface side, $\sigma_{y,+}$ refers to the stress in direction of the local y-axis on the positive surface side and $\sigma_{y,-}$ refers to the stress in direction of the local y-axis on the negative surface side.

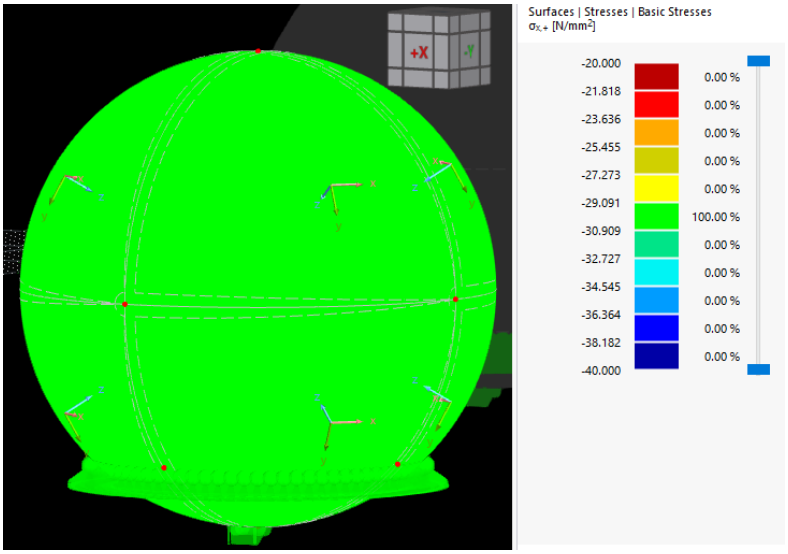

Figure 4-29 Surface stress $\sigma_{x,+}$ (stress in radial direction on positive surface side) for the sphere at a depth of 1000 m.

In Figure 4-29, surface stress $\sigma_{x,+}$ is given. The results of the other stress types are given in Appendix H. The maximum compressive stress in the sphere is 31 MPa, there are no tensile stresses. Because this is unreinforced concrete, the concrete is less ductile. Therefore, the compressive and tensile strength are lowered with a factor α_{cc} = 0.8. From this, it follows that the minimum required concrete class is C60/75, which has a design compressive strength of 32 MPa.

The stresses in the sphere during construction will be analysed at three different times: when the sphere is 50%, 75% and at 100% (Figure 4-30). The stresses will not be analysed at 25%, because then only the prefab element is present.

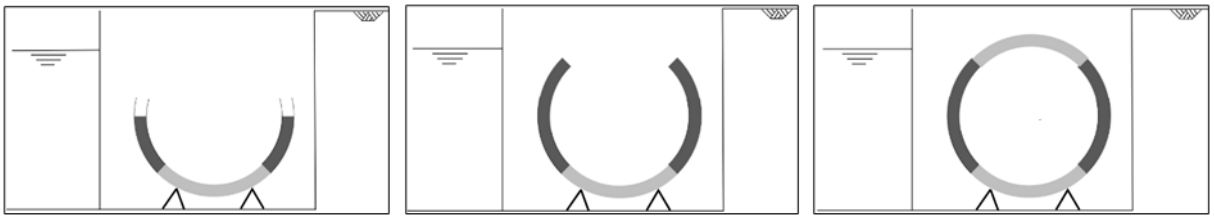

Figure 4-30 The stresses will be analysed at 3 different stages during construction: at 50%, 75% and 100%.

The results can be found in Table 4-6. The results of the stresses in the entire sphere are given in Appendix H.

Table 4-6 Maximum stress results in the sphere at 3 stages of construction: at 50%, 75% and 100%. Local x-direction is radial direction, local y-direction is axial-direction.

Stress type	50%	75%	100%
$\sigma_{x,+}$ [N/mm^2]	$-0.270 < \sigma_{x,+} < 0.208$	$-0.483 < \sigma_{x,+} < 0.308$	$-0.576 < \sigma_{x,+} < 0.407$
$\sigma_{x,-}$ [N/mm^2]	$-0.580 < \sigma_{x,-} < 0.455$	$-1.042 < \sigma_{x,-} < 0.574$	$-1.238 < \sigma_{x,-} < 0.625$
$\sigma_{y,+}$ [N/mm^2]	$-0.447 < \sigma_{y,+} < 0.882$	$-1.039 < \sigma_{y,+} < 1.389$	$-1.256 < \sigma_{y,+} < 1.601$
$\sigma_{y,-}$ [N/mm^2]	$-0.954 < \sigma_{y,-} < 0.458$	$-1.800 < \sigma_{y,-} < 0.578$	$-2.156 < \sigma_{y,-} < 0.628$

Conclusion

The maximum compressive stress in the sphere is 2.156 MPa and the maximum tensile stress in the sphere is 1.601 MPa, both at 100% of construction. The compressive stress is lower than the design compressive strength of concrete C60/75 (f_{cd} = 32 MPa, with α_{cc} = 0.8) and the tensile stress is also lower than the design tensile strength of concrete C60/75 (f_{ctd} = 1.62 MPa, with α_{ct} = 0.8). The tensile stress is therefore critical. Concrete class C60/75 is sufficient to be on the safe side.

4.3.3. Verification of 3DCP in water + cast in place

Determination of minimal height h_1

The plastic collapse of the submerged printed formwork is evaluated the same way as the plastic collapse of the formwork in case of printing in dry. The only parameter that is changed is the density. The normal density is replaced by the submerged density (density – 1000 kg/m^3). The following parameters are used:

b	$= 0.1$	[m]
h	$= 0.01$	[m]
d_{max}	$= h = 0.01$ (maximum printing angle of 45 ^{o}C)	[m]
ρ	$= 2200 - 1000 = 1200$	[kg/m^3]
g	$= 9.81$	[m/s^2]

The results for the lowest layer are shown in Figure 4-31. Each green and red dot represents an added layer on top.

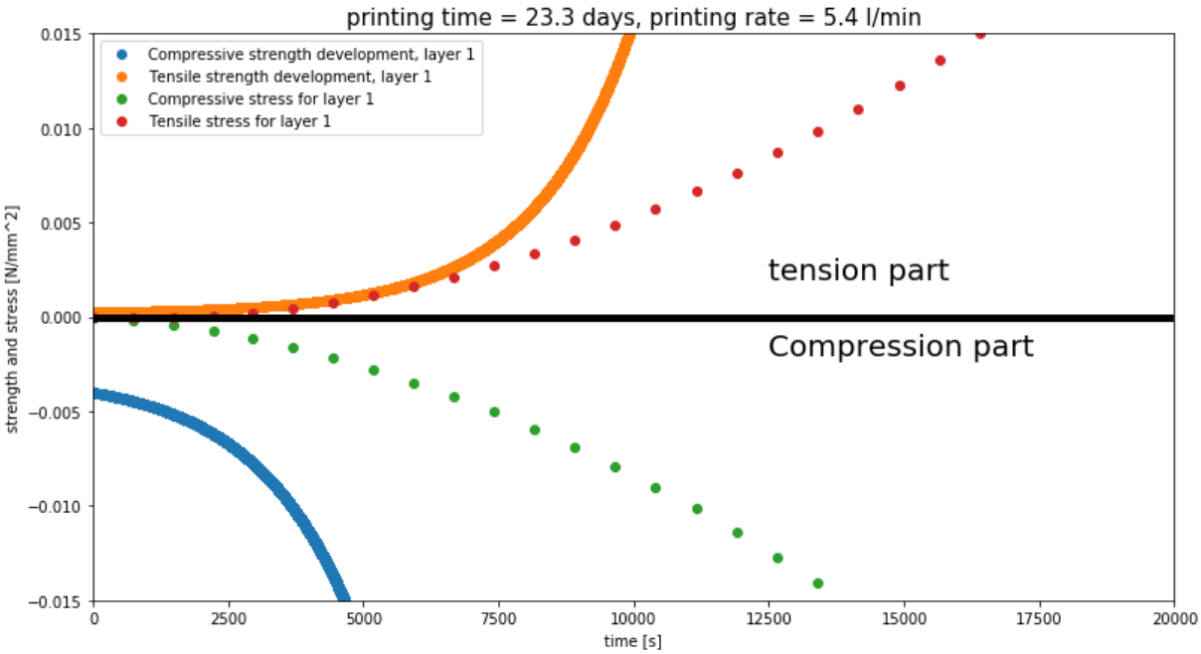

Figure 4-31 Development of stress and strength of lowest layer for submerged construction. Each dot represents an added layer on top.

Based on an iterative process, it follows that the maximum printing rate, with the chosen dimensions, is 5.4 l/min.

Verification of concrete pressure on printed formwork

The stresses due to the concrete pressure onto the formwork are verified the same way as in case of construction in the dry. The difference is the submerged weight of the concrete that is used in this case.

The maximum pressure $\sigma_{hk,max}$ can be calculated with Table 4-2 and Table 4-3 (NEN 8670, 2021). Again, consistency class F6 and a setting time of 20 hours are assumed to be on the safe side. The maximum vertical rate of placement is at the onset of casting. In case of a construction time of 23.3 days, the maximum rate of placement at onset of casting is 0.25 m/h. Then, the maximum lateral pressure (according to the Eurocode) equals:

$$\max\left[25 + 38 \cdot \nu \cdot \mathrm{KI}\,;30\right] = \max[\,25 + 38 \cdot 0.025 \cdot 4\,;30] \;= 30\ \mathrm{kN/m^2}$$

However, in this case, the concrete has reached a height of 0.50 m after 20 hours. This corresponds to a lateral pressure of 7.5 kN/m^2 in case a hydrostatic pressure gradient is assumed (the submerged weight of concrete is used: 15 kN/m^3). Therefore, the maximum pressure of 30 kN/m^2 is not reached. The stresses will be the highest at the onset of printing and casting, where the printed formwork is at an angle of 45 degrees. Per meter width, this results in a characteristic load of 7.5 kN/m and a design load of 11.25 kN/m (Figure 4-32).

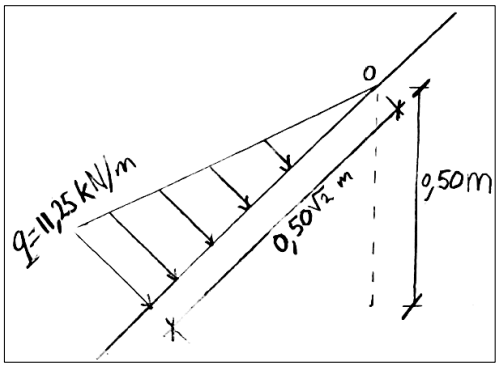

Figure 4-32 Modelling concrete pressure on the formwork.

The stresses in local x-direction and local y-direction at both sides of the printed formwork are calculated using RFEM (Figure 4-33).

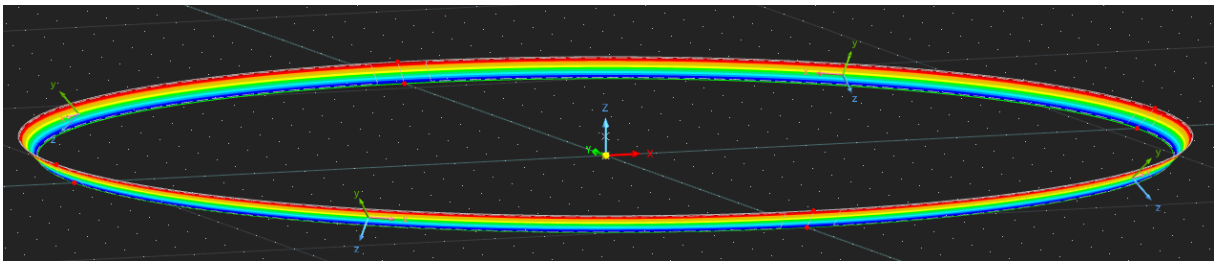

Figure 4-33 graphical result and representation of local axis system.

The results of the stresses in x-direction and y-direction are given in Table 4-7 for the positive surface side (positive z = outside) and negative surface side (negative z = inside).

Table 4-7 Results of stresses due to concrete pressure on formwork

Stress type	$\sigma_{x,+}$	$\sigma_{x,-}$	$\sigma_{y,+}$	$\sigma_{y,-}$
Stress [N/mm^2]	$-0.069 < \sigma_{x,+} < 0.788$	$0.0 < \sigma_{x,-} < 0.906$	$-0.021 < \sigma_{y,+} < 0.106$	$-0.140 < \sigma_{y,-} < 0$

The maximum stress that determines the minimum height of the formwork before the concrete can be cast is $\sigma_{x,-}$ which is 0.906 MPa.

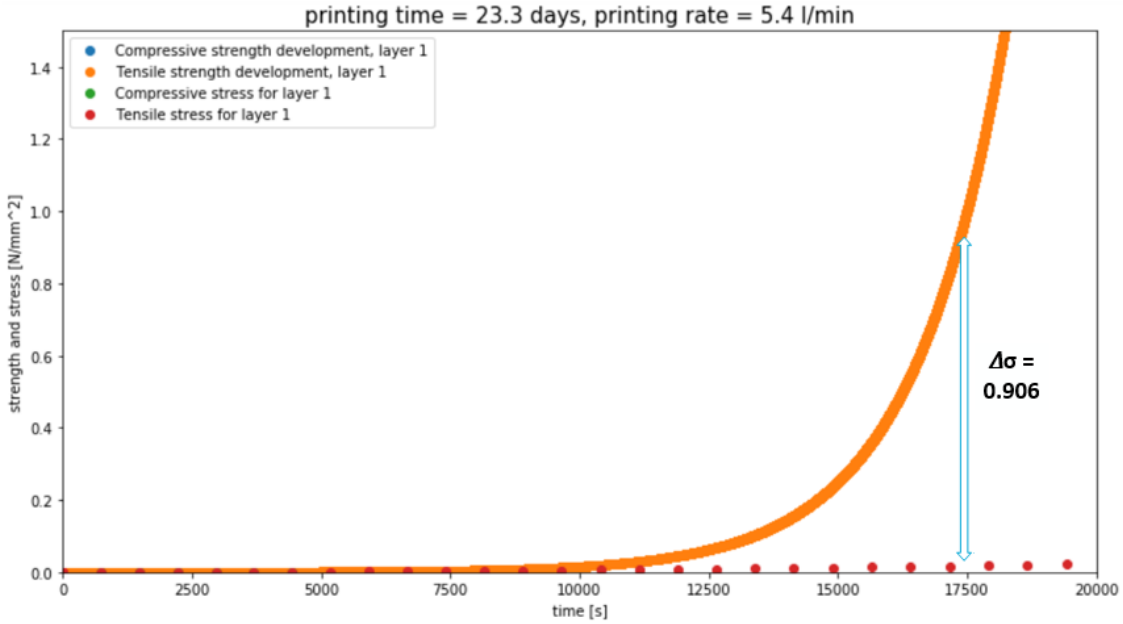

Figure 4-34 Difference between strength and stress required to cast the concrete in the formwork.

The difference between stress and strength is large enough from the 25th printed layer (each dot is one layer). Therefore, the minimum height h_1 of the printed formwork is 0.25 m in case the thickness of a printed layer is 0.01 m.

Determination of maximum height h2

Case 1: Free wall

The verification of elastic buckling is done in the same way as for 3DCP-variant 1 (construction in the dry). The difference is the density that is used, because the submerged density is used. In case of a free wall, the buckling height, depending on the y-value, is given in Figure 4-35. It should be kept in mind that the wall is only vertical for $y=0$. The red part is in case of printing under an angle larger than 45 degrees, the green part shows the result for a wall with an angle between 45 and 0 degrees. However, the order of the buckling height at the onset of printing does not differ from a vertical wall. Besides that, bending stresses become more important than buckling when the inclination increases.

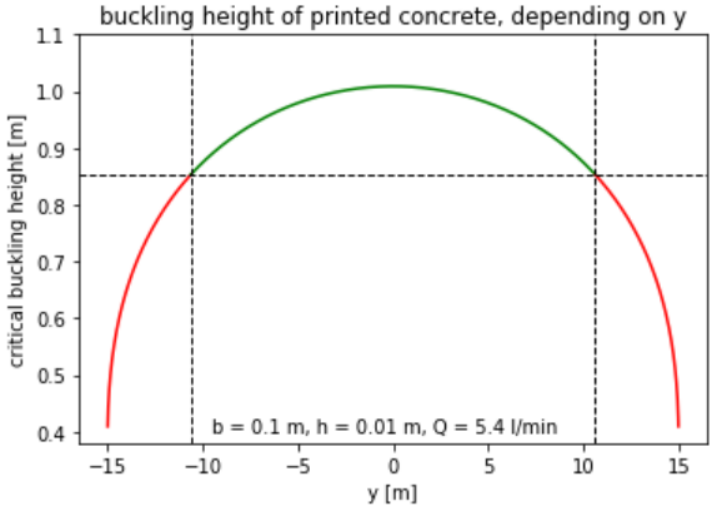

Figure 4-35 Buckling height of printed concrete, in case of submerged vertical printing. The critical buckling height depends on the y-value.

It follows that the buckling height for a free vertical wall, with these parameters, is 1.01 m.

Case 2: Simply supported or Fully-clamped wall

Also for this case, the same procedure is followed as for construction method 1. Instead of the normal density, the submerged density is applied. Again, as an estimation, part of the circle will be assumed to be straight with a maximum curvature of 10^{o}. The buckling length will be calculated for the two most interesting parameters: at the onset of printing (angle of 45^{o}, case 1) and at $y=0$ (case 2), where the wall is vertical.

The corresponding parameters for both cases are (note that for this case a larger pump rate is used, because the same pump rate as for free buckling results in a normalized curing rate which is outside the range of the design graphs):

Table 4-8 Parameters for both cases

Parameter	**Case 1**	**Case 2**
Q [m^3/s]	$1.53*10^{-4}$	$1.53*10^{-4}$
R [m]	10.6	15
b [m]	0.1	0.1
h [m]	0.01	0.01
v_n [m/s] (Q/(b*h))	0.153	0.153
T [s] $((\pi*2*R)/v_n)$	435	616
$\bar{w}$ [-]	12.41	17.57

The normalized buckling length for case 1 can be found using Figure 4-36.

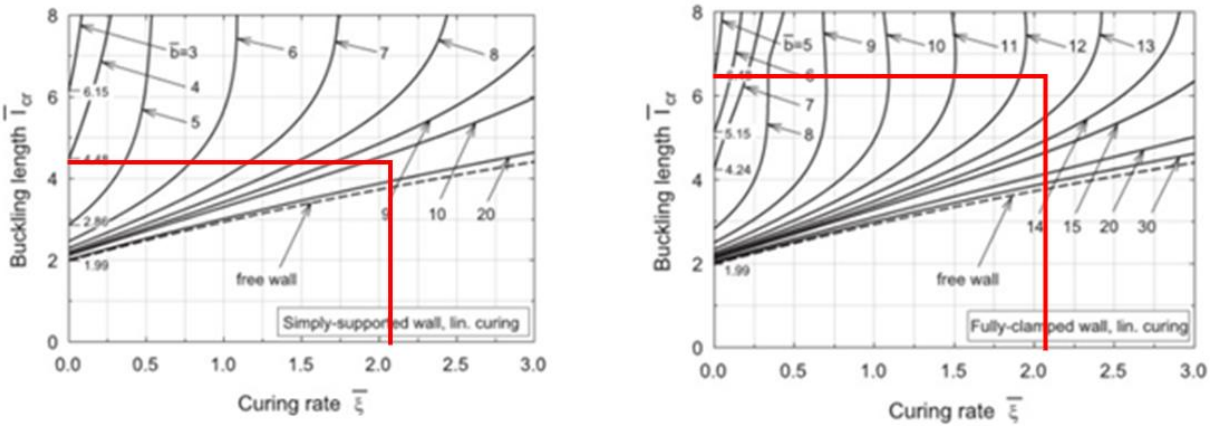

Figure 4-36 The normalized curing rate and normalized width gives the normalized buckling length l_{cr} in case of simply supported wall and fully-clamped wall. The parameters which define the curing rate and normalized width corresponds to the y-value corresponding to an angle of 45 ^{o}.

Then, the actual buckling length can be calculated, in case of simply supported and fully-clamped wall:

$$l_{cr,s-s} = \frac{\bar{l}_{cr}}{\left(\frac{\rho \cdot g \cdot b}{D_0}\right)^{\frac{1}{3}}} = \frac{4.4}{\left(\frac{2200 \cdot 9.81 \cdot 0.1}{7.152}\right)^{\frac{1}{3}}} = 0.65 \text{ [m]}$$

$$l_{cr,f-c} = \frac{\bar{l}_{cr}}{\left(\frac{\rho \cdot g \cdot b}{D_0}\right)^{\frac{1}{3}}} = \frac{6.5}{\left(\frac{2200 \cdot 9.81 \cdot 0.1}{7.152}\right)^{\frac{1}{3}}} = 0.98 \text{ [m]}$$

Thus: $0.65 < l_{cr} < 0.98$ [m]

The normalized buckling length for case 2 can be found using Figure 4-37.

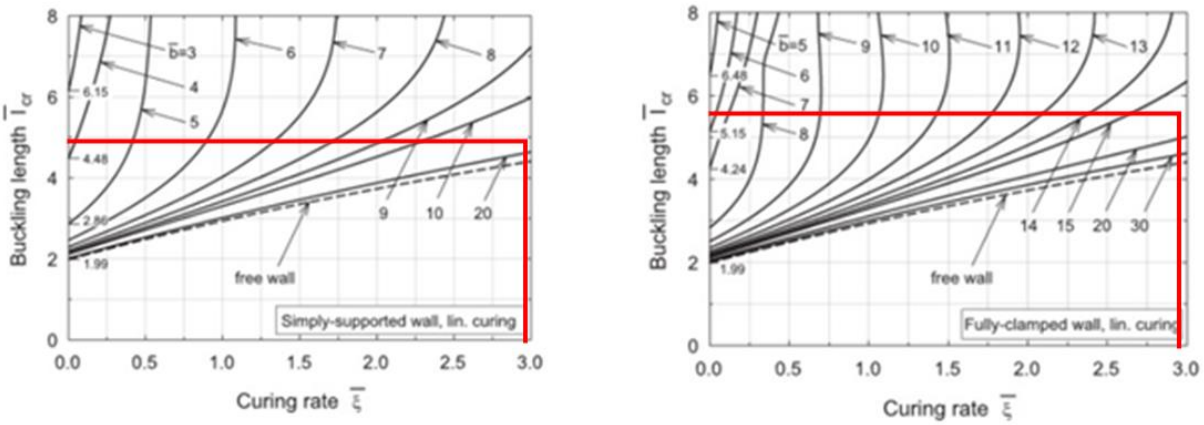

Figure 4-37 The normalized curing rate and normalized width gives the normalized buckling length l_{cr} in case of simply supported wall and fully-clamped wall. The parameters which define the curing rate and normalized width corresponds to the y-value corresponding to an angle of 0 ^{o} (y=0).

Then, the actual buckling length can be calculated, in case of simply supported and fully-clamped wall:

$$l_{cr,s-s} = \frac{\bar{l}_{cr}}{\left(\frac{\rho \cdot g \cdot b}{D_0}\right)^{\frac{1}{3}}} = \frac{4.9}{\left(\frac{2200 \cdot 9.81 \cdot 0.1}{7.152}\right)^{\frac{1}{3}}} = 0.72 \text{ [m]}$$

$$l_{cr,f-c} = \frac{\bar{l}_{cr}}{\left(\frac{\rho \cdot g \cdot b}{D_0}\right)^{\frac{1}{3}}} = \frac{5.6}{\left(\frac{2200 \cdot 9.81 \cdot 0.1}{7.152}\right)^{\frac{1}{3}}} = 0.83 \text{ [m]}$$

Thus: $0.72 < l_{cr} < 0.83$ [m]

Conclusion regarding maximum height h_2

The buckling behaviour of the printed formwork can be modelled best by a wall which is supported at the sides by a rotational stiffness. However, the model does not provide this and therefore, to be on the safe side, the value in case of a simply-supported wall will be used. Then, the maximum height h_2 of the formwork before the concrete is cast is 0.72 m. The buckling length in case of a vertical wall is used, because this gives the best estimate of what will happen in reality.

Verification of wall thickness and required concrete class

The condition in use phase is the same for the three 3DCP-construction variants which are investigated. From this it follows that the concrete class should be at least C60/75 (Section 4.3.2) and a wall-thickness of 2.5 m. The stresses in the sphere regarding this construction method are analysed at three different stages during construction: at 50%, 75% and 100%. This is depicted in Figure 4-38.

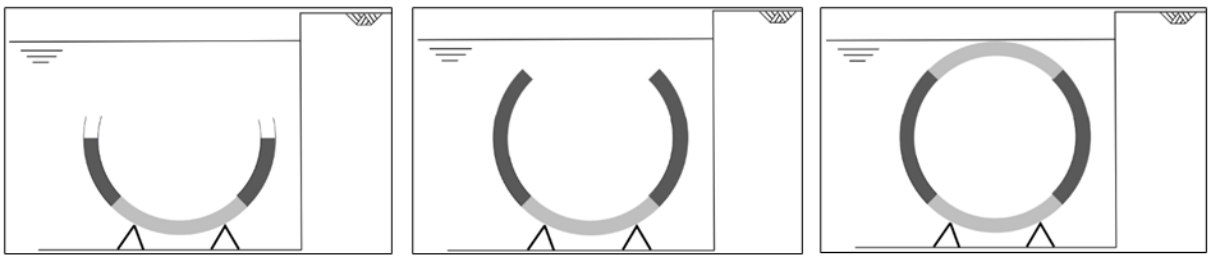

Figure 4-38 The stresses will be analysed at 3 different stages during construction: at 50%, 75% and 100%.

The method used is the same as for construction in the dry (Section 4.3.2), only the weight used is the submerged weight. The results can be found in Table 4-9. The results of the stresses in the entire sphere are given in Appendix H.

Table 4-9 Maximum stress results in the sphere at 3 stages of construction: at 50%, 75% and 100%. Local x-direction is radial direction, local y-direction is axial-direction.

Stress type	50%	75%	100%
$\sigma_{x,+}$ [N/mm^2]	$-0.162 < \sigma_{x,+} < 0.125$	$-0.290 < \sigma_{x,+} < 0.185$	$-0.345 < \sigma_{x,+} < 0.244$
$\sigma_{x,-}$ [N/mm^2]	$-0.348 < \sigma_{x,-} < 0.273$	$-0.625 < \sigma_{x,-} < 0.344$	$-0.743 < \sigma_{x,-} < 0.375$
$\sigma_{y,+}$ [N/mm^2]	$-0.268 < \sigma_{y,+} < 0.622$	$-0.623 < \sigma_{y,+} < 0.994$	$-0.754 < \sigma_{y,+} < 1.140$
$\sigma_{y,-}$ [N/mm^2]	$-0.755 < \sigma_{y,-} < 0.274$	$-1.367 < \sigma_{y,-} < 0.345$	$-1.658 < \sigma_{y,-} < 0.376$

Conclusion

The maximum compressive stress in the sphere is 1.658 MPa and the maximum tensile stress in the sphere is 1.140 MPa, both at 100% of construction. The compressive stress is lower than the design compressive strength of concrete C60/75 (f_{cd} = 32 MPa) and the tensile stress is lower than the design tensile strength of concrete 60/75 (f_{ctd} = 1.64 MPa). Therefore, there is no need for a higher concrete class; strength class C60/75 is sufficient for this construction method.

4.3.4. Verification of 3DCP + cast in place on pontoon

Determination of minimal height h_1 and h_2

Starting point for this construction method is that printing and casting is 'in the dry'. Therefore, plastic collapse and elastic buckling will be calculated emerged and is therefore the same as variant 1 (3DCP + cast in place, Section 4.3.2). This also holds for the calculation of plastic collapse. Therefore the values for h_1 (=0.2 m) and h_2 (=0.65 m) are the same for this construction method.

Verification of wall thickness and required concrete class

The condition in use phase is the same for the three 3DCP-construction variants which are investigated. From this it follows that the concrete class should be at least C60/75 (Section 4.3.2) and a wall-thickness of 2.5 m. The stresses in the sphere regarding this construction method are analysed at three different stages during construction: at 50%, 75% and 100%. This is depicted in Figure 4-39.

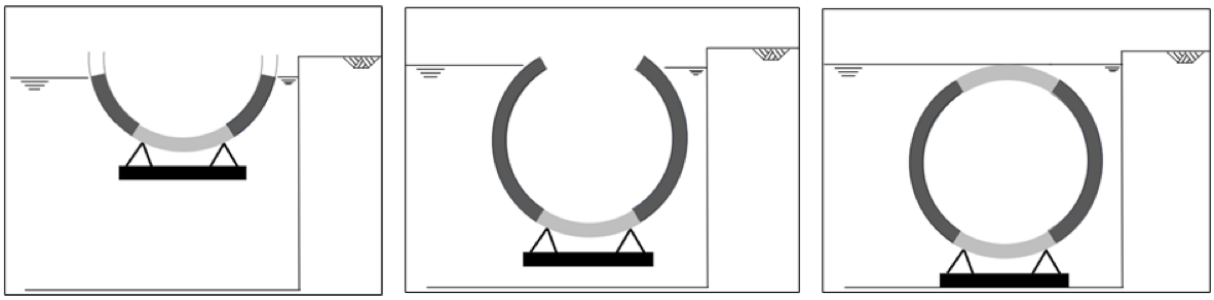

Figure 4-39 The stresses will be analysed at 3 different stages during construction: at 50%, 75% and 100%.

The difference between the loads in this case and in case of construction in the dry is the hydrostatic pressure at the outside of the sphere. This hydrostatic pressure will become larger when the draft becomes larger. The results of the stresses can be found in Table 4-10. The results of the stresses in the entire sphere are given in Appendix H.

Table 4-10 Maximum stress results in the sphere at 3 stages of construction: at 50%, 75% and 100%. Local x-direction is radial direction, local y-direction is axial-direction.

Stress type	50%	75%	100%
$\sigma_{x,+}$ [N/mm^2]	$-0.236 < \sigma_{x,+} < -0.043$	$-0.507 < \sigma_{x,+} < -0.178$	$-0.647 < \sigma_{x,+} < -0.155$

$\sigma_{x,-}$ [N/mm^2]	$-0.415 < \sigma_{x,-} < -0.046$	$-0.758 < \sigma_{x,-} < -0.120$	$-0.900 < \sigma_{x,-} < -0.072$
$\sigma_{y,+}$ [N/mm^2]	$-0.403 < \sigma_{y,+} < 0.000$	$-0.922 < \sigma_{y,+} < -0.001$	$-1.028 < \sigma_{y,+} < -0.154$
$\sigma_{y,-}$ [N/mm^2]	$-0.416 < \sigma_{y,-} < 0.023$	$-0.759 < \sigma_{y,-} < 0.084$	$-0.902 < \sigma_{y,-} < -0.072$

Conclusion
The maximum compressive stress in the sphere is 1.028 MPa at 100% of construction and the maximum tensile stress in the sphere is 0.084 MPa at 75% of construction. The compressive stress is lower than the design compressive strength of concrete C60/75 (f_{cd} = 32 MPa) and the tensile stress is lower than the design tensile strength of concrete C60/75 (f_{ctd} = 1.64 MPa). Therefore, there is no need for a higher concrete class; strength class C60/75 is sufficient for this construction method.

4.4. Selection of best 3DCP-construction method

To end up with the most promising 3DCP-construction method, the three 3DCP-construction methods will be evaluated based on the following evaluation criteria:

- Feasibility of construction method;
- Reliability of construction method;
- Required concrete class;
- Time span for casting concrete;
- Construction time.

Evaluation of 3DCP + cast in place

- Feasibility of construction method

Construction in the dry is the most commonly used construction method. Printing of concrete is done almost always in the dry and research is also mostly based on construction in the dry. Although concrete printing is not completely new, printing structures with dimensions as in this case are not performed yet. It will be a challenge to install a printer which is able to print the entire formwork, as this is not done yet.

- Reliability of construction method

Construction in the dry is a proven construction method and quality can be ensured which leads to a high reliability. However, 3DCP is an upcoming technology in the construction sector. Moreover, structures with these dimensions have not been printed before, because for large structures, they are made of different smaller printed elements. This is not preferred in this case, as this would be more sensitive to leakage due to seams.

- Required concrete class

Based on the conditions in the use-phase, the required concrete strength class is C60/75 in case a thickness of 2.5 m is applied. From the verification of construction stages it followed that for this construction method, there is no need for a higher strength class; C60/75 is sufficient.

- Time span for casting concrete

The minimal height of the formwork before concrete can be cast is 0.2 m (based on strength requirements) and the maximum height before the concrete should be cast is 0.65 m (based on stiffness requirements).

- Construction time

The printing time is 30.3 days for one sphere. The development of the tensile strength is the determining factor for this. Besides that, the bottom and top element should be made. The

construction time is therefore at least 31 days. It will also be a challenge to have a dry-dock with sufficient dimensions to construct a sphere and the number of spheres that could be built simultaneously depends on the dimensions of the dry-dock. This could negatively affect the construction time for multiple spheres.

Evaluation of submerged 3DCP + cast in place

- Feasibility of construction method

Submerged construction is used less than construction in the dry. Underwater concrete floors are an example of submerged construction, and therefore submerged casting concrete is feasible to a certain extend. However, it is unknown whether submerged concrete printing is feasible, especially for the spheres. When this is done in salty water, the instruments will be strongly affected which could lead to damage to the instruments.

- Reliability of construction method

For a submerged structure, it is more difficult to verify whether the structure has reached the desired quality. Besides that, the construction of underwater concrete floors show that it is a challenge to reach the desired quality. Besides that, it is yet unknown wat the properties are of fresh and hardened submerged printed concrete, resulting in a lower reliability.

- Required concrete class

Based on the conditions in the use-phase, the required concrete strength class is C60/75 in case a thickness of 2.5 m is applied. From the verification of construction stages it followed that for this construction method, concrete strength class C60/75 is sufficient.

- Time span for casting concrete

The minimal height of the formwork before concrete can be cast is 0.25 m (based on strength requirements) and the maximum height before the concrete should be cast is 0.72 m (based on stiffness requirements).

- Construction time

The printing time is 23.3 days for one sphere. The development of the tensile strength is the determining factor for this. Besides that, the bottom and top element should be made. The construction time is therefore at least 24 days. An advantage of this method is that the number of spheres that could be constructed simultaneously does not depend on the size of a dry-dock which positively affects the construction time for multiple spheres.

Evaluation of 3DCP + cast in place on a pontoon

- Feasibility of construction method

The construction of large platforms in Norway (e.g. Troll A) show that is possible to construct large structures on a pontoon. A particular challenge for this case is the printer which should be build on the pontoon to print the formwork. A continuous transport of concrete, both for printing and casting is required, which will be a challenge.

- Reliability of construction method

Printing and casting will always be in the dry in this case. This does not differ from entire construction in the dry. However, due to the increasing weight the sphere will sink. It could be that the printed concrete, which is not yet complete hardened, can be attacked by the water at the outside and/or is not complete watertight. This should be monitored to achieve high reliability.

- Required concrete class

Based on the conditions in the use-phase, the required concrete strength class is C60/75 in case a thickness of 2.5 m is applied. From the verification of construction stages it followed that for this construction method, concrete strength class C60/75 is sufficient.

- Time span for casting concrete

The minimal height of the formwork before concrete can be cast is 0.2 m (based on strength requirements) and the maximum height before the concrete should be cast is 0.65 m (based on stiffness requirements).

- Construction time

The printing time is 30.3 days for one sphere. The development of the tensile strength is the determining factor for this. Besides that, the bottom and top element should be made. The construction time is therefore at least 31 days. An advantage of this method is that the number of spheres that could be constructed simultaneously does not depend on the size of a dry-dock which positively affects the construction time for multiple spheres.

Conclusion

The score of the evaluation criteria regarding construction with 3DCP for each construction method is given in Table 4-11. Feasibility and reliability are weighed with a factor 2, the other criteria with a factor 1. This is because it is most important that there is a feasible and reliable solution to construct the spheres.

Table 4-11 Score of different 3DCP construction methods based on evaluation criteria.

	3DCP + cast in place		**3DCP + cast in place submerged**		**3DCP + cast in place on pontoon**	
Feasibility	4	8	2	4	3	6
Reliability	5	10	2	4	4	8
Strength class	2	2	2	2	2	2
Time span for casting	4	4	5	5	4	4
Construction time	3	3	5	5	4	4
Total		27		20		24

It can be concluded that, based on the scores for the evaluation criteria, that 3DCP + cast in place in the dry has the highest potential to come to an optimal and scalable design. Therefore, this construction method is advised to use.

5. Verifying the suitability of unreinforced concrete, based on crack width and watertightness

In this chapter, an estimation of the increase of concrete temperature, based on hydration heat, is made for different cement compositions. By doing so, the impact of the different cement composition on the temperature of concrete is shown (Section 5.1). Combining the temperature differences and the expansion coefficient, thermal shrinkage can be calculated. The concrete temperature at the edges, influenced by the (lower) surrounding temperature, is lower than the temperature inside the concrete, which results in differential shrinkage and thus cracking. Thermal shrinkage, as well as the (infinite) drying and autogenous shrinkage, are given in Section 5.2. The consequences regarding watertightness are also given in Section 5.2. This chapter is based on the preferred 3DCP-variant, construction in the dry. The focus is on tensile stresses due to thermal shrinkage. This is based on an adiabatic temperature increase, which will not differ for the different 3DCP-variants discussed in Section 4.3.

5.1. Calculation of adiabatic temperature increase based on different concrete mixtures

When cement reacts with water, heat is released. This results in warming of the concrete. In case the heat at the edges is released into the environment, temperature differences will develop between the centre and the edge(s) of the structure. This results in differential shrinkage which may cause cracking. In case no reinforcement is used, crack width cannot be controlled. It is therefore required that there are no cracks in the unreinforced concrete.

This temperature increase is calculated with an adiabatic calculation, which gives an conservative estimate of the temperature increase. In reality, the temperature increase is semi-adiabatic, which means that part of the heat is released into the environment, resulting in a lower temperature increase. A semi-adiabatic process would require an complex calculation process, which is outside the scope of this thesis. The adiabatic approach assumes that all the heat that is released from the chemical reaction of the cement constituents with water, results in warming of the concrete; no heat is lost into the environment. This is depicted in Figure 5-1.

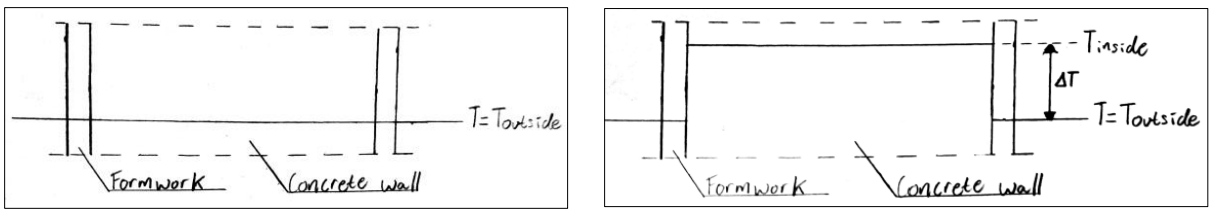

Figure 5-1 Temperature at inside and outside at start of casting concrete (left) and temperature inside and outside after the heat is released from the chemical reaction (right), resulting in a temperature difference.

An estimation of the temperature inside the concrete can be made with the hydration kinetics of different cement types. In this report, the ASTM classification is used. The hydration heat and temperature of the concrete over time will be calculated for type I to V to see their difference.

- Type I is used for general purpose. This one is calculated to see the difference between type I and the other cement types;
- Type II is used in case moderate sulphate resistance is required. As the spheres will be placed at the seabed, they are constantly in seawater (which is the reason why the spheres are also classified as XS2);
- Type III is used to gain high early strength. A higher early strength will sooner reduce the load on the formwork;
- Type IV is used in cases that low heat is desired and is therefore often used in thick-walled structures. Therefore this type will be calculated too;
- Type V is used when the concrete should be sulphate resistant. This type will be calculated to see the difference in temperature increase between type II and V.

The average composition of ASTM1 to ASTM5 is given in Table 5-1.

Table 5-1 Average composition of Portland cement types (Young, 2001).

ASTM type	Description	C_3S [%]	C_2S [%]	C_3A [%]	C_4AF [%]
I	General purpose	55	17	10	7
II	Moderate sulphate resistant	55	20	6	10
III	High early strength	55	17	9	8
IV	Low Heat cement	35	40	4	12
V	Sulphate resistant	55	20	4	12

The hydration kinetics of the main four constituents of cement are given in Figure 5-2.

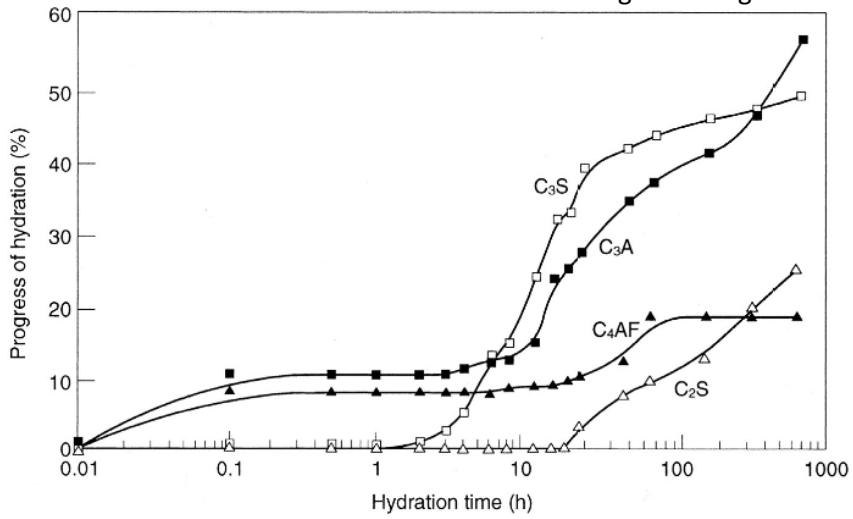

Figure 5-2 Hydration kinetics of ordinary Portland cement (Hewlett & Liska, 2017).

In Table 5-2, the degree of hydration (%) is given for the main four constituents, at time t after hydration is started (related to Figure 5-2).

Table 5-2 Degree of hydration of Bogues constituents at time t, derived from Figure 5-2.

constituent \ time (hr)	0.01	0.1	1	2	5	10	20	50	100	200	500
C_3S [%]	0	0	0	1	10	21	38	43	47	48	49
C_2S [%]	0	0	0	0	0	0	4	9	12	16	24
C_3A [%]	1	9	10	10	12	15	28	37	40	42	52
C_4AF [%]	0	7	8	8	8	9	11	18	20	20	20

With the degree of hydration, hydration heat of constituents (given in Section 2.3) and composition of the cement types, the temperature of the concrete at time t can be calculated. An example is shown for t=0.1 hr. The following parameters are used:

- ASTM type 1
- 1 m^3 of concrete
- c = specific heat = 900 J/(kg*^{o}C)
- C = cement content = 350 kg/m^3
- ρ = 2300 kg/m^3

$$\Delta T_{t=0.1} =$$

$$\frac{0.55 \cdot \alpha_{C_3S} \cdot 500 \cdot 10^3 + 0.17 \cdot \alpha_{C_2S} \cdot 260 \cdot 10^3 + 0.10 \cdot \alpha_{C_3A} \cdot 865 \cdot 10^3 + 0.07 \cdot \alpha_{C_4AF} \cdot 420 \cdot 10^3}{c} \cdot \frac{C}{\rho}$$

$$= \frac{0.55 \cdot 0 \cdot 500 \cdot 10^3 + 0.17 \cdot 0 \cdot 260 \cdot 10^3 + 0.10 \cdot 0.09 \cdot 865 \cdot 10^3 + 0.07 \cdot 0.07 \cdot 420 \cdot 10^3}{900} \cdot \frac{C}{\rho} = 1.66\ ^0\text{C}$$

The complete result for all cement types is given in Figure 5-3. This is calculated with Python, the script can be found in Appendix J.

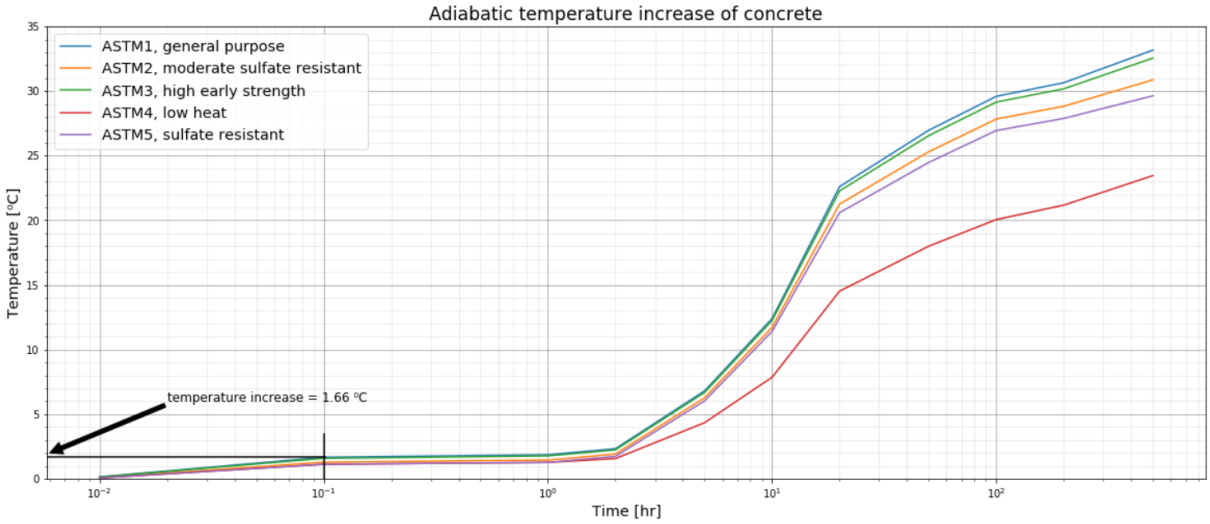

Figure 5-3 Adiabatic temperature increase of concrete, ASTM types I to V.

It can be seen that the temperature increase of the low heat cement is significantly lower than the other types of cement. Besides that, it is interesting to see that the difference in temperature increase between ASTM2 and ASTM5 is really small.

5.2. Verification of suitability of unreinforced concrete

Differential thermal shrinkage leads to tensile stresses and cracks will develop in case the tensile stresses become larger than the tensile strength of the concrete. In case of the spheres, the aim is to use unreinforced concrete. Consequently, when cracks develop, they are not controlled anymore. It is therefore important to verify whether the tensile stresses will become larger than the tensile strength of unreinforced concrete. This is done based on the thermal shrinkage, infinite drying shrinkage and infinite autogenous shrinkage.

Calculation of thermal shrinkage
The temperature at the outer side of the sphere is the temperature of the surrounding (variant 1) or from the water (variant 2 & 3). As lowest temperature, 5 ^{o}C is used for both the surrounding temperature and water temperature. Lower temperatures may occur in winter, but then the spheres will not be constructed.

The thermal expansion coefficient for concrete is 10*10^{-6} / ^{o}C. Then, the maximum tensile stresses due to the temperature difference are calculated as follows (C60/75 is used in this calculated, resulting in E_{cm} = 39000 MPa):

$$\sigma_t = \varepsilon \cdot E_{cm} = \alpha_c \cdot \Delta T \cdot E_{cm} = 10 \cdot 10^{-6} \cdot \Delta T \cdot 39000 \quad (5\text{-}1)$$

Calculation of drying shrinkage and autogenous shrinkage
Drying shrinkage and autogenous shrinkage are both described in Eurocode 2 (EN 1992, 2011). These two components both depend on time: drying shrinkage develops slowly and ranges from days to months, whereas autogenous shrinkage is linearly linked to the hardening of the concrete, which is mostly in the first days.

The initial drying shrinkage can be determined with Table 5-3. In this case, the sphere is submerged so the relative humidity is high. As starting point, relative humidity of 90% is chosen. Because the lowest required concrete class is C35/45, this is used as initial input.

Table 5-3 Value of the nominal unrestricted drying shrinkage of concrete with cement CEM and class N [in $^{0}/_{00}$]

$f_{ck}/f_{ck,cube}$ (MPa)	Relatieve vochtigheid ($^{0}/_{0}$)					
	20	40	60	80	90	100
20/25	0.62	0.58	0.49	0.30	0.17	0.00
40/50	0.48	0.46	0.38	0.24	0.13	0.00
60/75	0.38	0.36	0.30	0.19	0.10	0.00
80/95	0.30	0.28	0.24	0.15	0.08	0.00
90/105	0.27	0.25	0.21	0.13	0.07	0.00

If 1 meter length is used, and the wall thickness is 2.5 m, the total shrinkage equals (entire calculation can be found in Appendix I):

$$\varepsilon_{cd,\infty} = k_h \cdot \varepsilon_{cd,0} = 0.7 \cdot \ 0.13 \cdot 10^{-3} = 9.1 \cdot 10^{-5}$$

$$\varepsilon_{ca,\infty} = 2.5 \cdot (f_{ck} - 10) \cdot 10^{-6} = 2.5 \cdot (35 - 10) \cdot 10^{-6} = 6.25 \cdot 10^{-5}$$

$$\varepsilon_{cs,\infty} = \varepsilon_{cd,\infty} + \varepsilon_{ca,\infty} = 1.535 \cdot 10^{-4}$$

From this, it can be concluded that the thermal shrinkage is three times larger than the sum of the autogenous and drying shrinkage. In this report, autogenous and drying shrinkage are therefore not considered anymore, because thermal shrinkage is much more important.

Crack width

As a starting point, it is assumed that the initial temperature of the concrete is 20 ^{o}C. Then, the maximum temperature difference (considering a surrounding temperature of 5 ^{o}C) leads to the maximum tensile stresses given in Table 5-4 for each cement type.

Table 5-4 Maximum tensile stresses, in case of adiabatic temperature increase.

Cement type	**ASTM 1**	**ASTM 2**	**ASTM 3**	**ASTM 4**	**ASTM 5**
ΔT_{max} [^{o}C]	48.1	46.0	47.6	38.5	44.8
Max tensile stress [N/mm^2]	18.8	17.9	18.6	15.0	17.5

The stresses due to thermal shrinkage are higher than the tensile strength of concrete with strength class C60/75 (f_{ctd} = 1.64 MPa, with α_{ct} = 0.8), resulting in cracking. In case no reinforcement is added, the concrete will crack when the tensile strength is exceeded and the cracks cannot be controlled anymore.

Semi-adiabatic conditions

There are two important aspects which may result in tensile stresses due to thermal cracking which are lower than in case of a adiabatic approach. First of all, the printed formwork acts as insulation. this causes a larger temperature of the concrete at the edges, which lowers the temperature differences between the edge and the centre of the wall (depicted in Figure 5-4).

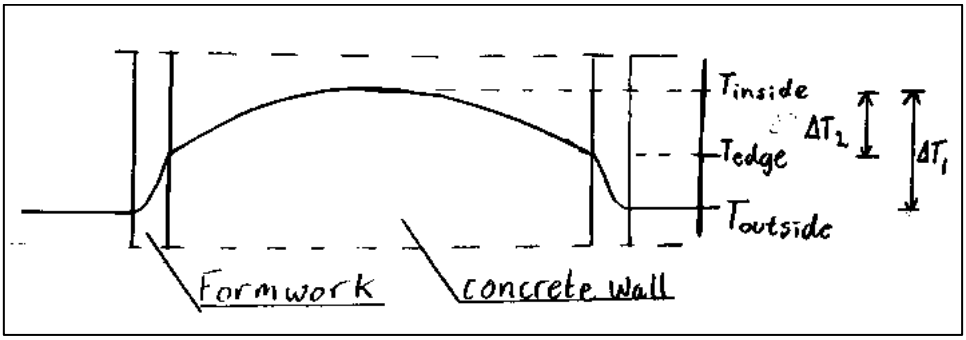

Figure 5-4 The temperature difference ΔT_1 is smaller than ΔT_2, because the printed formwork will act as insulation (to a certain extent).

Secondly, the vertical construction rate determines how much heat may be released into the environment, which lowers the temperature of the concrete. This is a semi-adiabatic approach. Because the vertical construction rate is less than 0.5 m/day, heat is also released on top of the structure (Figure 5-5). As can be seen in Figure 5-3, the temperature increase is maximum between 2 and 20 hours. This may result in a significant amount of heat that is released into the environment, resulting in a much lower concrete temperature.

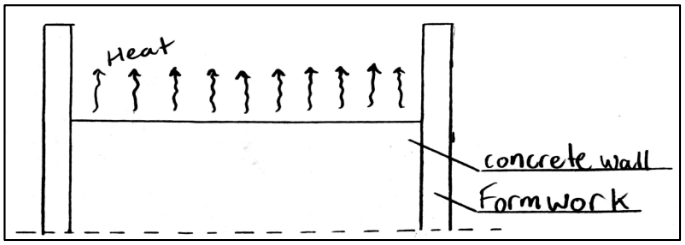

Figure 5-5 Hydration heat is released on top.

Potential solutions to lower thermal shrinkage

The total shrinkage results in stresses that are higher than the strength of the concrete and therefore cracks will occur. In case no reinforcement is added (which is aimed in this case), the crack width cannot be controlled. This should be avoided and therefore, measures should be taken to lower the shrinkage. These measures can be divided in two groups: changing the concrete mixture and without changing the concrete mixture.

Measures regarding the concrete mix

- Accelerators can be used in order to reach a larger hydration rate sooner after casting the concrete. In that case, more heat is released in the same time. Due to the small vertical growth, more heat will be released into the environment which reduces the temperature differences at the end, resulting in less shrinkage.
- More cement should be replaced by other binders, which result in lower heat release when the binders hydrate. This lowers the temperature of the concrete.
- A higher initial concrete temperature could lead to a lower maximum temperature than for a lower initial concrete temperature. This is because the hydration rate will be larger in case of a higher initial temperature, through which more heat is released into the environment.

Measures besides mixture changes

- An insulation layer could be used to avoid large temperature differences between the edge and the centre of the concrete. The insulation layer should be used long enough, to avoid a thermal 'shock'. If the insulation layer is removed too early, the concrete will still crack.
- The concrete can be cooled with cooling pipes. These pipes should be installed in the formwork (Figure 2-10). Water flows through these pipes when the concrete is cast, which leads to lower temperatures locally, because the heat is taken by the water. These pipes should be installed manually during construction, which costs labour.
- Another option is to add liquid nitrogen to the concrete mixture. Nitrogen converts from liquid to gas when the temperature is -196 °C. The heat that is used for this transition is coming from the hydration heat. This concept is also applied for construction of inclined walls in the Callandtunnel (Kruizenga, Zegwaard, & Obladen, 2003). This lowers the initial temperature and lowers the maximum temperature (Figure 5-6).

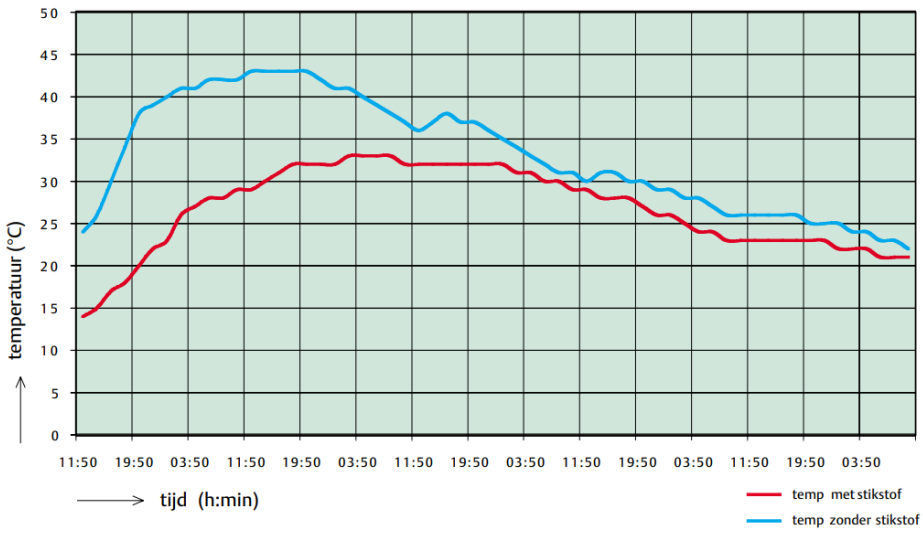

Figure 5-6 Temperature increase without added nitrogen (blue line) and with added nitrogen (red line) in the Callandtunnel (Kruizenga, Zegwaard, & Obladen, 2003)

It is important to add enough nitrogen, to avoid that the temperature increases when the nitrogen does not influences the temperature anymore. It is also important that the concrete should be mixed continuously when the nitrogen is added to avoid freezing of the concrete.

- The method of adding nitrogen could be optimised by constructing the spheres when the environmental temperature is higher, which lead to a smaller temperature differences between the edge and the centre of the concrete.

Consequences regarding watertightness

The requirement regarding watertightness is that the crack width should not be larger than 0.05 mm. In case unreinforced concrete is used, the tensile stress must be lower than the tensile strength. In cast that is not possible, reinforced concrete or fibre-reinforced concrete should be used. In that case, the crack width should be controlled by the reinforcement, in order to have a maximum crack width of 0.05 mm. Another option could be to use a sheet cover all around the sphere, to reach the desired watertightness.

6. Discussion of assumptions made during the design

This chapter gives an overview of the impact of choices that haven been made throughout the report. Examples of choices are calculations based on experimental measurements instead of design values, the applicability of Suiker's model to predict the critical buckling height and the setting time of concrete.

- In Section 2.1, three models are given regarding the strength development of 3DCP. The applicability of the models depend at which timescale the strength increase will be verified. The model of Perrot fits best for the purpose used in this report. The equation of Perrot is based on experimental values and is therefore not a design value, as the experimental values show a certain spreading, as can be seen in Figure 6-1.

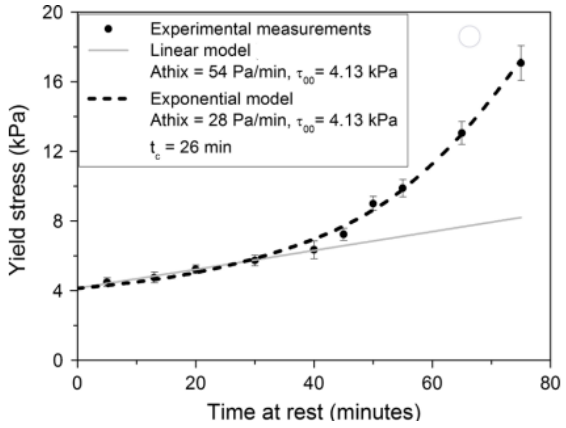

Figure 6-1 Exponential model of Perrot through experimental measurements (Perrot, Rangeard, & Pierre, 2016).

A design fit or 'design equation' would give lower values for the yield stress at the same time. In case this would be used, the strength increase is slower, which will decrease the maximum print rate which increases the construction time.

- The same as for the strength increase holds for the increase of stiffness, which is used to calculate the critical buckling height. As can be seen in Figure 6-2, the dashed line is fitted through the experimental data. This gives a value of 0.0026/s for the curing rate of the stiffness. In case the red (fictitious) design value would be used for the curing rate of stiffness, the value would be 0.000076/s.

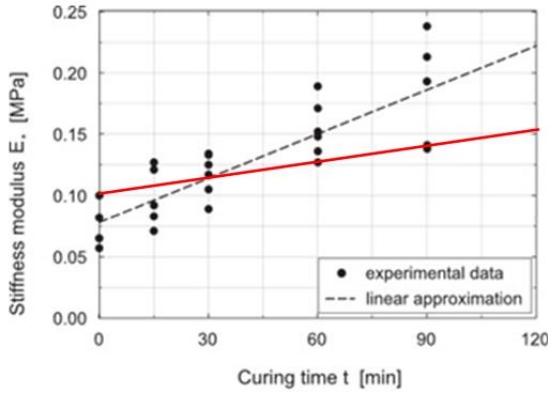

Figure 6-2 Curing rate stiffness based on experiments (black dashed line) and fictitious design curing rate of stiffness (red line).

A lower curing rate of stiffness influences the critical buckling height. In case of a free wall, the critical buckling height decreases from 0.85 m to 0.51 m (reduction of 40%), in case of a simply-supported wall the critical buckling height decreases from 0.65 m to 0.43 m (reduction of 34%) and in case of a fully clamped wall the critical buckling height decreases from 0.70 m to 0.48 m (reduction of 32%). This is significantly lower than the characteristic values that have been used to calculate the maximum height of the formwork h_2. Although this is significantly lower, it will not be a problem, because the minimal height h_1 is still lower than h_2.

- The development of the tensile strength of 3DCP is unknown at this stage. Therefore, the relationship of conventional concrete is used. In case of conventional concrete, the tensile design strength is a factor 11 lower in case of concrete class C12/15 and a factor 24 in case of concrete class C80/95. In the design, a factor 15 is used to estimate the tensile strength of 3DCP. However, in case higher strength classes are used for 3DCP, this could be an underestimation. A slower print rate would be required to ensure that the printed formwork will not collapse.

Symbol	Description	C12/15	C16/20	C20/25	C25/30	C30/37	C35/45	C40/50	C45/55	C50/60	C55/67	C60/75	C70/85	C80/95	C90/105
f_{cd} (MPa) (for α_{cc}=1.00)	Design compressive strength (for α_{cc}=1.00)	8.00	10.67	13.33	16.67	20.00	23.33	26.67	30.00	33.33	36.67	40.00	46.67	53.33	60.00
f_{ctd} (MPa) (for α_{ct}=1.00)	Design tensile strength (for α_{ct}=1.00)	0.73	0.89	1.03	1.20	1.35	1.50	1.64	1.77	1.90	1.97	2.03	2.15	2.26	2.35

Figure 6-3 Design compressive strength and design tensile strength of concrete strength classes.

- The model from Suiker to calculate the critical buckling height is based on a vertical wall. However, in case of the sphere, printing is only vertical at the middle of the sphere. This is important to realize when the buckling height is calculated at the onset of printing, at 45°. The values that are found are slightly lower than the values for the vertical wall at the middle of the sphere. This is due to the smaller diameter, through which the lowest printed layer has gained less stiffness in the same time as the interlayer time is smaller and thus the vertical growth higher.

  However, the stresses due to eccentricity of the layers on top are more important at the onset of casting than the buckling height. When the formwork approaches the middle of the sphere, the angle becomes smaller and buckling becomes more important, but then the calculated values in case of a vertical wall becomes more accurate.

  The critical buckling height of the simply-supported wall is used to determine the maximum height of the formwork h_2. However, a section of the wall of the sphere can be modelled as a

wall with a support that has a certain rotational stiffness. Therefore, the critical height h_2 is a conservative estimation. Besides that, there is a factor of safety of 20% in the model itself (Suiker, 2018).

- The print rate that is used to calculate the critical buckling height in case the wall is simply-supported or fully clamped, is higher than the maximum print rate that follows from the strength requirement. For example, the maximum print rate for variant 1 (3DCP + cast in place in the dry) is 4.2 l/min (= $7*10^{-5}$ m^3/s), see Figure 4-15. If this print rate would be used, the normalized curing rate of the stiffness would be 5.26 (in case the parameters belonging to the middle of the sphere are used). In that case, it is assumed that the buckling height (both normalized and actual) are higher in reality. However, this is outside the range of the design graphs that are used to determine the buckling height, see Figure 6-4. The print rate that is used is chosen such that a comparison could be made for the different variants, based on the same print rate. It follows that this is 9.2 l/min (= $1.5*10^{-4}$ m^3/s).

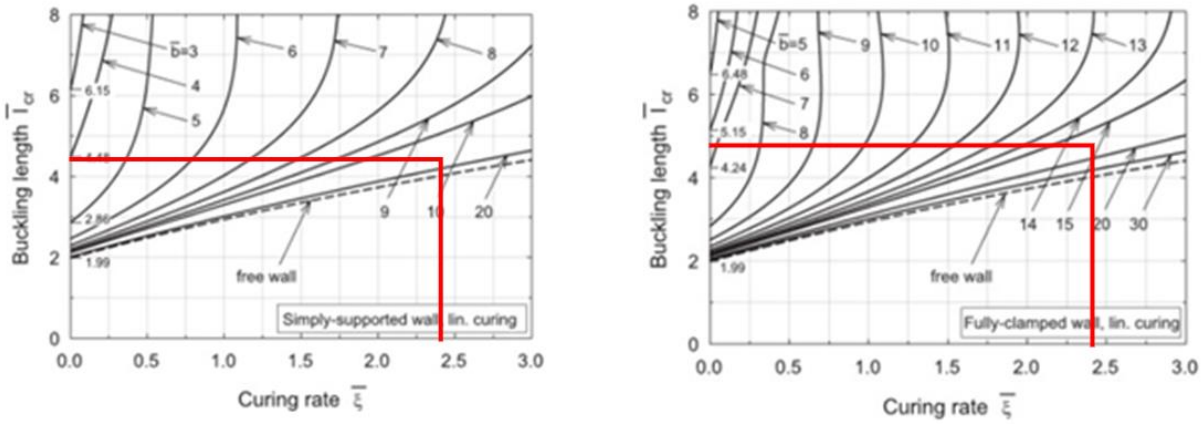

Figure 6-4 Design graphs used to determine the normalized buckling height. The normalized curing rate ranges from 0 to 3 (Suiker, 2018). In this case, the values for the middle of the sphere are used, in case of construction in the dry.

- The model that is used to calculate the buckling height is based on a straight wall. However, in case of the spheres, the wall is curved. The width (w) of the wall is assumed to be straight with a curvature of 10°, see Figure 6-5.

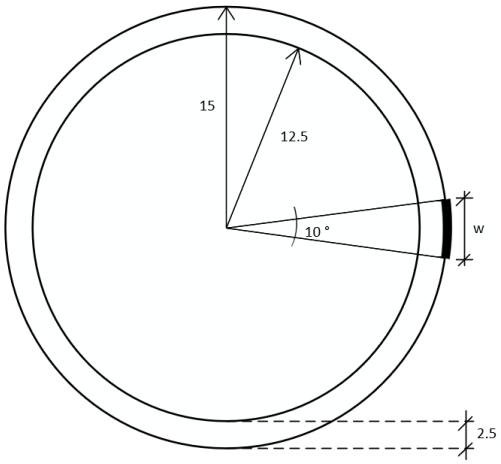

Figure 6-5 A cross-section is given at the middle of the sphere. Part of the sphere is assumed to be straight with a curvature of 10°.

A smaller curvature (smaller angle) would result in a better approximation of a straight wall. However, in that case, the combination of the normalized width and the normalized curing

rate of stiffness is outside the range of the design graphs that are used (Figure 6-6). A larger curvature than 10° would give a poorer approximation.

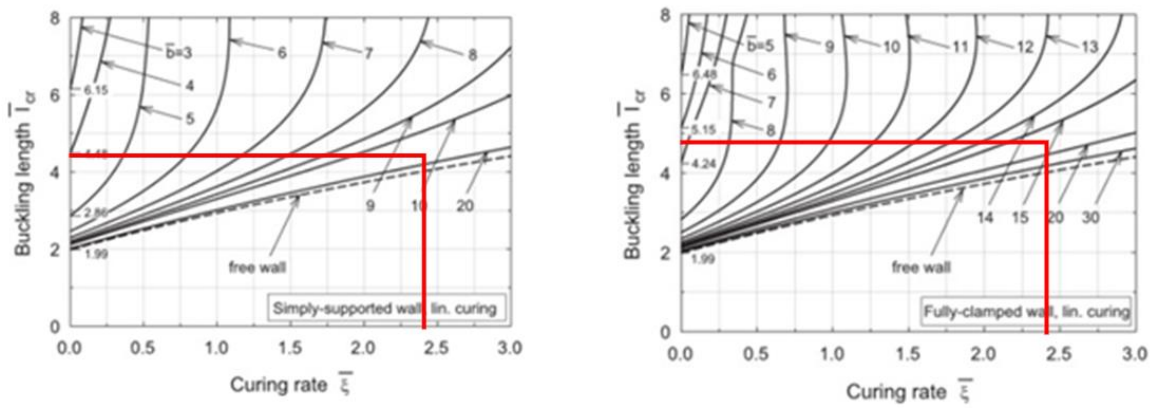

Figure 6-6 A smaller normalized width, combined with the same normalized curing rate, is outside the range of the design graphs.

- An important assumption that is made in case of submerged printing and casting (2nd 3DCP-variant) is that the only difference is the submerged weight of the concrete. It is unknown whether the strength development of the printed concrete is the same as in case it is printed in the dry. It this would be slower, the construction time increases and if this would be faster, the construction time decreases. Besides that, the submerged weight is also used to calculate the critical buckling height. In case the strength increase is slower, the critical buckling height will also decrease, resulting in a lower maximum value for h_2.

- The minimum height h_1 of the formwork before the concrete can be cast, depends on the load of the fresh concrete onto the formwork. In this thesis, the stress is calculated based on a concrete mix with a consistency class F6 and a setting time of 20 hours. A different consistency class would not influence the maximum load onto the formwork in this case. However, in case the setting time would be smaller, the maximum load on the formwork is smaller, which leads to a lower minimum height h_1. A faster setting time can generally be reached with a lower w/c ratio.

7. Conclusions and recommendations

In this chapter, the main conclusions and several recommendations are given. First, in Section 7.1, the sub-research questions are answered, in order to answer the main research question. Several recommendations for further design optimisation and further research are given in Section 7.2

7.1. Conclusions

The conclusions will be given based on the research questions. To answer the main question, first the sub-research questions will be answered.

Sub-research question 1

- *Does the best construction method make use of 3DCP?*

In Chapter 4, five different construction methods are described, of which two 3DCP-construction methods. Besides 3DCP-methods, conventional casting, slip/jump forming and prefab are investigated. The result of the scores on the evaluation criteria is given in Table 7-1. The first 3DCP is printing the entire sphere, the second one is printing the formwork, in between which the concrete is cast.

Table 7-1 Scores for main construction method based on 5 evaluation criteria. Scores regarding ease of construction, construction time and costs are based on personal communication (A. van Dalfsen, personal communication, April 19, 2022).

	3DCP + cast in place	Fully printed	Slip/jump forming	Conventional casting	prefab
Ease of construction	+	+	-	-	+
Construction time	+	-	+	+	+
Costs	+	+	-	-	+
Scalability	++	++	-	--	-
Watertightness	++	+	+	+	-

Based on a qualitative comparison, the 3DCP-variant in which 3DCP is used to print the formwork has the highest score and is therefore used for the design. The bottom and top element are made from prefab elements, because the maximum inclination for printing is 45°.

Sub-research question 2

- *How can 3DCP be used in an optimal way to construct the spheres?*

Based on the best 3DCP-construction method, 3 different variants are investigated: construction in the dry, submerged construction and construction on a pontoon. These 3 variants are evaluated based on feasibility, reliability, required concrete strength class, time span for casting and construction time.

The minimum height of the printed formwork (h_1) before the concrete can be cast is based on the strength and stress in the formwork, in which the self-weight of the formwork and the load of the fresh concrete are taken into account. It follows that:

- Construction in the dry: $h_1 = 0.20$ m
- Submerged construction: $h_1 = 0.25$ m
- Construction on pontoon: $h_1 = 0.20$ m

The maximum free height (h_2) of the formwork before the concrete should be cast is based on elastic buckling of the formwork with a model from Suiker. Although there are some limitations for the use

of the model for the printed formwork, an estimation is given. It follows that the maximum free height of the formwork before the concrete should be cast is as follows:

- Construction in the dry: h_2 = 0.65 m
- Submerged construction: h_2 = 0.72 m
- Construction on pontoon: h_2 = 0.65 m

It is required that the sphere is buoyant, to enable transport of the spheres. From this, it followed that the maximum thickness is limited to 2.5 m. From this requirement, it follows that the required concrete class for construction in the dry is C60/75. This required concrete strength class is sufficient regarding construction for variant 1, 2 and 3. The choice is made based on evaluation criteria, given in Table 7-2.

Table 7-2 Scores for different 3DCP methods

	3DCP + cast in place		**3DCP + cast in place submerged**		**3DCP + cast in place on pontoon**	
Feasibility	4	8	2	4	3	6
Reliability	5	10	2	4	4	8
Strength class	2	2	2	2	2	2
Time span for casting	4	4	5	5	4	4
Construction time	3	3	5	5	4	4
Total		27		20		24

As a final answer to the sub-question: The best method to use 3DCP for construction of the spheres is to use 3DCP and cast in place, in the dry.

Sub-research question 3

- *Is it possible to use unreinforced concrete for the spheres?*

The verification of the suitability of unreinforced concrete is based on the tensile stresses in the concrete that will develop due to shrinkage. A distinction is made between thermal shrinkage, autogenous shrinkage and drying shrinkage, from which thermal shrinkage is evaluated in more detail. The maximum temperature differences between the outside and the centre of the wall (leading to differential shrinkage) are calculated based on different cement compositions. The result is given in Table 7-3.

Table 7-3 Maximum tensile stresses, in case of adiabatic temperature increase

Cement type	**ASTM 1**	**ASTM 2**	**ASTM 3**	**ASTM 4**	**ASTM 5**
ΔT_{max} [°C]	48.1	46.0	47.6	38.5	44.8
Max tensile stress [N/mm^2]	18.8	17.9	18.6	15.0	17.5

It is important to note that these values are in case of fully adiabatic conditions. In reality, the temperature increase is semi-adiabatic, which leads to lower temperature differences and lower tensile stresses. However, to use unreinforced concrete, it should be sure that the tensile strength is not exceeded. It is therefore required to do further investigation into the thermal shrinkage, before unreinforced concrete is used.

Main research question

The main research question is as follows:

- *How does the optimal design of a concrete sphere, that will be used for energy storage at large water depth, look like?*

It is concluded that 3D Concrete Printing can be used best to construct the formwork. The formwork consists of an printed outer and printed inner shell, in between which the concrete can be cast conventionally. The best way to do this is in the dry. A disadvantage of this construction method is the maximum inclination that can be printed. In this thesis, a maximum inclination angle of 45° is used. The bottom and top part could be made of prefab elements. The construction sequence is as follows:

- Building and installation of temporary concrete factory on site;
- Building and installation of 3D concrete printer in a dry dock;
- Printing outer and inner shell;
- After a time step, simultaneously casting concrete in between the outer and inner shell. The free height of the formwork should be between h_1 (0.2 m) and h_2 (0.65 m);
- Prefab bottom and top element, which will be placed with a crane. It is important that the seams are injected to ensure watertightness;
- Inundation of dry dock and transport of spheres to installation site.

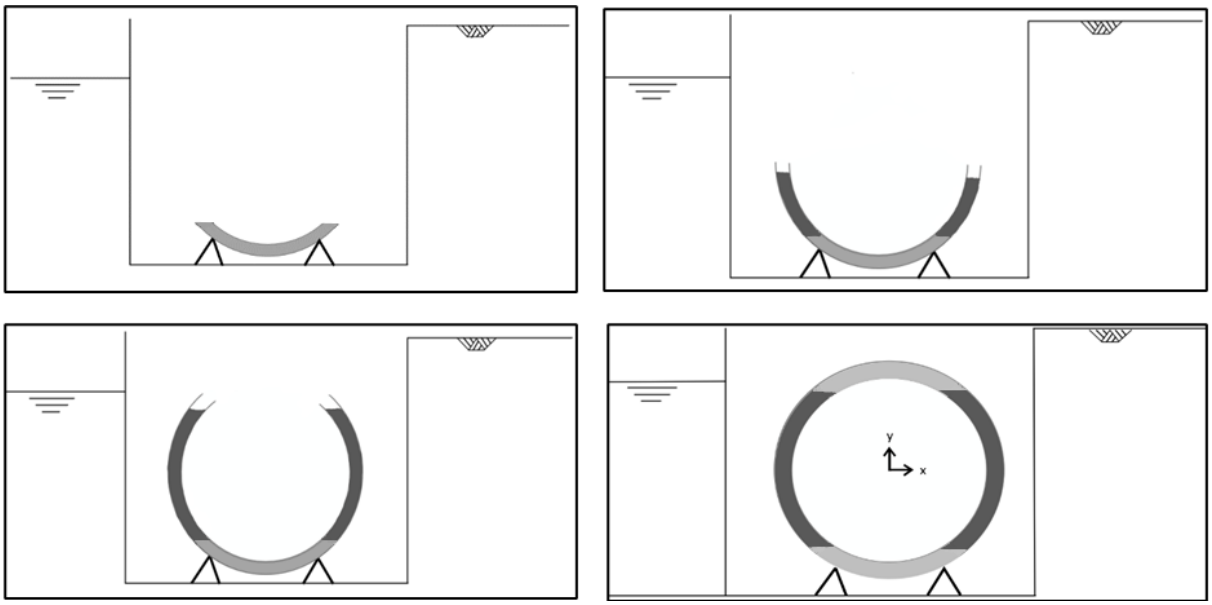

Figure 7-1 Construction sequence of the spheres with construction in a dry dock. The bottom and top element are prefab (light grey).

7.2. Recommendations

In this section, recommendations are given for further design optimisations and further research. In particular, recommendations regarding the suitability of unreinforced concrete are given, because this is a critical factor in the design at this stage.

Recommendations for design optimisation:

- The construction time of one sphere is now based on the maximum print speed at 45°, thus at the onset of printing. This is based on the increase of strength and stress of the lowest layer. The bending moment of an second layer on a layer below is the largest at the onset of printing, but it is approximately zero at the middle of the sphere. Therefore, the increase of stress per layer decreases when the middle of the sphere is reached. It is therefore recommended to relate the print speed on the height of the sphere, because this will decrease the total construction time.

- As a starting point for the verification of required concrete strength class, a wall thickness of 2.5 m is used. It is recommended to further investigated whether the thickness can be decreased, while the required concrete class will increase. Less concrete would be required in that case, although more cement is used for a higher concrete strength class. It is recommended to investigate what the optimal combination of thickness and strength class will be.
- In the design, the sphere is supported at an angle of 45°. Because of that, the stresses increase locally. It is recommended to investigate whether a lower strength class or lower thickness could be used in case the sphere is supported in the middle of the sphere, where the wall is vertical. In that case, there is only a normal force which has to be transferred from the sphere to the pedestal/foundation. Another advantage of this is that due to a larger volume, the buoyancy of the entire system increases and the extra volume could be also be used for energy storage, which increases the overall efficiency.
- Due to a lower feasibility and reliability of submerged printing, construction in the dry is chosen to be most promising. However, the construction time is lowest in case of submerged construction. It is therefore recommended to do further research into the fresh and hardened properties of submerged printed concrete.

Recommendations regarding suitability of unreinforced concrete

- The suitability of unreinforced concrete is verified in Chapter 5. From that, it followed that the thermal shrinkage will result in stresses larger than the tensile strength. It is important to note that this is in case of an adiabatic calculation, whereas the temperature increase is semi-adiabatic in reality. It is therefore strongly recommended to do further research into the increase of concrete temperature:
    - It is recommended to investigate the semi-adiabatic temperature increase without further measures;
    - It is recommended to investigate the semi-adiabatic temperature increase in case (liquid) nitrogen (or ice instead of water) is added to the concrete mix, because this could significantly decrease temperature differences (Kruizenga, Zegwaard, & Obladen, 2003);
    - It is recommended to investigate the semi-adiabatic temperature increase in case cooling pipes are used to lower the temperature inside the concrete;
- It is recommended to investigate whether it is possible to use fibre-reinforced concrete for the wall of the sphere. The fibres in the act as reinforcement, which leads to a significant increase of the tensile strength (Marcalikova, Racek, Mateckova, & Cajka, 2020). In case the tensile strength of fibre-reinforced concrete is enough, no further measures need to be taken to lower the temperature difference for example;

Recommendation regarding tensile strength development 3DCP

- It is recommended to do research into the tensile strength development of 3DCP. In this report, it is related to the ratio of the compressive and tensile strength of conventional concrete. It followed that the tensile strength determines the maximum print rate. It is therefore important to investigate how this tensile strength develops in practice, because it could decrease the construction time drastically.
- Research showed that the tensile strength of 3DCP can go up to 5.7 MPa and a tensile strain of 11.4% in case of 3D printable Engineered Cementitious Composites (Zhu, et al., 2019). It is therefore recommended to investigate whether this type of printable concrete would decrease the construction time, because the tensile strength of 3DCP is the limiting factor.

Literature

3Dprint. (2015, September 8). *EXCLUSIVE: Lewis Grand Hotel Erects World's First 3D Printed Hotel, Plans to Print Thousands of Homes in the Philippines Next*. Retrieved July 13, 2022, from 3Dprint: https://3dprint.com/94558/3d-printed-hotel-lewis-grand/

3Printr. (2016, June 2). *3D Concrete printing market to reach $56.4 Million by 2021*. Retrieved June 15, 2022, from 3Printr: https://www.3printr.com/3d-concrete-printing-market-reach-56-4-million-2021-1239664/

Asia News. (2020, August 22). *Torrential rains threaten the Three Gorges Dam in Hubei*. Retrieved June 13, 2022, from Asia News: https://www.asianews.it/news-en/Torrential-rains-threaten-the-Three-Gorges-Dam-in-Hubei-50843.html

AXPO. (n.d.). *Limmern pumped storage plant: Battery in the mountains*. Retrieved June 14, 2022, from axpo: https://www.axpo.com/ch/en/about-us/energy-knowledge.detail.html/energy-knowledge/limmern-pumped-storage-power-plant.html

Bitew, G., Han, M., Mekonnen, S., Patrobers, S., Khan, Z., & Tuan, L. (2019). Pumped energy storage system technology and its AC–DC interface topology, modelling and control analysis: a review. *The Journal of Engineering, 2019*(16), 705-710. doi:https://doi.org/10.1049/joe.2018.8379

Blain, L. (2021, June 24). *New undersea energy storage system harnesses the power of buoyancy*. Retrieved June 20, 2022, from New Atlas: https://newatlas.com/energy/buoyancy-energy-storage-iiasa/

Breugel, K. v. (1991). *Simulation of hydration and formation of structure in hardening cement-based materials.* PhD thesis.

Breugel, K. v., Veen, C. v., Walraven, J., & Braam, C. (1996). *Betonconstructies onder Temperatuur- en Krimpvervormingen.* Den Bosch: ENCI Media.

Buhagiar, D., Sant, T., Farrugia, R., Aquilina, L., Farrugia, D., & Strati, F. (2019, August). Small-scale Experimental Testing of a Novel Marine Floating Platform with Integrated Hydro-pneumatic Energy Storage. *Energy Storage, 24*(2352-152X), 100774. doi:https://doi.org/10.1016/j.est.2019.100774

Cemex. (n.d.). *What are aggregates and how are they used?* Retrieved July 5, 2022, from Cemex USA: https://www.cemexusa.com/products-and-services/aggregates/background-on-aggregates#:~:text=Aggregate%20materials%20help%20to%20make,and%20maintenance%20of%20rigid%20structures.

Choi, M., Roussel, N., Kim, Y., & Kim, J. (2013, March). Lubrication layer properties during concrete pumping. *Cement and Concrete Research, 45*(0008-8846), 69-78. doi:https://doi.org/10.1016/j.cemconres.2012.11.001

Civil Giant. (n.d.). *Bogues Compounds*. Retrieved October 7, 2022, from Civil Giant: https://www.civilgiant.com/bogues-compound/#hydration-of-bogues-compound

Day, R., & Clarke, J. (2003). 2 - Plastic and thermal cracking. In R. Day, & J. Clarke, *Advanced Concrete Technology* (pp. 3-17). Butterworth-Heinemann. doi:https://doi.org/10.1016/B978-075065686-3/50249-4

de Vries, P. (2005). Thermische krimp in jong beton. *Agrabeton*.

Dick, C., Puchta, M., & Bard, J. (2021). StEnSea - Results from the pilot test at Lake Constance. *Energy Storage, 42*(2352-152X), 103083. doi:https://doi.org/10.1016/j.est.2021.103083

Droste-Franke, B., Carrier, M., Kaiser, M., Schreurs, M., Weber, C., & Ziesemer, T. (2014). *Improving Energy Decisions Towards Better Scientific Policy Advice for a Safe and Secure Future Energy System.* Springer Publishers.

EN 1990. (2019). Grondslagen voor het constructief ontwerp. NEN.

EN 1992. (2011). Eurocode 2: Design of concrete structures - Part 1-1: General rules and rules for buildings. NEN.

Eurocode 2. (2006). *Eurocode 2: Design of concrete structures - Part 3: Liquid retaining and containtment structures.* Delft: NEN .

Everett, H. (2021, September 9). *World's longest 3D pinted concrete pedestrian bridge unveiled in Nijmegen*. Retrieved July 6, 2022, from 3D printing industry: https://3dprintingindustry.com/news/worlds-longest-3d-printed-concrete-pedestrian-bridge-unveiled-in-nijmegen-195951/

Ferrell, M. (2022, April 26). *How the Ocean Could be the Future of Energy Storage*. Retrieved June 15, 2022, from Undecided with Matt Ferrell: https://undecidedmf.com/episodes/how-the-ocean-could-be-the-future-of-energy-storage

FLASC. (n.d.). *Technology*. Retrieved June 23, 2022, from FLASC: https://www.offshoreenergystorage.com/

Gajda, J., & Nasvik, J. (2017, June 21). *Why Thermal Cracking Happens & How to Control It*. Retrieved July 8, 2022, from For Construction Pros: https://www.forconstructionpros.com/concrete/article/20862452/why-thermal-cracking-happens-how-to-control-thermal-cracking

GE Renewable Energy. (n.d.). *Linth-Limmern - Securing Future Electricity Supply*. Retrieved June 15, 2022, from GE Renewable Energy: https://www.ge.com/renewableenergy/stories/linthal-securing-future

Gebhard, L., Mata-Falcon, J., Anton, A., Dillenburger, B., & Kaufmann, W. (2021). *Structural behaviour of 3D printed concrete beams with various reinforcement strategies.* Engineering Structures.

Geuss, M. (2017, July 3). *German institute sucessfully tests underwater energy storage sphere*. Retrieved June 10, 2022, from Ars Technica: https://arstechnica.com/science/2017/03/german-institute-successfully-tests-underwater-energy-storage-sphere/

Hagrey, S., Köhn, D., & Rabbel, W. (2014, May). Geophysical assessments of renewable gas energy compressed in geologic pore storage reservoirs. *SpringerPlus, 3*(1), 267. doi:10.1186/2193-1801-3-267

Hewlett, P., & Liska, M. (2017). *Lea's Chemistry of Cement and Concrete.* Butterworth Heinemann. doi:https://doi.org/10.1016/C2013-0-19325-7

Hoogeveen, M. (2020). *Integration of manufacturing and structural design of 3D concrete printed bridges.* Tu Delft.

Hunt, J., Zakeri, B., Barros, A. d., Filho, W., Marques, A., Barbosa, P., . . . Farenzena, M. (2021, August). Buoyancy Energy Storage Technology: An energy storage solution for islands, coastal regions, offshore wind power and hydrogen compression. *Energy Storage, 40*, 102746. doi:https://doi.org/10.1016/j.est.2021.102746

Hydrostor. (n.d.). *Technology*. Retrieved June 22, 2022, from Hydrostor: https://www.hydrostor.ca/technology/

International Energy Agency. (2022). *Global Energy Review 2021 - Renewables*. Retrieved June 8, 2022, from International Energy Agency: https://www.iea.org/reports/global-energy-review-2021/renewables

International Hydropower Association. (2018). *The world's water battery: pumped hydropower storage and the clean energy transition.* London: International Hydropower Association.

Jiao, D., Schryver, R. D., Shi, C., & Schutter, G. D. (2021, September). Thixotropic structural build-up of cement-based materials: A state-of-the-art review. *Cement and Concrete Composites, 122*(0958-9465), 104152. doi:https://doi.org/10.1016/j.cemconcomp.2021.104152

Juenger, M., Hema, J., & Solt, S. (2007). *The Effects of Liquid Nitrogen on Concrete Properties.* Center for Transportation Research at The University of Texas at Austin.

Kalhara. (2021). *How to manage heat of hydration in concrete*. Retrieved July 6, 2022, from Civil medium: https://civilmedium.com/how-to-manage-heat-of-hydration-in-concrete/

Khoshnevis, B. (2004, January). Automated construction by contour crafting - Related robotics and information technologies. *Automation in Construction , 13*(1), 5-19. doi:https://doi.org/10.1016/j.autcon.2003.08.012

Khoshnevis, B., & Zhang, J. (2013, January). Optimal machine operation planning for construction by Contour Crafting. *Automation in Construction, 29*(0926-5805), 50-67. doi:https://doi.org/10.1016/j.autcon.2012.08.006

Kim, K., Park, S., Kim, W., Jeong, Y., & Lee, J. (2017). Evaluation of shear strength of RC beams with multiple interfaces formed before initial setting using 3D printing technology. *Materials, 10*(12), 1349. doi:https://doi.org/10.3390/ma10121349

KNMI. (2010, December). *Hoe warmen broeikasgassen de aarde op?* Retrieved June 2, 2022, from KNMI: https://www.knmi.nl/kennis-en-datacentrum/achtergrond/hoe-warmen-broeikasgassen-de-aarde-op

KNMI. (n.d.). *Klimaatdashboard*. Retrieved August 18, 2022, from Koninklijk Nederlands Meteorologisch Instituut: https://www.knmi.nl/klimaatdashboard

Kruger, J., Zeranka, S., & Zijl, G. v. (2019, November). An ab initio approach for thixotropy characterisation of (nanoparticle-infused) 3D printable concrete. *Construction and Building Materials, 224*(0950-0618), 372-386. doi:https://doi.org/10.1016/j.conbuildmat.2019.07.078

Kruizenga, E., Zegwaard, J., & Obladen, B. (2003, Februari). Koelen met stikstof. *Cement*, p. 5.

Lagundžija, S., & Thiam, M. (2017). *Temperature reduction during concrete hydration in massive structures.* MSc Thesis, Royal Institute of Technology, Stockholm.

Larosche, C. (2009). 3 - Types and causes of cracking in concrete structures. In C. Larosche, & N. Delatte (Ed.), *Failure, Distress and Repair of Concrete Structures* (pp. 57-83). Woodhead Publishing. doi:https://doi.org/10.1533/9781845697037.1.57

Lindsey, R. (2020, August 14). *Climate Change: Atmospheric Carbon Dioxide*. Retrieved June 6, 2022, from Climate.gov: https://www.climate.gov/news-features/understanding-climate/climate-change-atmospheric-carbon-dioxide

Lu, T., Li, Z., & Huang, H. (2021). *Restraining effect of aggregates on autogenous shrinkage in cement.* Construction and Building MATERIALS.

Marcalikova, Z., Racek, M., Mateckova, P., & Cajka, R. (2020). Comparison of tensile strength fiber reinforced concrete with different types of fibers. *Procedia Structural Integrity, 28*, 950-956. doi:https://doi.org/10.1016/j.prostr.2020.11.068

MarineScotland. (n.d.). *Maps NMPI*. Retrieved August 31, 2022, from MarineScotland: https://marinescotland.atkinsgeospatial.com/nmpi/default.aspx?layers=1332

Marrewijk, C. v. (2020). *Form Finding for a Submerged Floating Tunnel.* Delft University of Technology. Delft: TU Delft.

Martinelli, E., Koenders, E., & Caggiano, A. (2013, July). A numerical recipe for modelling hydration and heat flow in hardening concrete. *Cement and Concrete Composites, 40*(0958-9465), 48-58. doi:https://doi.org/10.1016/j.cemconcomp.2013.04.004

Milieu Centraal. (n.d.). *Wat is het broeikaseffect?* Retrieved May 31, 2022, from Milieu Centraal: https://www.milieucentraal.nl/klimaat-en-aarde/klimaatverandering/wat-is-het-broeikaseffect/#:~:text=steeds%20strengere%20regels.-,CO2%20is%20het%20belangrijkste%20broeikasgas,niet%20zelf%20in%20de%20lucht.

NEN 8670. (2021). Additional regulations to NEN-En 13670: Execution of concrete structures. NEN.

Netbeheer Nederland. (n.d.). *Netcapaciteit*. Retrieved May 31, 2022, from Netbeheer Nederland: https://www.netbeheernederland.nl/dossiers/netcapaciteit-60

Ocean grazer. (n.d.). *Ocean Battery*. Retrieved June 8, 2022, from Ocean Grazer: https://oceangrazer.com/

Oceanmotion. (n.d.). *Ocean's vertical structure*. Retrieved August 30, 2022, from Ocean motion: http://oceanmotion.org/html/background/ocean-vertical-structure.htm

Panda, B., Paul, S., Mohamed, N., Tay, Y., & Tan, M. (2018, January). Measurement of tensile bond strength of 3D printed geopolymer mortar. *Measurement, 113*(0263-2241), 108-116. doi:https://doi.org/10.1016/j.measurement.2017.08.051

Parmar, T. (n.d.). *What is LOW HEAT CEMENT?- Know All The Low Heat Cement Uses Here!* Retrieved July 20, 2022, from Civil Giant: https://www.civilgiant.com/low-heat-cement/#:~:text=Low%20heat%20cement%20is%20a,S%20content%20is%20about%2046%20%25.

PBL. (2011). *Een delta in beweging.* Planbureau voor de Leefomgeving. Den Haag: Uitgeverij PBL.

Perrot, A., Rangeard, D., & Pierre, A. (2016, April). Structural built-up of cement based materials used for 3D-printing extrusion techniques. *Materials and Structures, 49*(4), 1213-1220. doi:https://doi.org/10.1617/s11527-015-0571-0

Pitorac, L., Vereide, K., & Lia, L. (2020, September). Technical Review of Existing Norwegian Pumped Storage Plants. *Energies, 13*, 4918. doi:10.3390/en13184918

Qiu, Y., & Zhang, G. (2017). Stress and damage in concrete induced by pipe cooling at mesoscopic scale. *Advnces in Mechanical Engineering, 9*(2). doi:https://doi.org/10.1177/1687814017690509

RCAM Technologies. (n.d.). *Energy Storage*. Retrieved June 7, 2022, from RCAM Technologies: https://rcamtechnologies.com/

Renz, A., & Solas, M. (2016). *Shaping the Future of Construction. A Breakthrough in Mindset and Technology.* Canada: World Economic Forum.

Roussel, N. (2006, May). A thixotropy model for fresh fluid concretes: Theory, validation and applications. *Cement and Concrete Research, 36*(10), 1797-1806. doi:https://doi.org/10.1016/j.cemconres.2006.05.025

Roussel, N. (2018, October). Rheological requirements for printable concretes. *Cement and Concrete Research, 112*, 76-85. doi:https://doi.org/10.1016/j.cemconres.2018.04.005

Rudenko, A. (n.d.). Retrieved July 4, 2022, from Total Kustom: www.totalkustom.com

Stocks, M., Stocks, R., Lu, B., Cheng, C., & Blakers, A. (2020). Global Atlas of Closed-Loop Pumped Hydro Energy Storage. *Joule, 5*(1), 270-284. doi:https://doi.org/10.1016/j.joule.2020.11.015

Structural Guide. (n.d.). *Thermal Cracking of Concrete*. Retrieved July 20, 2022, from Structural Guide: https://www.structuralguide.com/thermal-cracking-of-concrete/

Suiker, A. (2018, March). Mechanical performance of wall structures in 3D printing processes: Theory, design tools and experiments. *International Journal of Mechanical Sciences, 137*, 145-170. doi:https://doi.org/10.1016/j.ijmecsci.2018.01.010

Tasri, A., & Susilawati, A. (2019, July). Effect of cooling water temperature and space between cooling pipes of post-cooling system on temperature and thermal stress in mass concrete. *Building Engineering, 24*(2352-7108), 100731. doi:https://doi.org/10.1016/j.jobe.2019.100731

TeachEngineering. (n.d.). *Engineering Design Process*. Retrieved August 18, 2022, from Teach Engineering: https://www.teachengineering.org/populartopics/designprocess

TU/e. (2021, April 30). *Printend uit de wooncrisis: 'keiharde noodzaak'*. Retrieved July 15, 2022, from Eindhoven University of Technology: https://www.tue.nl/nieuws/nieuwsoverzicht/30-04-2021-printend-uit-de-wooncrisis-keiharde-noodzaak/

U.S. Energy Information Administration. (2021, May 21). *Energy and the environment explained*. Retrieved June 2, 2022, from U.S. Energy Information Administration.: https://www.eia.gov/energyexplained/energy-and-the-environment/where-greenhouse-gases-come-from.php#:~:text=Carbon%20dioxide,-In%202019%2C%20CO&text=Fossil%20fuel%20combustion%20(burning)%20for,of%20total%20CO2%20emissions.

United Nations. (2015). *Paris Agreement.* Paris: United Nations.

Urschel, W. (1931). *US Patent No. US1995692A.* Retrieved from https://patentimages.storage.googleapis.com/e5/3c/e2/1c417f3b41892a/US1995692.pdf

Wang, L., Yang, H., Zhou, S., Chen, E., & Tang, S. (2018). Hydration, mechanical property and C-S-H structure of early-strength low-heat cement-based materials. *Materials Letters, 217*(0167-577X), 151-154. doi:https://doi.org/10.1016/j.matlet.2018.01.077

Water Encyclopedia. (n.d.). *Waves*. Retrieved September 8, 2022, from Water Encyclopedia: http://www.waterencyclopedia.com/Tw-Z/Waves.html

Wolfs, R. (2019). *Experimental characterization and numerical modelling of 3D printed concrete.* Eindhoven: Eindhoven University of Technology.

Wolfs, R., Bos, F., & Salet, T. (2019, May). Hardened properties of 3D printed concrete: The influence of process parameters on interlayer adhesion. *Cement and Concrete Research, 119*(0008-8846), 132-140. doi:https://doi.org/10.1016/j.cemconres.2019.02.017

Young, J. (2001). portland Cements. In *Encyclopedia of Materials: Science and Technology* (pp. 7768-7773). Oxford. doi:https://doi.org/10.1016/B0-08-043152-6/01398-X

Zhang, C., Nerella, V., Krishna, A., Wang, S., Zhang, Y., Mechtcherine, V., & Banthia, N. (2021, September). Mix design concepts for 3D printable concrete: A review. *Cement and Concrete Composites, 122*(0958-9465), 104155. doi:https://doi.org/10.1016/j.cemconcomp.2021.104155

Zhu, B., Pan, J., Nematollahi, B., Zhou, Z., Zhang, Y., & Sanjayan, J. (2019, November). Development of 3D printable engineered cementitious composites with ultra-high tensile ductility for digital construction. *Materials & Design, 181*, 108088. doi:https://doi.org/10.1016/j.matdes.2019.108088

Appendices

A. Overview of offshore energy storage types

Energy storage in concrete spheres at seabed level is based on gravitational energy storage. However, there are also other types of offshore energy storage, making use of gravitational energy. These are shortly explained in this appendix. This shows the relevance of this thesis.

Energy can be stored in multiple ways when it is stored as potential energy. For example, a pendulum has maximum potential energy when the velocity is zero and has no potential energy when the velocity (which is kinetic energy) is maximum. A stretched or compressed spring has potential energy, which decreases when the spring is released, as the potential energy is converted to kinetic energy. When water is lifted, work is done (kinetic energy) and the potential energy increases. Energy stored in a battery is stored as chemical energy and is a form of potential energy. Even food is a form of potential energy. So, potential energy can be stored in multiple ways and is daily used without thinking about it.

Potential energy storage is also used in the case of Pumped Hydro Energy Storage (PHES). The system consists of two reservoirs, which are connected to each other by pipes or channels and have different elevation. This difference in elevation is the head-difference. When water is pumped from the lower reservoir to the upper reservoir, the potential energy increases proportional to the head difference, as can be seen in Eq. A.1. Pumped Hydro Energy Storage accounts for more than 95% of installed global energy storage (Stocks, Stocks, Lu, Cheng, & Blakers, 2020). Due to an 'increasing penetration of wind and solar, reduced dispatchable generation and the need for greater grid flexibility … an increase of nearly 50% is expected to be commissioned by 2030' (International Hydropower Association, 2018).

$$E_P = m * g * h \tag{A.1}$$

Where:

m	= mass	[kg]
g	= gravitational constant	[m/s^2]
h	= height	[m]

There are two principal categories of Pumped Hydro Energy Storage. One is the closed-loop, where energy is generated only from water that is previously pumped to an upper reservoir, so there is no (significant) natural inflow to either reservoir (Figure A - 1). This is pure storage of energy. The second one is the open-loop in which at least one of the reservoirs is connected to a natural flow of water. If there is a significant natural inflow of water in the upper reservoir, there is no need to pump water from the lower to the upper reservoir to generate electricity. Hydropower dams are an example of this type of storage (Figure A - 2). The storage capacity depends on the size of the reservoirs and the height difference, whereas the electricity that is generated depends on the turbine size (International Hydropower Association, 2018).

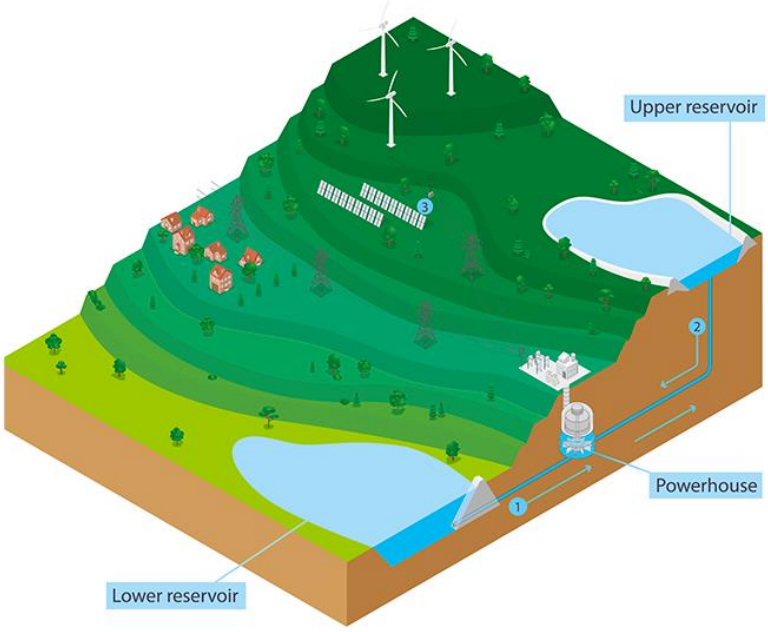

Figure A - 1 Closed-loop pumped hydropower storage (International Energy Agency, 2022)

Figure A - 2 Three Gorges Dam, China. This is an open-loop storage, because there is a natural flow into the upper reservoir from the Yangtze River (Asia News, 2020).

The energy storage in the spheres is a closed-loop Pumped Hydro Energy Storage. Water is pumped out of the spheres, 'stored' in the ocean, and the same amount of water is let in back into the spheres. Apart from leakage into the spheres, there is no natural flow in or out of the spheres. Therefore, the focus is on closed-loop storage systems.

Closed-loop PHES

Pumped Hydro Energy Storage represents most of the energy storage globally. There is a significant inflow in at least one of the reservoirs needed in case of open-loop PHES and often a dam is built which can have significant environmental impact. Closed-loop PHES overcomes these problems. Researchers of the Australian National University concluded that there is a potential for 616.000 PHES-sites in general, which has a potential energy storage of 23.000 TWh (Stocks, Stocks, Lu, Cheng, & Blakers, 2020).

An example of closed-loop PHES in Europe is the Limmern pumped storage plant, which is called 'the battery of the mountains'. It consists out of 5 lakes, each at different elevation. The highest and largest

two are presented in Figure A - 3, which can generate 1000 MW together. The full storage plant can generate 1520 MW, which is as powerful as a nuclear power plant, it can store up to 34 GWh and has an overall efficiency of more than 80%. The system is able to react fast: 2 minutes are needed to start-up the plant and only 3 minutes to switch the pump to turbine mode (GE Renewable Energy, n.d.). With a water level of 2474 m above sea level, it is the highest reservoir in Europe.

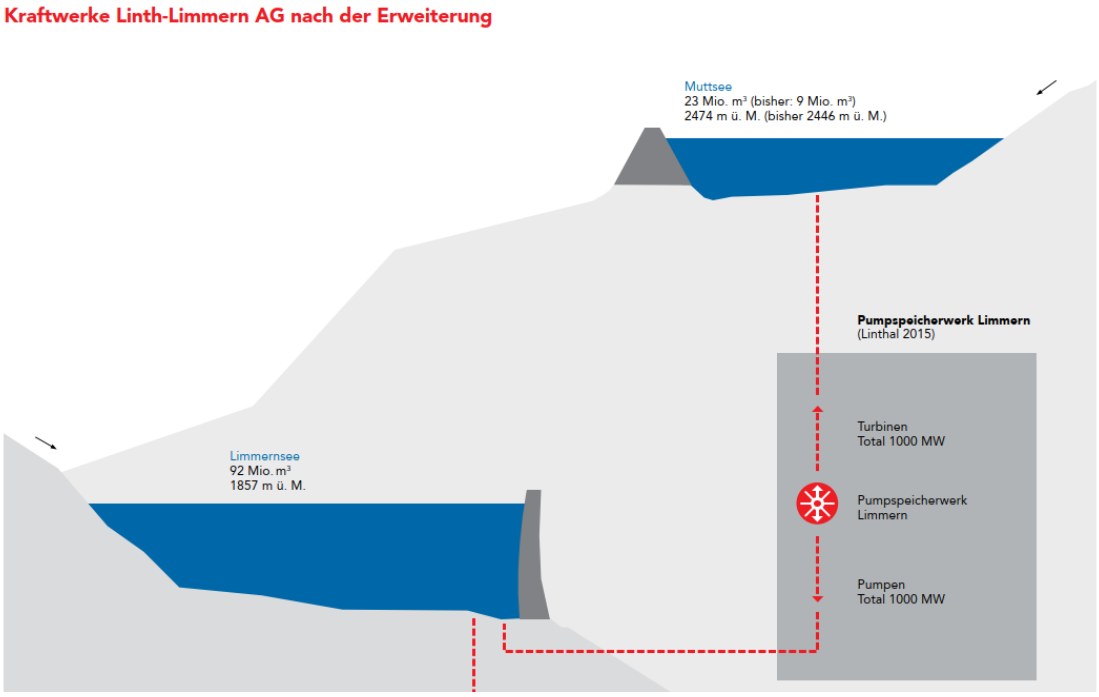

Figure A - 3 Schematization of the closed-loop PHES plant in Limmern. Water is pumped from the Limmernsee to the Muttsee when demand is lower than supply and water flows from the Muttsee through turbines to the Limmernsee when supply is lower than demand (AXPO, n.d.).

Offshore (Pumped Hydro) Energy Storage

The amount of stored energy is proportional to the difference in height (the 'head difference') and the amount of the water that is pumped to a higher level. To store a larger amount, the head difference should be higher or the capacity of the reservoirs should increase. However, a suitable landscape shape is needed for PHES using natural reservoirs. Therefore, a promising solution is to store energy at sea. Four concepts are described below to explain the need for energy storage in concrete spheres at large depth.

BEST

Although PHES is a promising technology to store energy at sea, there are also other techniques to store energy at sea. One of these is to store energy at sea using buoyancy: Buoyancy Energy Storage Technology (BEST). This has been developed by researchers at the International Institute for Applied Systems Analysis (IIASA), Austria. Energy is stored at the seabed with a compressed gas like air or hydrogen. The system is connected to floating solar panels or wind turbines. When there is a surplus of generated energy, buoyant tubes are pulled down to the seabed and are thus stored as potential energy. BEST uses a platform anchored at the sea bed which is connected to a 100 x 100 m array of high-density polyethylene pipes, in which the compressed gas is stored (Hunt, et al., 2021). The researchers concluded that the system could have great potential in storing energy close to the coastline near islands with no mountains. Although the current estimated costs are high, the estimated LCOS could be reduced to $50/MWh (Blain, 2021) in the future if several optimisations are performed, which is much less than the LCOS of lithium-ion batteries, which is around $200/MWh (Ferrell, 2022).

FLASC

FLASC is another example of storing energy at sea. FLASC stands for Floating Liquid piston Accumulator using Seawater under Compression and this concept is developed from researchers of the University of Malta. In this concept, in charging mode, water is pumped into a closed chamber containing pre-charged air Figure A - 4. When the stored energy is needed, the pressurized water is released through a turbine to generate electricity (FLASC, n.d.). The intended depth for full-scale is between 100 and 400 m. This technology won several awards in the last years. With a first prototype, tests were done in 2017 in the Grand Harbour of the Maltese Islands. The stored energy was generated with solar panels and the system showed high efficiencies and system availability (FLASC, n.d.).

The efficiency decreases for larger depths, because thermal effects will become a problem. According to the gas law, when a volume of air is compressed, the pressure increases by which the temperature also increases. If the heat is not captured somehow, energy is lost to the surrounding sea water in the form of heat and the overall efficiency decreases. This concepts is therefore intended to use at depths up to 400 m, because at larger depth a larger pressure is needed to store the same amount of energy due to the increase of hydrostatic pressure. Present systems using compressed air for energy storage attempt to solve this with thermal storage to increase the efficiency, of which an example is Hydrostor, which captures the heat of the compressed air (Hydrostor, n.d.). Although it increases efficiency, the complexity and costs increases as well. Other solutions, which are used by FLASC, is to make sure that the increase in temperature is limited by cooling the air with the surrounding water and limit the pressure increase (Buhagiar, et al., 2019). The LCOS for this storage type is unknown yet, but according to Ferrel, this system could save $554.000/MWh for the entire life span, with respect to lithium-ion batteries (Ferrell, 2022).

Ocean Grazer

Another energy storage system for offshore use is the one developed by Ocean Grazer. This system makes use of the hydrostatic pressure. When there is a surplus of energy, generated by (floating) wind turbines or solar panels, water is pumped from a reservoir underground into a flexible reservoir placed on the seabed. When the energy is needed, the water stored in the flexible reservoir is pushed back due to the hydrostatic pressure into the reservoir underground. According to Ocean Grazer, the system is flexible deployable, scalable and durable (Ocean grazer, n.d.).

Figure A - 4 Concept of the Ocean Battery. The pump-turbine module and the concrete reservoir are placed underground, the flexible rubber 'bag' is placed on the seabed (Ocean grazer, n.d.)

Although the system looks promising, there are also disadvantages. One of these is that the concrete reservoirs and the pump-turbine module will be placed underground (see Figure A - 4). As stated before, the amount of energy increases linearly with depth. Besides this, the efficiency of the pump-

turbine module increases also with depth. However, if water depth increases, it will also be more difficult to install the pump-turbine module and the concrete reservoir underground.

Besides that, maintenance of the pump-turbine will be difficult, because it is buried in the ground. To (partly) overcome this problem, it is intended to fill the concrete reservoirs with fresh water instead of seawater, as fresh water leads to less maintenance. However, this will also be difficult, because the volume of the concrete reservoirs is 20.000 m^3 (Ocean grazer, n.d.). It will be a challenge to transport the reservoirs if they are filled with fresh water, but it is also a challenge to fill the reservoirs with such amount of fresh water at sea, when the system is deployed at large depth.

Fraunhofer

One of the concepts that is similar to the one that will be optimised in this report, is StEnSea, which stands for 'Stored Energy at Sea'. The Fraunhofer Institute has developed a pilot project, in collaboration with Hochtief Solutions AG. This consists also of concrete spheres, which were placed on the seabed. With a diameter of 30 m and a depth of 700 m, the storage equals 20 MWh and could generate 5 MW for four hours, if a pump-turbine module would be used of 5 MW (Geuss, 2017). StEnSea has got several awards, including one from Green Awards, where they ended in the top 3 in the category 'Best innovation of the year'.

In 2017 tests were done at Lake Constance at 100 m depth. For this test, a scaled prototype was made which is shown in Figure A - 5. This prototype has an outer diameter of 3 m and an inner volume of approximately 8 m^3. The prototype was made on land and transported with heavy duty vehicles to the lake. To avoid cavitation a pressure hose was made above the pump-turbine module (Dick, Puchta, & Bard, 2021). The cylindrical parts below and above the sphere are to create space for the pump-turbine.

During the tests, the pressure hose gave some disadvantages, because conventional pressure hoses are usually designed for high internal pressures and not for external pressures. However, for full scale spheres, cavitation can be avoided much more easy, with a water column of a few meters. Another disadvantage is that the pump is integrated in the system, which makes maintainability of the pump difficult. The next step will be testing a prototype of 1:3 scale and test it offshore (Dick, Puchta, & Bard, 2021). It is an cost-competitive option: the LCOS is estimated at $44-$220/MWh (Ferrell, 2022).

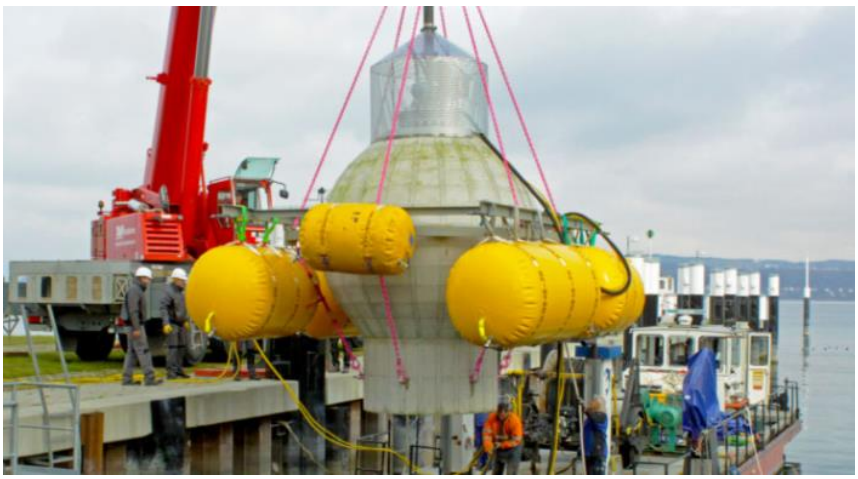

Figure A - 5 Scaled prototype of the concrete sphere used for energy storage, developed by researchers of the Fraunhofer Institute (Geuss, 2017). The yellow balloons are needed to give enough buoyancy.

B. Overview of development and current applications of 3DCP

3DCP is an upcoming and promising technique. To investigate whether 3DCP can be used to construct the spheres, it is important to know how it is developed and for what purposes it is developed. This information is mainly used in steps 2.3 (the concepts, based on main construction methods, will be developed) and 2.4 (a qualitative verification is made for the main construction method) of the design method.

3DCP is a relatively new development and therefore it is until today not widely used as structural concrete. Although 3DCP is a relatively new, the technique of building walls and structures with machines goes back to the 1930's. Several patents under the name of William E. Urschel describes a machine which could be used to deposit materials in the form of a strip for cylindrical or spherical walls (US Patent No. US1995692A, 1931). Other patents followed, but in absence of a 3D model, 3DCP was not there yet.

Since the end of the last century, the 3D printing industry increased and developed more and more. One of the techniques that was developed is Contour Crafting (CC), developed by Khoshnevis at the University of Southern California. Initially relatively small objects were printed with mainly ceramic materials, but at the beginning of the 21th century, the Contour Crafting technique was scaled up and more developed and also concrete was printed (Khoshnevis, 2004). From this, two different approaches were distinguished: One method used the printed concrete as a formwork, where the inner space was conventionally cast. For this method, reinforcement can still be applied. In case of the second method, the inner structure is also printed, whereby concrete is used in a more efficient way. In this case however, it is much more difficult to add reinforcement. Figure B - 1 illustrates both techniques.

(a) (b)

Figure B - 1 Printed concrete structures. (a) represents a printed formwork with conventionally cast concrete in between and in case of (b) the inner structure is also printed (Khoshnevis & Zhang, 2013).

Although more research is needed before 3DCP will be used on large scale in the construction sector, it is already been used on small scale. One project named 'Project Milestone' in The Netherlands are the printed houses in Eindhoven (Figure B - 2a). These houses fully meets all the Dutch building requirements. The first house is delivered in 2021 and consists of 24 elements that were printed in a factory in Eindhoven. After that, the elements were transported to the construction site and placed on a foundation (TU/e, 2021).

Another application of 3DCP used for structural purposes in The Netherlands is a bridge for cyclists and pedestrians. The bridge is 29 m long and is the longest 3D printed bridge in the world. The project was undertaken by Rijkswaterstaat, in cooperation with BAM and Weber Beamix, and the bridge was placed in the Dutch city of Nijmegen, due to Nijmegen's election as European Green Capital in 2018. From architectural point of view, there is much more freedom because a formwork is not needed. Also for this project, the bridge consists of elements that were printed in a factory and assembled on the construction site (Everett, 2021). This technique is also used in case of prefab structures, were the structure is made in elements and assembled on the construction site. The technique of printing elements in a factory and assemble them on the construction site is promising for the future.

(a) (b)

Figure B - 2 Printed house in Eindhoven (a) (TU/e, 2021) and printed bridge in Nijmegen (b) (Everett, 2021).

In both cases, the structure consists of elements which were printed off-site and assembled on-site. Other examples show that it is also possible to print on-site. In that case, transport costs are lowered. Total Kustom, an enterprise founded by Rudenko in Minnesota (USA), realized some examples of on-site 3DCP. In 2014, Rudenko designed and printed a small castle in his backyard, Figure B - 3a. The main part was printed on-site, although the top parts were printed separately and assembled afterwards (Rudenko, n.d.). The goal was to show that outside printing is possible and to verify whether the printer would need any adjustments to print on larger scale.

After this success, Rudenko was approached by an entrepreneur to print an entire hotel room, as part of the Lewis Grand Hotel in The Philippines. This room was 10.5 by 12.5 by 3 meters and was fully printed on-site. To ensure continuity of the process, a large tent was built in which the room was printed. The printing process took about 100 hours. This process includes several stops to install plumbing, wiring and rebars. If these things could be done simultaneously with printing and/or automatically, the printing process could be significantly reduced. The assembly of the printer took most of the time: 2 months (3Dprint, 2015).

(a) (b)

Figure B - 3 Printed castle by Rudenko (a) and printed hotel room in The Philippines (b) (3Dprint, 2015)

C. Calculation of draft of the empty sphere

As the draft of the spheres is an important design aspect, a calculation of the draft of the sphere with conceptual dimensions is shown in this appendix. It is required that the spheres will have enough buoyancy to keep floating. This is used in step 2.7 (a quantitative verification is made for the variants) of the design.

The spheres should be transported from the construction location to the location where the will be deployed. Therefore, the depth should be everywhere enough at the route of transportation. To verify whether the available depth is sufficient, the draft of the spheres is calculated. The weight and size of the spheres determines the draft of the spheres. This could be used to optimise the design. Besides that, it could be used to verify whether the spheres are added to the pedestal and foundation before transport or after transport, because that will influence the draft. In this appendix, the draft of an empty sphere is calculated.

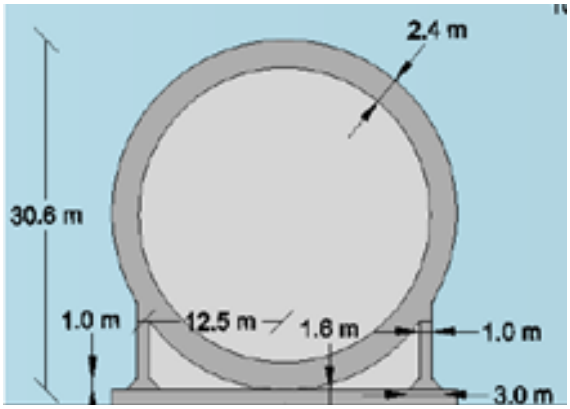

Figure C - 1 Dimensions of the sphere.

Sphere outer diameter R_{out} = 30.6/2 = 15.3 m
Sphere inner diameter R_{in} = 25.8/2 = 12.9 m
Thickness t = 2.4 m

The volume of the concrete:

$$V_c = \frac{4}{3} \cdot \pi \cdot R_{out}^3 - \frac{4}{3} \cdot \pi \cdot R_{in}^3 = \frac{4}{3} \cdot \pi \cdot 15.3^3 - \frac{4}{3} \cdot \pi \cdot 12.9^3 = 6010 \text{ m}^3$$

Then, the weight of concrete:

$$W_c = \gamma_c * V_c = 24 * 6010 = 144.240 \text{ kN}$$

This weight has to balance the buoyancy. From that, the height of the sphere above the waterline is calculated. This is calculated with the following equation:

$$Buoyancy = \left(\frac{4}{3} \cdot \pi \cdot R_{out}^3 - \frac{1}{3} \cdot \pi \cdot h^2 \cdot (3 \cdot R_{out} - h) \right) * \gamma_w$$

In which h is the height of the sphere above the waterline. The buoyancy should be equal to the weight of the empty sphere. From this, the height of the sphere above the waterline can be calculated. From that, the draft is calculated.

$$Buoyancy = \left(\frac{4}{3} \cdot \pi \cdot 15.3^3 - \frac{1}{3} \cdot \pi \cdot h^2 \cdot (3 \cdot 15.3 - h)\right) * 10 = 144.240 \quad \rightarrow \quad h = \ 3.7 \text{ m}$$

This results in a draft of 30.6 – 3.7 = 26.9 m.

D. Model of Roussel to estimate buckling height printed concrete

Besides the model of Suiker which is used to calculate the buckling height in step 2.7 (a quantitative verification is made for the variants), Roussel also developed a model to predict the buckling height. This model is given in this appendix, which shows the difference between the model of Suiker and the model of Roussel.

Roussel developed a formulation for the critical height H_c at which self-buckling is expected to occur in a slender vertical structure submitted to its own weight (Roussel, 2018). If one linear meter of a wall of width δ is considered, the formulation simplifies to the one given in Eq. C.1.

$$H_c \cong \left(\frac{8 \cdot EI}{\rho \cdot g \cdot A}\right)^{\frac{1}{3}} \cong \left(\frac{2 \cdot E \cdot \delta^2}{3 \cdot \rho \cdot g}\right)^{\frac{1}{3}} \quad \text{(C.0-1)}$$

For a stable structure, the modulus of elasticity should therefore be higher than:

$$E = \frac{3 \cdot \rho \cdot g \cdot H^3}{2 \cdot \delta^2} \quad \text{(C.0-2)}$$

Where:

E	= modulus of elasticity	[N/mm^2]
I	= quadratic moment of inertia	[mm^4]
A	= horizontal rectangular cross-sectional area	[mm^2]
δ	= width of deposited layer	[mm]

Roussel did some experiments, where the elastic modulus and compressive strength were measured. Buckling failure was measured after 29 layers, whereas Eq. C.1 predicted buckling after 20 layers. Eq. C.1 therefore underestimates the ability of the structure to resist buckling, but still allows for a rough estimate (Roussel, 2018).

By using the relation between the Young's modulus E and the shear modulus G and the relation between yield stress and shear modulus, the requirement on Young's modulus originating from a strength-based failure criterion can be given.

$$E = 2G(1 + \nu) \quad and \quad \tau_c = G\gamma_c \quad \text{(C.0-3)}$$

Then

$$E > \frac{2\rho g H}{\gamma_c \sqrt{3}}(1 + \nu) \quad \text{(C.0-4)}$$

By equaling Eq. C.1 and Eq. C.4, the transition height between plastic failure and buckling can found.

$$H_T = 2\delta \sqrt{\frac{1+\nu}{3\gamma_c \sqrt{3}}} \quad \text{(C.0-5)}$$

Where:

G	= shear modulus
ν	= Poisson ratio (typical value of 0.3 (Roussel, 2018)
γ_c	= critical shear strain at flow onset (typical value = 2% (Roussel, 2018)

E. Semi-adiabatic temperature description

In step 2.9 (the hydration heat is estimated, crack width calculations are performed and watertightness will be verified) of the design, the adiabatic temperature increase is used. In reality however, the temperature increase is semi-adiabatic. This semi-adiabatic formulation gives a more accurate prediction and is given in this appendix. It shows the difference between the adiabatic and semi-adiabatic calculation.

Non-adiabatic formulation

In practice, part of the hydration heat is transferred to the surroundings with elapse of time. This makes that the hydration process is semi-adiabatic. The start of the hydration is a adiabatic process, but as time goes on, some heat is released into the surroundings. This will also slow down the hydration process, as the rate of the process depends on temperature (Martinelli, Koenders, & Caggiano, 2013). The development of the temperature and the hydration process are described using the differential equation of Fourier. The expression for 1D is given in Eq. D.1.

$$\rho_c \cdot c_c \cdot \frac{\partial T}{\partial t} = \lambda_c \cdot \frac{\partial^2 T}{\partial x^2} + q_c(x,t) \tag{D.1}$$

In this equation:

$$q_c(x,t) = C \cdot \frac{dQ_c}{dt} \tag{D.2}$$

Where:

T	= temperature inside the concrete	[K]
λ_c	= heat conduction coefficient	[W/(m · K)]
$q_c\,(x,t)$	= rate of the heat source	[J/(m^3 · s]
Q_c	= function describing heat by hydration per unit mass of cement	[-]

The relationship between the temperature and the rate of the chemical reaction can be expressed with the Arrhenius expression (Breugel, Veen, Walraven, & Braam, 1996).

$$V(T) = A_V \cdot e^{-\left(\frac{E_A}{R \cdot T}\right)} \tag{D.3}$$

Where:

$V(T)$	= rate of chemical reaction	[-]
A_V	= reference rate value	[-]
E_A	= apparent activation energy	[J/mol]
R	= universal gas constant	[8.3145 J/(mol · K)]

The Arrhenius equation is useful to define the relationship between the hydration heat Q in the semi-adiabatic process and the degree of hydration. The Arrhenius expression is used to link the actual heat production rate $q_c(T)$ and the corresponding heat production rate $q_a(T_a)$ in adiabatic conditions, from which the last one should be measured at the same stage of hydration. Then, when the semi-adiabatic process has reached the degree of hydration at time t, an equivalent time t_{eq} can be defined to identify the corresponding status of the hydration reaction in adiabatic conditions (Martinelli, Koenders, & Caggiano, 2013):

$$Q_a(t_{eq}) = \alpha_h(t) \cdot Q_{max} \tag{D.4}$$

Where:

$Q_a\,(t_{eq}) =$ heat released at an equivalent time in adiabatic conditions [J]

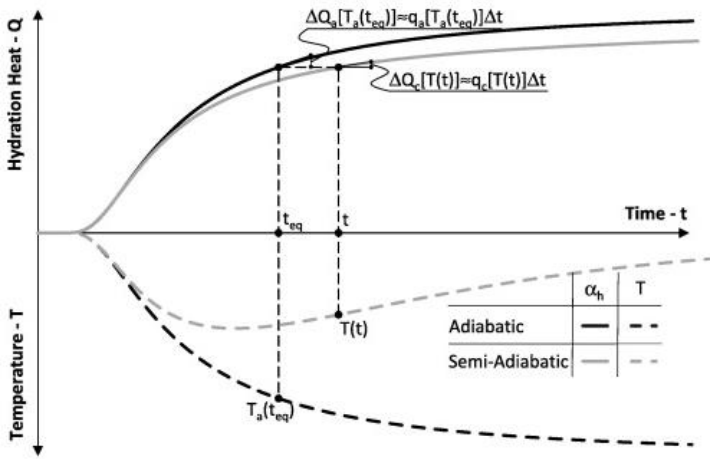

Figure E - 1 Hydration heat and temperature development in adiabatic and semi-adiabatic conditions (Martinelli, Koenders, & Caggiano, 2013)

Based on results of experimental testing on hardening concrete samples, in adiabatic conditions, two possible analytical expressions were given to approximate the time evolution of the hydration heat $Q_a(t)$ (Breugel, 1991):

$$Q_a(t) = Q^*_{max} \cdot (1 - e^{-r \cdot t}) \tag{D.5}$$

$$Q_a(t) = Q^*_{max} \cdot e^{-\left(\frac{\tau}{t}\right)^{\beta}} \tag{D.6}$$

Where:

$r, \tau \, and \, \beta$ = parameters introduced to control the shape of the heat evolution [-]

The expression for t_{eq} can be found with Eq D.7 or Eq D.8. The following two equations corresponds to these two functions respectively Eq. D.5 and Eq. D.6.

$$t_{eq} = -\frac{1}{r} \cdot \ln\left[1 - \frac{\alpha_h(t)}{a_{h,max}}\right] \tag{D.7}$$

$$t_{eq} = -\frac{\tau}{\left\{\ln\left[\frac{\alpha_h(t)}{\alpha_{h,max}}\right]\right\}^{\frac{1}{\beta}}} \tag{D.8}$$

The amount of heat that is produced by the general hydration process is the same for both the adiabatic and the semi-adiabatic process. However, the temperatures T and T_{eq} corresponding to time t and t_{eq} are not equal, due to the heat transfer. Again, the Arrhenius equation is used to describe the relationship (Martinelli, Koenders, & Caggiano, 2013):

$$\frac{q_c[T(t)]}{q_a[T_a(t_{eq})]} = \frac{e^{-\frac{E_A}{R \cdot T(t)}}}{e^{-\frac{E_A}{R \cdot T_a(t_{eq})}}} = e^{-\frac{E_A}{R} \cdot \frac{T_a(t_{eq}) - T(t)}{T_a(t_{eq}) \cdot T(t)}} \tag{D.9}$$

Now, the differential equation can be rewritten. The result is given in Eq. D.10.

$$\rho_c \cdot c_c \cdot \frac{\partial T}{\partial t} = \lambda_c \cdot \frac{\partial^2 T}{\partial x^2} + q_a\left[T_a(t_{eq})\right] \cdot e^{-\frac{E_A}{R} \cdot \frac{T_a(t_{eq}) - T(t)}{T_a(t_{eq}) \cdot T(t)}} \tag{D.10}$$

In this equation, the flow source in adiabatic conditions can be determined as follows (Martinelli, Koenders, & Caggiano, 2013):

$$q_a\left[T_a(t_{eq})\right] = C \cdot \frac{dQ_a}{dt}\Big|_{t=t_{eq}} \quad \text{(D.11)}$$

The problem can be solved with the initial conditions and boundary conditions. The initial condition is given in Eq. D.12. When the external sides are not insulated, the boundary conditions are given in Eq D.13. If the external sides are insulated, with a heat conduction coefficient λ_p and thickness t_p, the boundary conditions are given in Eq. D.14 and Eq. D.15.

$$T(x, t=0) = T_R \quad \text{(D.12)}$$

$$T\left(x = -\frac{L}{2}, t\right) = T_{left}(t), \qquad T\left(x = \frac{L}{2}, t\right) = T_{right}(t) \quad \text{(D.13)}$$

$$q_{left}(t) = \lambda_p \cdot \frac{T_{left}(t) - T_R}{t_p} = \lambda_c \cdot \frac{\partial T}{\partial x}\Big|_{x=-\frac{L}{2}} \quad \text{(D.14)}$$

$$q_{right}(t) = \lambda_p \cdot \frac{T_{right}(t) - T_R}{t_p} = -\lambda_c \cdot \frac{\partial T}{\partial x}\Big|_{x=\frac{L}{2}} \quad \text{(D.15)}$$

Where:

λ_p = heat conduction coefficient of insulation [W/(m · K)]]

t_p = thickness of insulation

F. Estimation of leakage through (un)cracked sphere

Because leakage is important regarding the efficiency of the system, leakage should be avoided as much as possible. To estimate the leakage, equations of Darcy are used. This is shown in this appendix and the results are used to emphasise the required crack width control in Section 2.2.

The leakage in uncracked stage can be estimated with the Darcy moisture flow, given in Eq. E.1.

$$Q = \left(\frac{A \cdot \Delta p}{\eta \cdot D}\right) \cdot \kappa \tag{E.1}$$

Typical values for concrete are:

Q	= leakage through concrete	[m^3/s]
A	= area through which leakage occurs = $4 \cdot \pi \cdot R^2 = 4 \cdot \pi \cdot 15^2 = 2827$	[m^2]
Δp	= pressure difference = $100*10^5$	[Pa]
η	= dynamic viscosity of fluid (temperature = 3 °C) = $1.6*10^{-3}$	[$N \cdot s/m^2$]
D	= thickness of the member = 2.5	[m]
κ	= intrinsic permeability = $1*10^{-18}$	[m^2]

For these values, the leakage is:

$$Q = \left(\frac{A \cdot \Delta p}{\eta \cdot D}\right) \cdot \kappa = \left(\frac{2827 \cdot 100 \cdot 10^5}{1.6 \cdot 10^{-3} \cdot 2.5}\right) \cdot 10^{-18} = 7 \cdot 10^{-6} \frac{\mathrm{m}^3}{\mathrm{s}} = 0.025 \frac{\mathrm{m}^3}{\mathrm{hr}}$$

The amount of leakage through a cracked concrete wall can also be calculated with the Darcy moisture flow, given in Eq. E.2. The leakage depends on the surface roughness, crack width, pressure difference, dynamic viscosity, thickness of the member and the length of the crack width.

$$Q = \alpha \cdot \left(\frac{\mathrm{w}^3 \cdot \Delta p}{\eta \cdot D}\right) \cdot \mathrm{L} \tag{E.2}$$

Typical values are:

α	= roughness factor = 0.01	[-]
w	= crack width = $0.05*10^{-3}$	[m]
L	= length of the crack = 2.5	[m]

As an estimation, 1 crack through the full cross-section per m^2 is assumed.

For these values, the leakage is:

$$Q = \mathrm{A} \cdot \alpha \cdot \left(\frac{\mathrm{w}^3 \cdot \Delta p}{\eta \cdot D}\right) \cdot \mathrm{L} = 2827 \cdot 0.01 \cdot \frac{\left(0.05 \cdot 10^{-3}\right)^3 \cdot 100 \cdot 10^5}{1.6 \cdot 10^{-3} \cdot 2.5} \cdot 2.5 = 0.022 \frac{\mathrm{m}^3}{\mathrm{s}} = 79.5 \frac{\mathrm{m}^3}{\mathrm{hr}}$$

G. Verification of plastic and elastic failure of 3DCP and verification of wall thickness

This appendix shows the calculation procedure for plastic collapse and elastic buckling. This is used in step 2.7 (a quantitative verification is made for the variants) of the design, where the different 3DCP-variants are verified. In this appendix, the calculations, with numbers, are shown. The results are given in Section 4.3.

Plastic collapse

The two failure modes of 3DCP, as described in Section 2.1, are plastic collapse and elastic buckling. In case of plastic collapse, the stress in the lowest layer is higher than the strength of the material. The increase of strength is described in Section 2.1, the stress can be divided into normal stress due to the weight of the layers on top and bending stresses, due to the eccentricity of the layers on top, in case the layers are inclined. This is represented in Figure G - 1. The normal stress $\sigma_{i,1}$ and bending stress $\sigma_{i,2}$ in layer i are given in Eq. F.1 and Eq. F.2 respectively, in case 1 m length is used.

$$\sigma_{i,1} = \frac{F}{A} = \frac{(h \cdot b \cdot 1) \cdot \rho \cdot g}{b * 1} \tag{F.1}$$

$$\sigma_{i,2} = \frac{M}{W} = \frac{F \cdot a}{\frac{1}{6} \cdot 1 \cdot b^2} \tag{F.2}$$

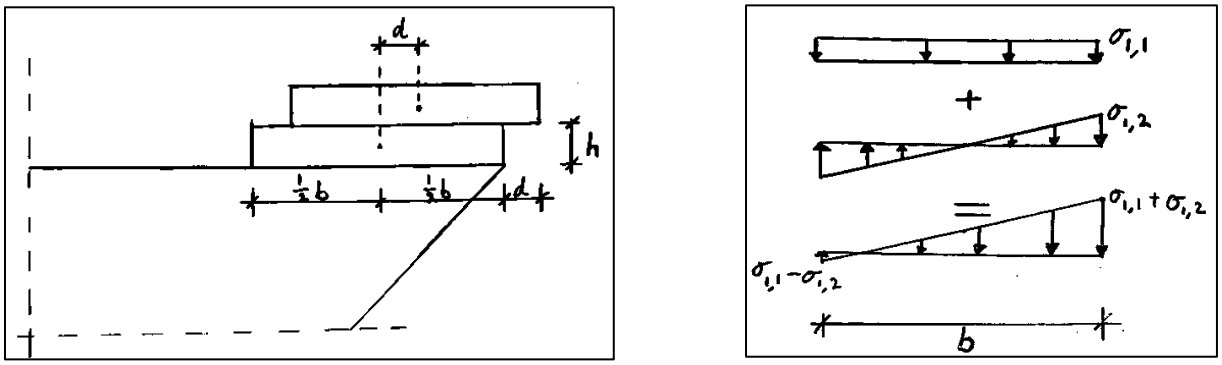

Figure G - 1 First printed layers of concrete at the prefab element (left) and stresses in lowest printed layer due to a layer on top.

The following parameters are used:

$b = 0.1$	[m]
$h = 0.01$	[m]
$d = h = 0.01$ (maximum printing angle of 45 °C)	[m]
$\rho = 2200$	[kg/m^3]
$g = 9.81$	[m/s^2]
$Q = 0.25/3600 = 6.94*10^{-5}$	[m^3/s]

The normal stress in the first layer, due to the weight of the second layer equals:

$$\sigma_{i,1} = \frac{F}{A} = \frac{(h \cdot b \cdot 1) \cdot \rho \cdot g}{b * 1} = \frac{(0.01 \cdot 0.1 \cdot 1) \cdot 2200 \cdot 9.81}{0.1 \cdot 1} = 220 \frac{\mathrm{N}}{\mathrm{m}^2} = 0.22 \cdot 10^{-3} \frac{\mathrm{N}}{\mathrm{mm}^2}$$

The bending stress in the first layer, due to the eccentricity of the second layer equals:

$$\sigma_{i,2} = \frac{M}{W} = \frac{F \cdot a}{\frac{1}{6} 1 \cdot b^2} = \frac{(0.01 \cdot 0.1 \cdot 1) \cdot 2200 \cdot 9.81 \cdot 0.01}{\frac{1}{6} \cdot 1 \cdot 0.1^2} = 129 \frac{\mathrm{N}}{\mathrm{m}^2} = 0.129 \cdot 10^{-3} \frac{\mathrm{N}}{\mathrm{mm}^2}$$

The total normal stress in the first layer varies over the cross-section, as represented in Figure G - 2.

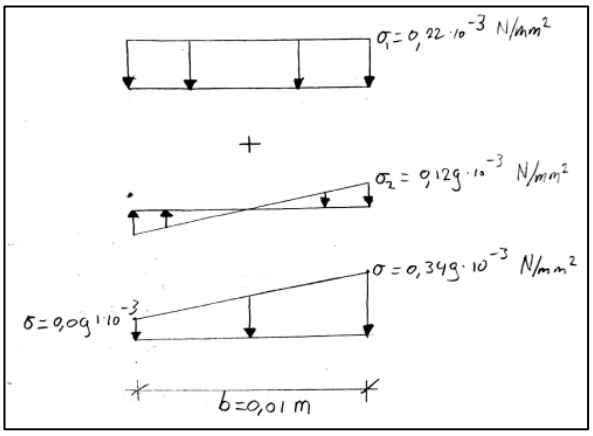

Figure G - 2 Total stress in layer 1 when layer 2 is added.

The extra normal stress in the first layer when the third layer is added equals:

$$\sigma_1 = \frac{F}{A} + \frac{M}{W} = \frac{(0.01 \cdot 0.1 \cdot 1) \cdot 2200 \cdot 9.81}{0.1 \cdot 1} + \frac{(0.01 \cdot 0.1 \cdot 1) \cdot 2200 \cdot 9.81 \cdot 0.02}{\frac{1}{6} 1 \cdot 0.1^2} = (0.22 + 0.258) \cdot 10^{-3} \frac{\mathrm{N}}{\mathrm{mm}^2}$$

Then, the total normal stress is represented in Figure G - 3.

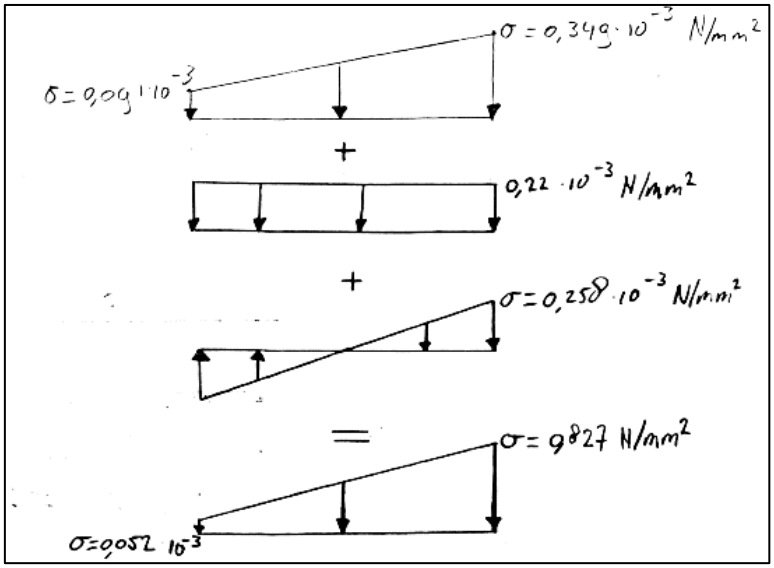

Figure G - 3 Total stress in layer 1 when layer 3 is added.

The stress in the lowest layer can be calculated for each layer that is added on top, to get the total stress in the lowest layer, for all layers that are added on top.

Verification of elastic buckling

Elastic buckling is the second failure mode of printed concrete. This has to do with the geometry and stability of the structure. The model that is used to predict the buckling height is presented in Section

2.1. The vertical wall growth velocity (Eq. F-3) can be simplified by modelling it as a continuous growing process, which depends on several printing parameters.

$$\dot{l} = \frac{Q}{v_n \cdot b \cdot T_l} \tag{F-3}$$

The increase of stiffness is given with the curing rate ξ_E. This curing rate can be determined by measuring the stiffness of the printed concrete at different time steps after the concrete is deposited. In this report, the initial stiffness and curing rate of stiffness are taken from Figure G - 4, based on experiments by Suiker (Suiker, 2018). From this, the linear relation equals:

$$E = 0.0781 + 0.0012 \cdot t \tag{F.4}$$

Then, the curing rate equals:

$$\xi_E^l = \frac{0.0781}{0.0012} = 0.0154\ \text{min}^{-1} = 2.6 \cdot 10^{-4}\ \text{s}^{-1}$$

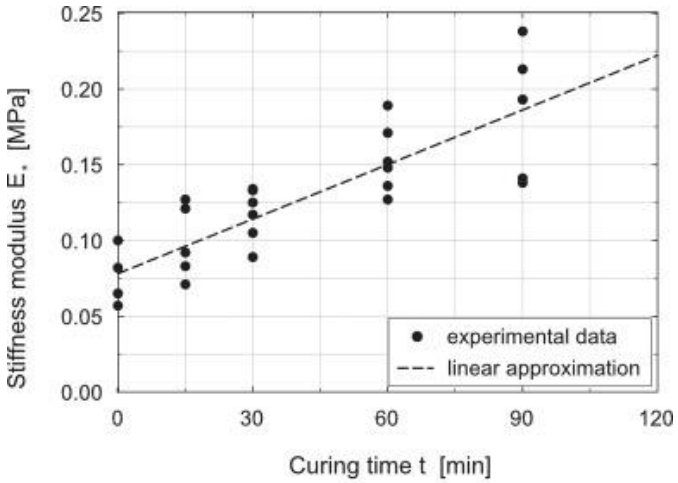

Figure G - 4 Initial stiffness and increase of stiffness for printed concrete, coming from experiments (Suiker, 2018)

Case 1: Free wall

In case of a free wall, the critical height can be calculated with the approximation given in Eq. F.5

$$\bar{l}_{cr} = \left(\frac{\rho \cdot g \cdot b}{D_0}\right)^{\frac{1}{3}} \cdot l_{cr} \tag{F.5a}$$

$$\bar{l}_{cr} = 1.98635 + 0.996 \cdot \left(\bar{\xi}_E^l\right)^{0.793} \tag{F.5b}$$

Where:

$$\bar{\xi}_E^l = \left(\frac{D_0}{\rho \cdot g \cdot b}\right)^{\frac{1}{3}} \cdot \frac{\xi_E^l}{\dot{l}} \tag{F.6}$$

$$D_0 = \frac{E_0 \cdot b^3}{12 \cdot (1 - \nu^2)} \tag{F.7}$$

Where:

l_{cr}	= critical buckling height	[m]
ξ_E	= curing rate elastic stiffness	[s^{-1}]
D_0	= initial bending stiffness	[Nm]
E_0	= initial elastic stiffness	[N/m^2]
ν	= Poisson's ratio = 0.3	[-]

The parameters depend on the number of the layer, as the cross-section changes over height. The calculation is shown for the middle of the sphere. The corresponding parameters are:

Q	$= 0.25/3600 = 6.94*10^{-5}$	[m^3/s]
R	$= 15$	[m]
b	$= 0.1$	[m]
h	$= 0.01$	[m]
v_n	$= Q/(b*h) = 0.0694$	[m/s]
T_l	$= (\pi*2*R)/v_n = 1358$	[s]

The vertical growth equals:

$$\dot{l} = \frac{Q}{v_n \cdot b \cdot T_l} = \frac{6.94 \cdot 10^{-5}}{0.0694 \cdot 0.1 \cdot 1358} = 7.36 \cdot 10^{-6}\,\frac{\mathrm{m}}{\mathrm{s}}$$

$$D_0 = \frac{E_0 \cdot b^3}{12 \cdot (1-\nu^2)} = \frac{0.0781 \cdot 10^6 \cdot 0.1^3}{12 \cdot (1-0.3^2)} = 7.152\ \mathrm{Nm}$$

$$\bar{\xi}_E^l = \left(\frac{D_0}{\rho \cdot g \cdot b}\right)^{\frac{1}{3}} \cdot \frac{\xi_E^l}{\dot{l}} = \left(\frac{7.152}{2200 \cdot 9.81 \cdot 0.1}\right)^{\frac{1}{3}} \cdot \frac{2.6 \cdot 10^{-4}}{7.36 \cdot 10^{-6}} = 5.27$$

$$\bar{l}_{cr} = 1.98635 + 0.996 \cdot \left(\bar{\xi}_E^l\right)^{0.793} = 5.71$$

and

$$l_{cr} = \frac{\bar{l}_{cr}}{\left(\frac{\rho \cdot g \cdot b}{D_0}\right)^{\frac{1}{3}}} = \frac{5.71}{\left(\frac{2200 \cdot 9.81 \cdot 0.1}{7.152}\right)^{\frac{1}{3}}} = 0.851\ \mathrm{m}$$

Case 2: Simply supported or Fully-clamped wall

In case of a simply supported and fully clamped wall, de design graphs of Figure G - 5 need to be used to find the dimensionless critical height, depending on the dimensionless linear curing rate and the dimensionless wall width. The dimensionless wall width can be calculated with Eq. F.8.

$$\bar{w} = \left(\frac{\rho \cdot g \cdot b}{D_0}\right)^{\frac{1}{3}} \cdot w \qquad \text{(F.8)}$$

Where:

w = wall width [m]

Eq. F.8 is based on a straight vertical wall. In this particular case, the cross-section is a circle and therefore there is no straight wall. As an estimation, part of the circle will be assumed to be straight with a maximum curvature of 10^o.

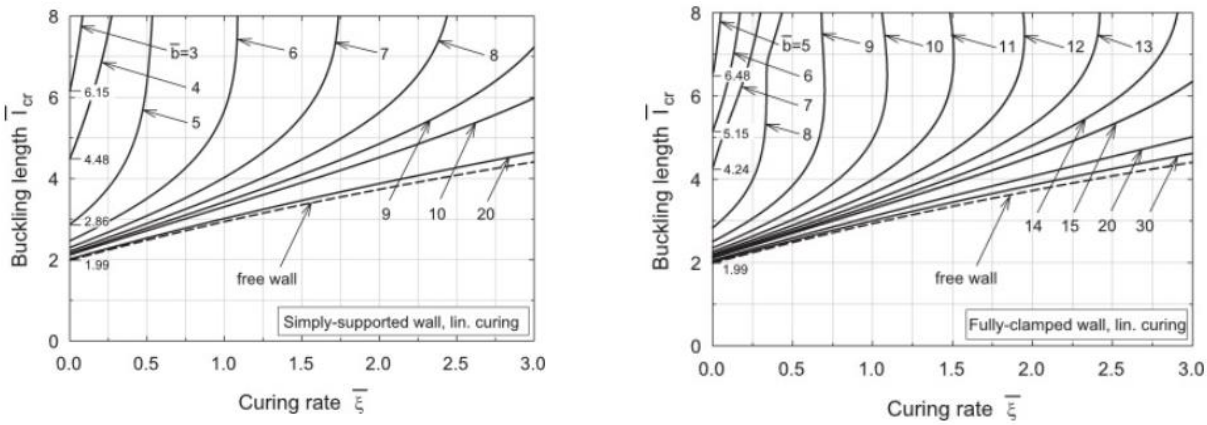

Figure G - 5 Design graphs to obtain the dimensionless critical buckling height in case of simply supported wall and fully-clamped wall (Suiker, 2018)

The buckling length will be calculated for the two most interesting parameters: at the onset of printing (angle of 45°) and at $y=0$, where the wall is vertical.

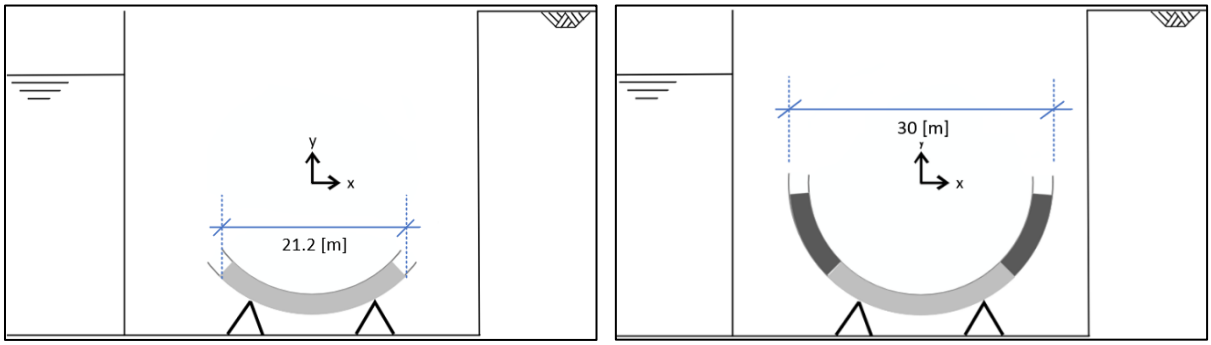

Figure G - 6 The buckling length is calculated for two cases: at the onset of printing (left) and when printing vertical (right)

The corresponding parameters for the first case are (note that for this case a larger pump rate is used, because the same pump rate as for free buckling results in a normalized curing rate which is out of the range of the design graphs):

Q	$= 0.55/3600 = 1.53*10^{-4}$	[m^3/s]
R	$= 10.6$	[m]
b	$= 0.1$	[m]
h	$= 0.01$	[m]
v_n	$= Q/(b*h) = 0.153$	[m/s]
T_l	$= (\pi*2*R)/v_n = 435$	[s]

The width (length) of the part with a maximum curvature of 10° equals:

$$w = \frac{10}{360} \cdot \pi \cdot 2 \cdot R = \frac{10}{360} \cdot \pi \cdot 2 \cdot 10.6 = 1.85 \text{ m}$$

The vertical growth equals:

$$\dot{l} = \frac{Q}{v_n \cdot b \cdot T_l} = \frac{1.53 \cdot 10^{-4}}{0.153 \cdot 0.1 \cdot 435} = 2.30 \cdot 10^{-5} \frac{\text{m}}{\text{s}}$$

$$\bar{\xi}_E^l = \left(\frac{D_0}{\rho \cdot g \cdot b}\right)^{\frac{1}{3}} \cdot \frac{\xi_E^l}{\dot{l}} = \left(\frac{7.152}{2200 \cdot 9.81 \cdot 0.1}\right)^{\frac{1}{3}} \cdot \frac{2.6 \cdot 10^{-4}}{2.30 \cdot 10^{-5}} = 1.69$$

$$\bar{w} = \left(\frac{\rho \cdot g \cdot b}{D_0}\right)^{\frac{1}{3}} \cdot w = \left(\frac{2200 \cdot 9.81 \cdot 0.1}{7.152}\right)^{\frac{1}{3}} \cdot 1.85 = 12.41$$

The normalized buckling length can be found, using Figure G - 7.

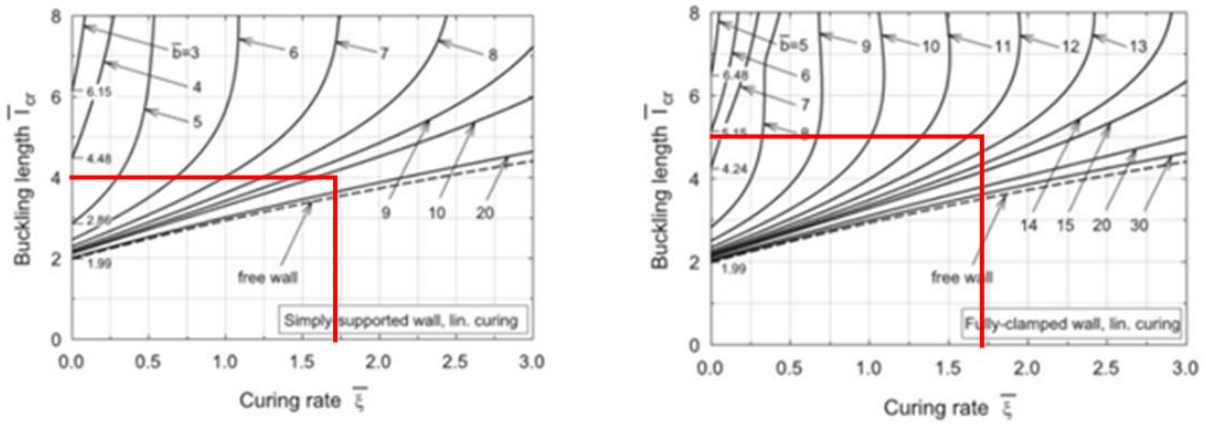

Figure G - 7 The normalized curing rate and normalized width gives the normalized buckling length l_{cr} in case of simply supported wall and fully-clamped wall. The parameters which define the curing rate and normalized width corresponds to the y-value corresponding to an angle of 45 °.

Then, the actual buckling length can be calculated, in case of simply supported and fully-clamped wall:

$$l_{cr,s-s} = \frac{\bar{l}_{cr}}{\left(\frac{\rho \cdot g \cdot b}{D_0}\right)^{\frac{1}{3}}} = \frac{4.0}{\left(\frac{2200 \cdot 9.81 \cdot 0.1}{7.152}\right)^{\frac{1}{3}}} = 0.60 \text{ [m]}$$

$$l_{cr,f-c} = \frac{\bar{l}_{cr}}{\left(\frac{\rho \cdot g \cdot b}{D_0}\right)^{\frac{1}{3}}} = \frac{5.0}{\left(\frac{2200 \cdot 9.81 \cdot 0.1}{7.152}\right)^{\frac{1}{3}}} = 0.75 \text{ [m]}$$

Thus: $0.60 < l_{cr} < 0.75$ [m]

The corresponding parameters for the second case are (note that for this case a larger pump rate is used, because the same pump rate as for free buckling results in a normalized curing rate which is out of the range of the design graphs):

Q	$= 0.5/3600 = 1.53*10^{-4}$	[m^3/s]
R	$= 15$	[m]
b	$= 0.1$	[m]
h	$= 0.01$	[m]
v_n	$= Q/(b*h) = 0.153$	[m/s]
T_l	$= (\pi*2*R)/v_n = 616$	[s]

The width (length) of the part with a maximum curvature of 10° equals:

$$w = \frac{10}{360} \cdot \pi \cdot 2 \cdot R = \frac{10}{360} \cdot \pi \cdot 2 \cdot 15 = 2.62 \text{ m}$$

The vertical growth equals:

$$\dot{l} = \frac{Q}{v_n \cdot b \cdot T_l} = \frac{1.53 \cdot 10^{-4}}{0.153 \cdot 0.1 \cdot 616} = 1.62 \cdot 10^{-5} \frac{\text{m}}{\text{s}}$$

$$\bar{\xi}_E^l = \left(\frac{D_0}{\rho \cdot g \cdot b}\right)^{\frac{1}{3}} \cdot \frac{\xi_E^l}{i} = \left(\frac{7.152}{2200 \cdot 9.81 \cdot 0.1}\right)^{\frac{1}{3}} \cdot \frac{2.6 \cdot 10^{-4}}{1.62 \cdot 10^{-5}} = 2.39$$

$$\bar{w} = \left(\frac{\rho \cdot g \cdot b}{D_0}\right)^{\frac{1}{3}} \cdot w = \left(\frac{2200 \cdot 9.81 \cdot 0.1}{7.152}\right)^{\frac{1}{3}} \cdot 2.62 = 17.57$$

The normalized buckling length can be found, using Figure G - 8.

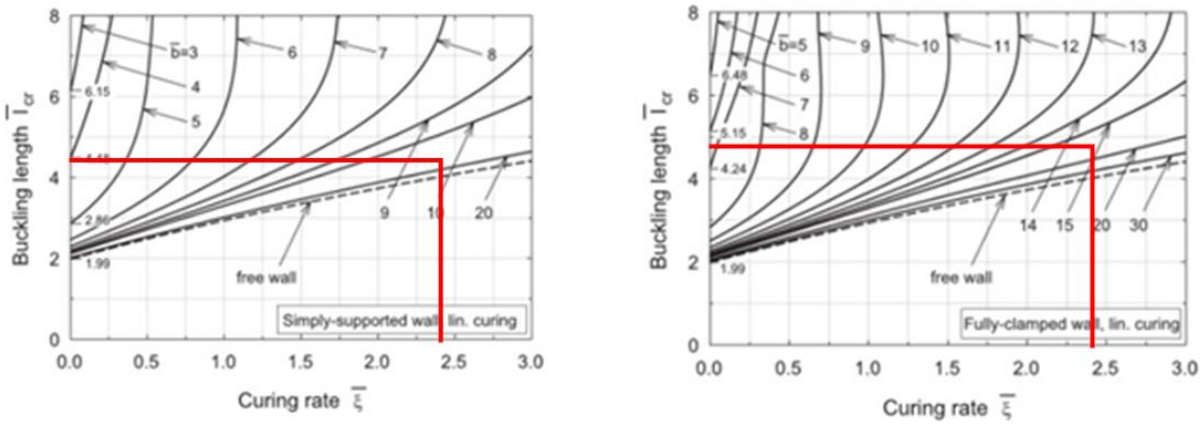

Figure G - 8 The normalized curing rate and normalized width gives the normalized buckling length l_{cr} in case of simply supported wall and fully-clamped wall. The parameters which define the curing rate and normalized width corresponds to the y-value corresponding to an angle of 0 ^{o} (y=0).

Then, the actual buckling length can be calculated, in case of simply supported and fully-clamped wall:

$$l_{cr,s-s} = \frac{\bar{l}_{cr}}{\left(\frac{\rho \cdot g \cdot b}{D_0}\right)^{\frac{1}{3}}} = \frac{4.4}{\left(\frac{2200 \cdot 9.81 \cdot 0.1}{7.152}\right)^{\frac{1}{3}}} = 0.65 \text{ [m]}$$

$$l_{cr,f-c} = \frac{\bar{l}_{cr}}{\left(\frac{\rho \cdot g \cdot b}{D_0}\right)^{\frac{1}{3}}} = \frac{4.7}{\left(\frac{2200 \cdot 9.81 \cdot 0.1}{7.152}\right)^{\frac{1}{3}}} = 0.70 \text{ [m]}$$

Thus: $0.65 < l_{cr} < 0.70$ [m]

The calculation is shown in case of construction in the dry. The same procedure is used in case of submerged construction and construction on a pontoon. The relevant parameters for these variants are given in Section 4.3.3 and Section 4.3.4.

H. RFEM results regarding the thickness of the sphere and required concrete class

In this appendix, the input used in RFEM is stated. Besides that, the elaborate results are shown for different construction methods. This is used in step 2.7 (a quantitative verification is made for the variants) of the design.

Input RFEM

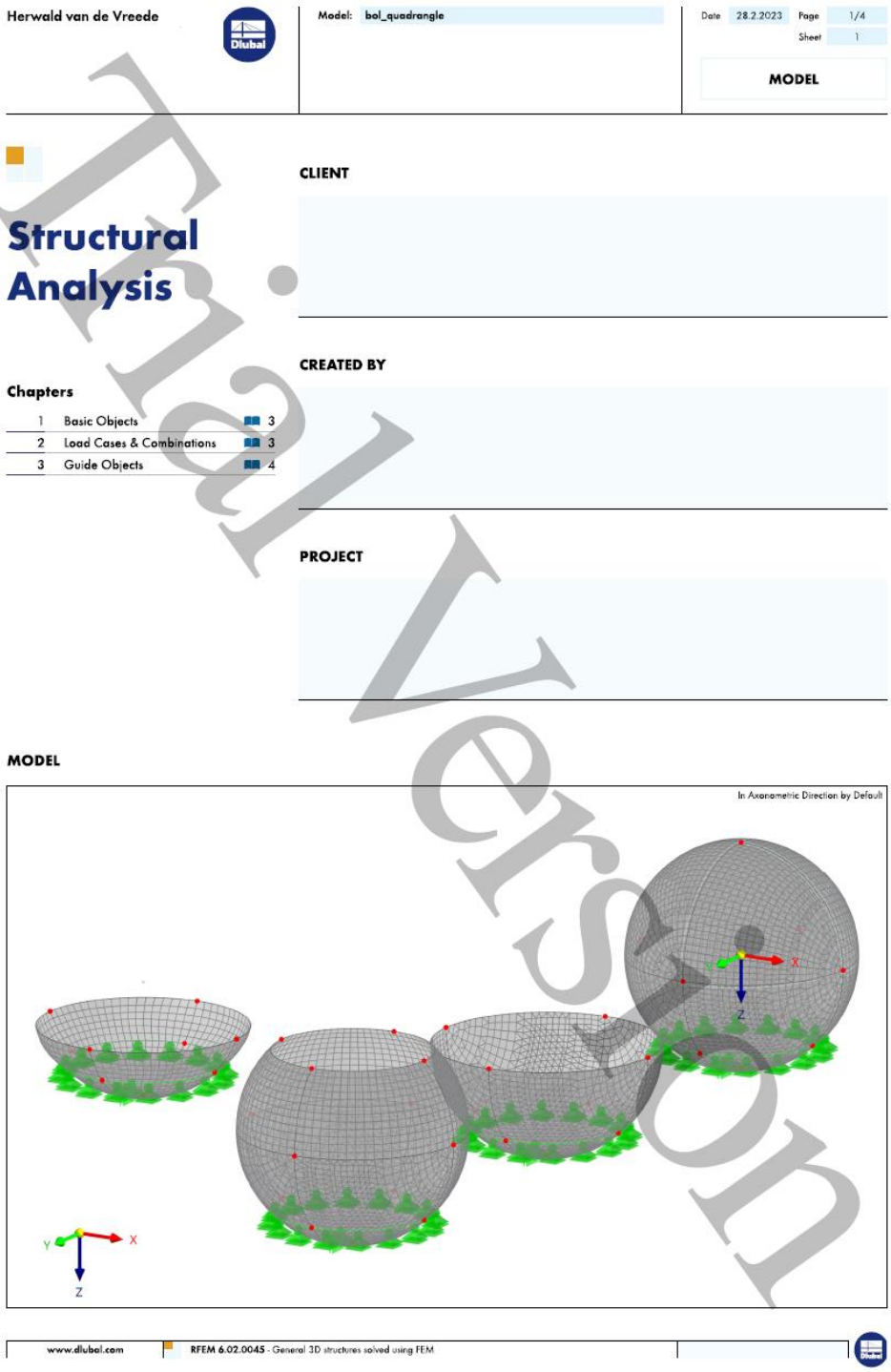

Herwald van de Vreede

Model: bol_quadrangle

Date 28.2.2023 Page 1/4 Sheet 1

MODEL

Structural Analysis

CLIENT

CREATED BY

PROJECT

Chapters

1	Basic Objects	3
2	Load Cases & Combinations	3
3	Guide Objects	4

MODEL

In Axonometric Direction by Default

www.dlubal.com RFEM 6.02.0045 - General 3D structures solved using FEM

CONTENTS

A MODEL - LOCATION

Location		
	Country	: --
	Street	:
	Zip / Postal code	:
	City	:
	State	:
	Latitude	: deg
	Longitude	: deg
	Altitude	: m

1 Basic Objects

1.1 MATERIALS

Material No.	Material Name	Material Type	Analysis Model
3	C60/75 | Isotropic | Linear Elastic	Concrete	Isotropic | Linear Elastic

1.2 THICKNESSES

Thick. No.	Type	Assigned to Surface No.	Material	Thickness Symbol	Value	Unit	Nodes	Direction
1	Uniform | d : 2500.0 mm | 3 - C60/75							
	Uniform	7-10,12-23,25-28,58-65	3	d	2500.0	mm		

2 Load Cases & Combinations

2.1 LOAD CASES

LC No.	Settings	Value	Unit	To Solve
1	G Self-weight			
	Analysis type	Static Analysis		☒
	Static analysis settings	SA1 - Geometrically linear		
	Action category	G Permanent		
	Self-weight - Factor in direction X	0.000	--	
	Self-weight - Factor in direction Y	0.000	--	
	Self-weight - Factor in direction Z	1.000	--	
2	G hydrostatic outside			
	Analysis type	Static Analysis		☒
	Static analysis settings	SA1 - Geometrically linear		
	Action category	G Permanent		

2.2 STATIC ANALYSIS SETTINGS

Settings No.	Description	Symbol	Value	Unit
1	Geometrically linear			
	Analysis type		Geometrically linear	
	Modify standard precision and tolerance settings		☐	
	Modify loading by multiplier factor		☐	
	Displacements due to member load of type 'Pipe internal pressure' (Bourdon effect)		☐	
	Method for equation system		Direct	
	Plate bending theory		Mindlin	
	Activate mass conversion to load		☐	
	Asymmetric direct solver		☒	
	Equilibrium for undeformed structure		☐	
2	Second-order (P-Δ) | Picard | 100 | 1			
	Analysis type		Second-order (P-Δ)	
	Iterative method for nonlinear analysis		Picard	
	Maximum number of iterations		100	
	Number of load increments		1	
	Modify standard precision and tolerance settings		☐	
	Ignore all nonlinearities		☐	
	Modify loading by multiplier factor		☐	
	Consider favorable effect due to tension in members		☒	
	Displacements due to member load of type 'Pipe internal pressure' (Bourdon effect)		☐	

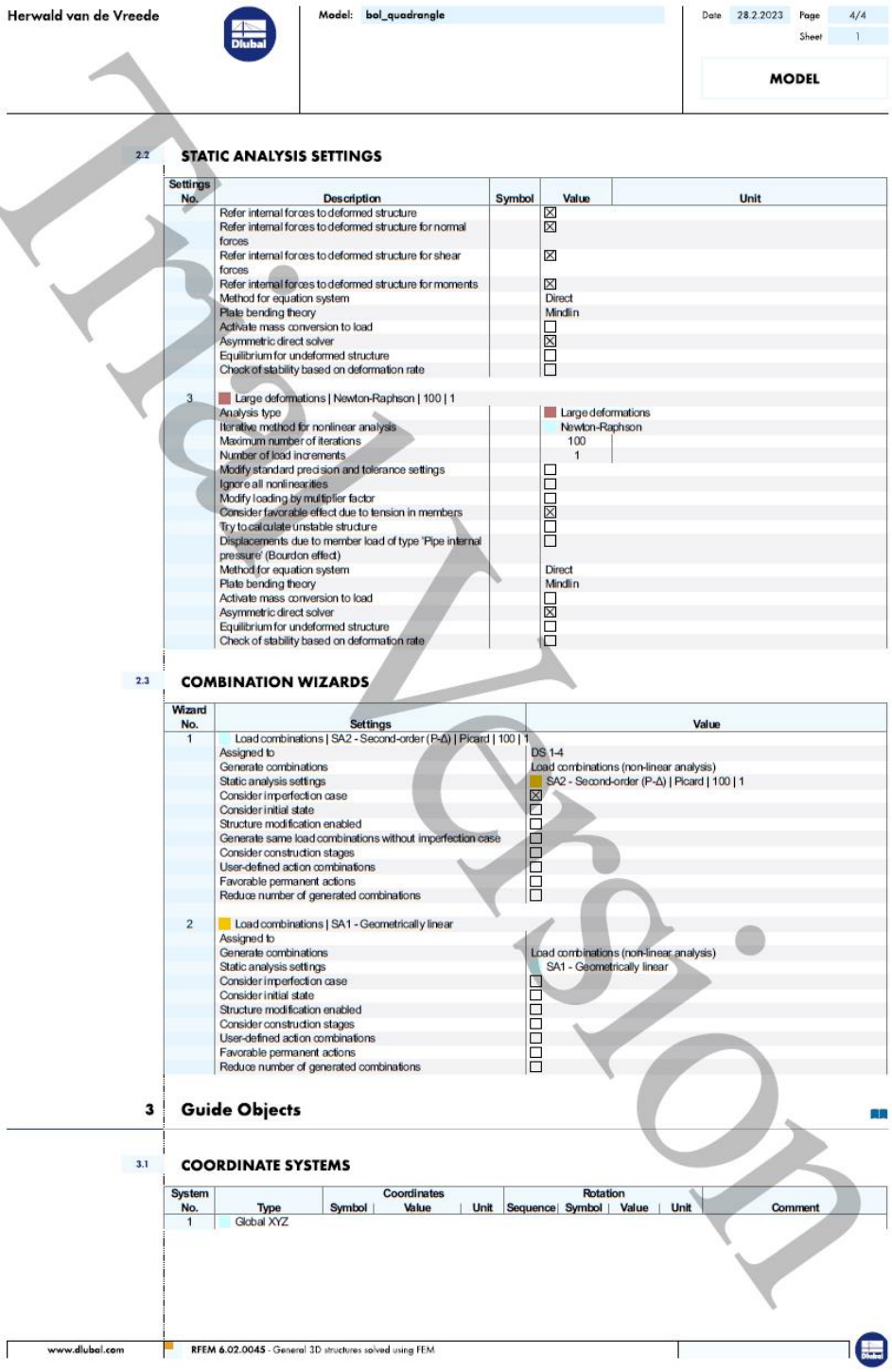

Herwald van de Vreede | Model: bol_quadrangle | Date 28.2.2023 | Page 4/4 | Sheet 1

MODEL

2.2 STATIC ANALYSIS SETTINGS

Settings No.	Description	Symbol	Value	Unit
	Refer internal forces to deformed structure		☒	
	Refer internal forces to deformed structure for normal forces		☒	
	Refer internal forces to deformed structure for shear forces		☒	
	Refer internal forces to deformed structure for moments		☒	
	Method for equation system		Direct	
	Plate bending theory		Mindlin	
	Activate mass conversion to load		☐	
	Asymmetric direct solver		☒	
	Equilibrium for undeformed structure		☐	
	Check of stability based on deformation rate		☐	
3	Large deformations | Newton-Raphson | 100 | 1			
	Analysis type		Large deformations	
	Iterative method for nonlinear analysis		Newton-Raphson	
	Maximum number of iterations		100	
	Number of load increments		1	
	Modify standard precision and tolerance settings		☐	
	Ignore all nonlinearities		☐	
	Modify loading by multiplier factor		☐	
	Consider favorable effect due to tension in members		☒	
	Try to calculate unstable structure		☐	
	Displacements due to member load of type 'Pipe internal pressure' (Bourdon effect)		☐	
	Method for equation system		Direct	
	Plate bending theory		Mindlin	
	Activate mass conversion to load		☐	
	Asymmetric direct solver		☒	
	Equilibrium for undeformed structure		☐	
	Check of stability based on deformation rate		☐	

2.3 COMBINATION WIZARDS

Wizard No.	Settings	Value
1	Load combinations | SA2 - Second-order (P-Δ) | Picard | 100 | 1	
	Assigned to	DS 1-4
	Generate combinations	Load combinations (non-linear analysis)
	Static analysis settings	SA2 - Second-order (P-Δ) | Picard | 100 | 1
	Consider imperfection case	☒
	Consider initial state	☐
	Structure modification enabled	☐
	Generate same load combinations without imperfection case	☐
	Consider construction stages	☐
	User-defined action combinations	☐
	Favorable permanent actions	☐
	Reduce number of generated combinations	☐
2	Load combinations | SA1 - Geometrically linear	
	Assigned to	
	Generate combinations	Load combinations (non-linear analysis)
	Static analysis settings	SA1 - Geometrically linear
	Consider imperfection case	☐
	Consider initial state	☐
	Structure modification enabled	☐
	Consider construction stages	☐
	User-defined action combinations	☐
	Favorable permanent actions	☐
	Reduce number of generated combinations	☐

3 Guide Objects

3.1 COORDINATE SYSTEMS

System No.	Type	Coordinates Symbol	Coordinates Value	Coordinates Unit	Rotation Sequence	Rotation Symbol	Rotation Value	Rotation Unit	Comment
1	Global XYZ								

www.dlubal.com | RFEM 6.02.0045 - General 3D structures solved using FEM

The sphere is support with a hinged support at 45 degrees (fixed displacement in global z-direction and fixed rotation around global z-axis), which represents the support of the pedestal. To avoid an error in RFEM, the translation is fixed in global x- and y-direction at the bottom of the sphere.

Results of deformations and stresses in the sphere in use phase.

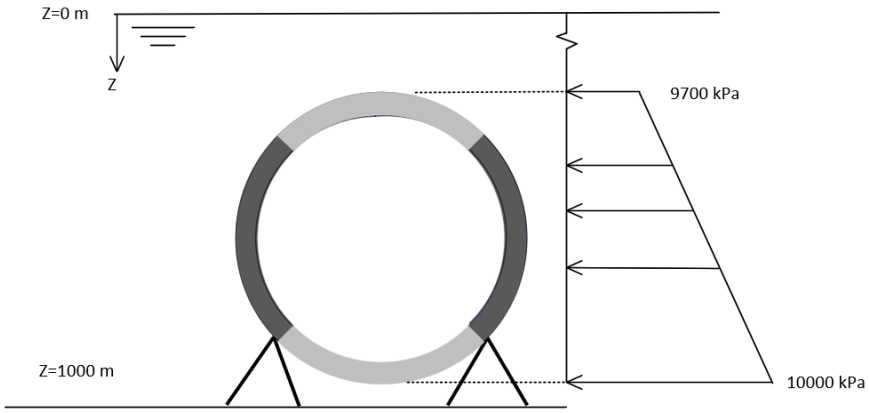

Figure H - 1 A hydrostatic pressure is applied at the outside of the sphere (the pressure is perpendicular to the surface). The support of the pedestal is modelled with a hinged support at an angle of 45°.

Result of global deformations:

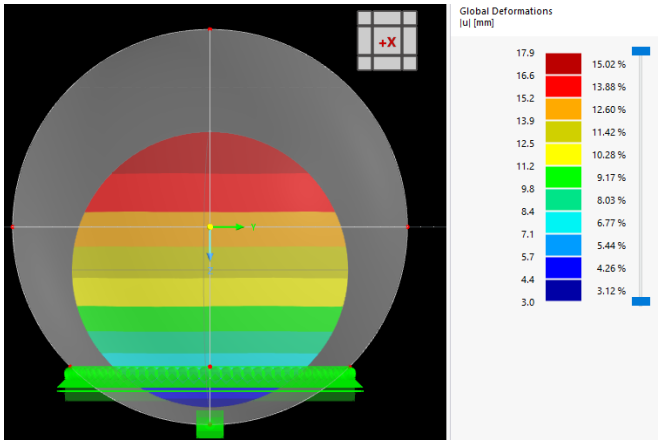

Figure H - 2 Global deformation of the sphere in use phase.

Result of stresses in local x-direction at inside (left) and outside (right)

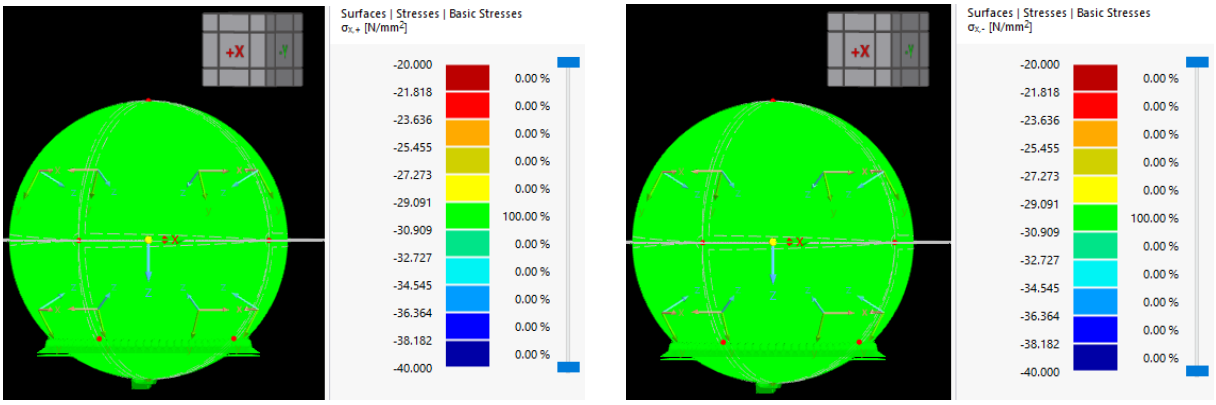

Figure H - 3 Result of stresses in local x-direction at inside (left) and outside (right)

Result of stresses in local y-direction at inside (left) and outside (right)

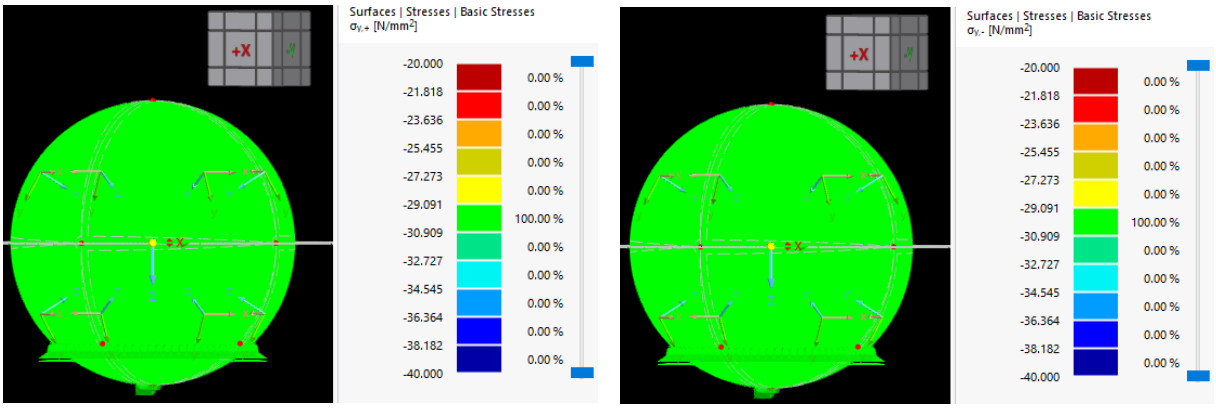

Figure H - 4 Result of stresses in local y-direction at inside (left) and outside (right).

Result of deformations and stresses for 3DCP construction method 1: 3DCP + cast in place

The results are shown at 3 different stages during construction: at 50%, 75% and 100%. This is represented in Figure H - 5.

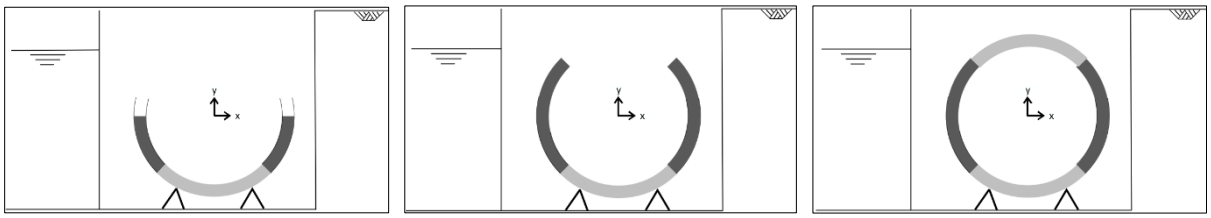

Figure H - 5 The stresses will be analysed at 3 different stages during construction: at 50%, 75% and 100%.

Results at 50% of construction:
Result of global deformations:

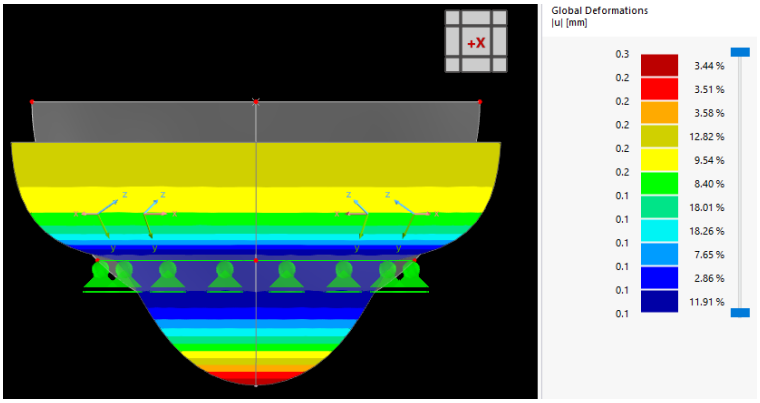

Figure H - 6 Global deformations at 50% of construction.

Result of stresses in local x-direction at inside (left) and outside (right)

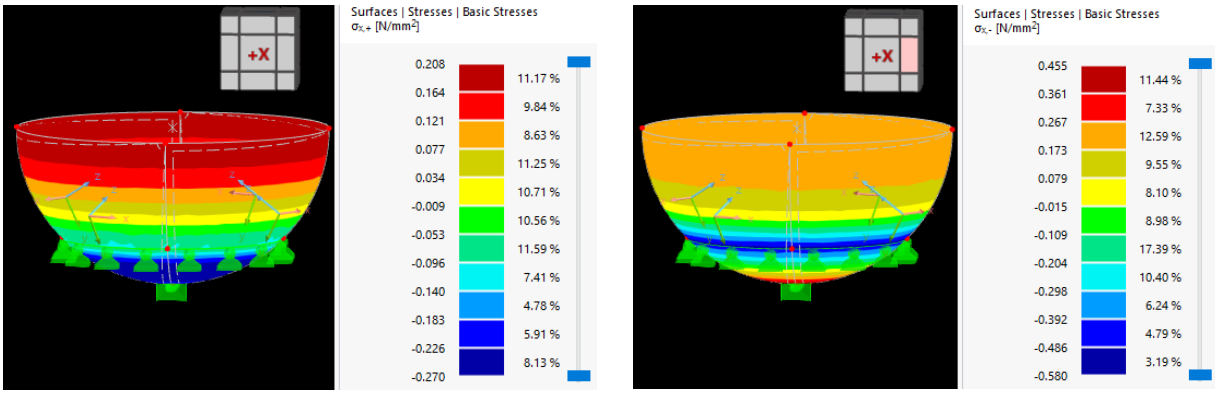

Figure H - 7 Result of stresses in local x-direction at inside (left) and outside (right).

Result of stresses in <u>local</u> y-direction at inside (left) and outside (right)

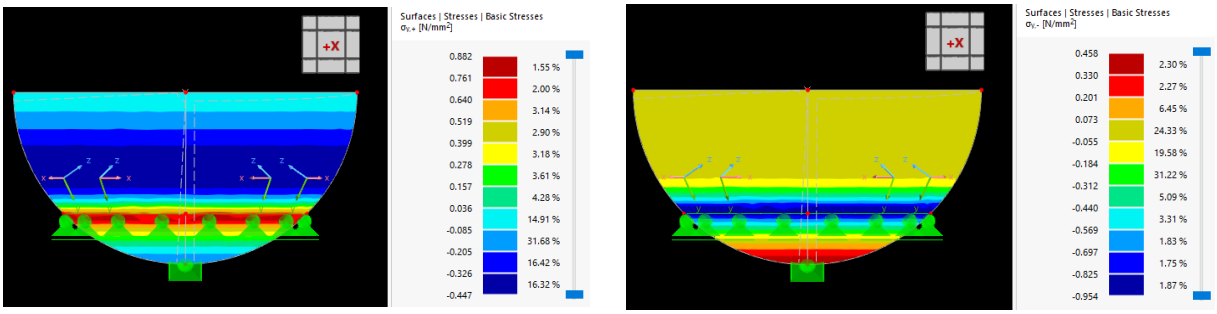

Figure H - 8 Result of stresses in local y-direction at inside (left) and outside (right).

<u>Results at 75% of construction:</u>
Result of <u>global</u> deformations:

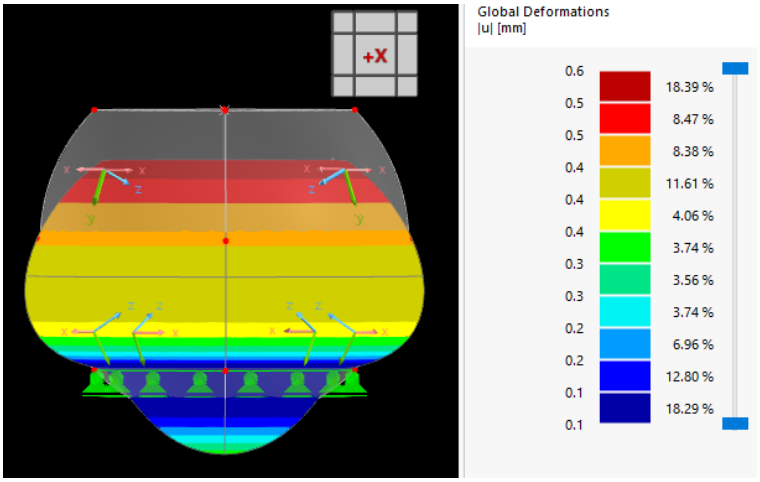

Figure H - 9 Global deformations at 75% of construction.

Result of stresses in <u>local</u> x-direction at inside (left) and outside (right)

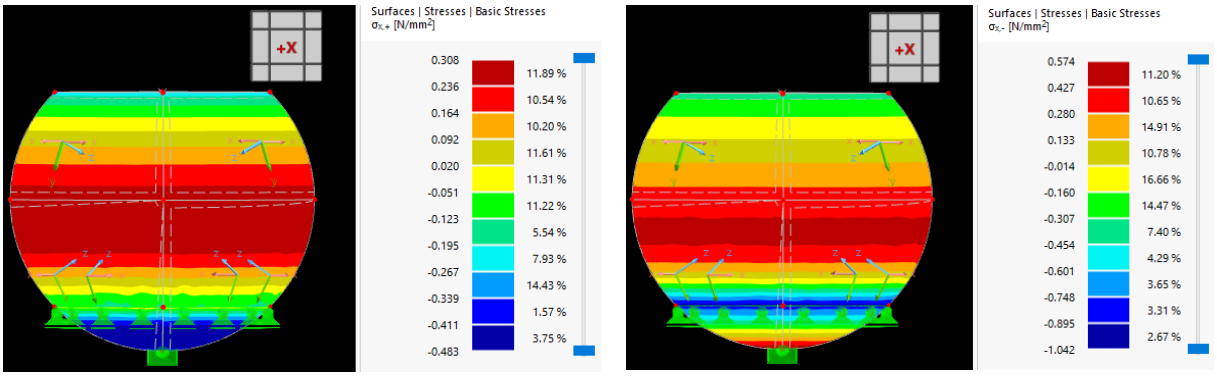

Figure H - 10 Result of stresses in local x-direction at inside (left) and outside (right)

Result of stresses in <u>local</u> y-direction at inside (left) and outside (right)

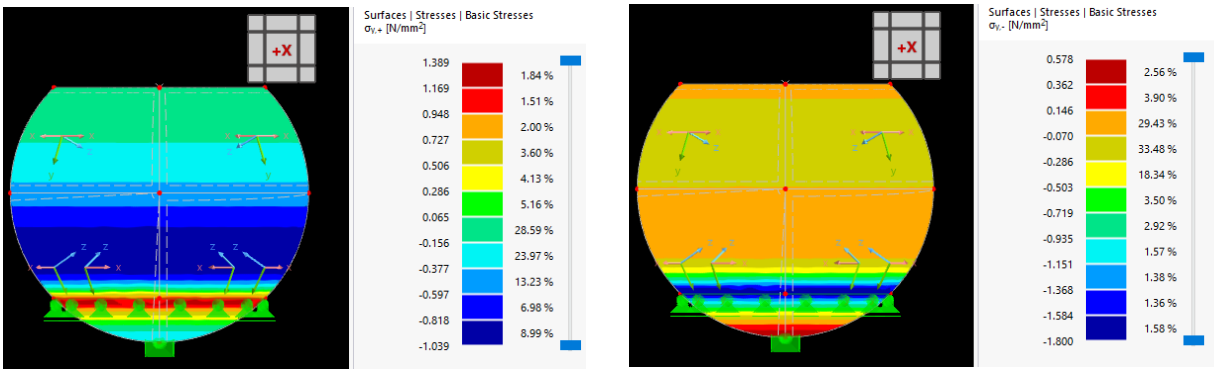

Figure H - 11 Result of stresses in local y-direction at inside (left) and outside (right).

<u>Results at 100% of construction:</u>
Result of <u>global</u> deformations:

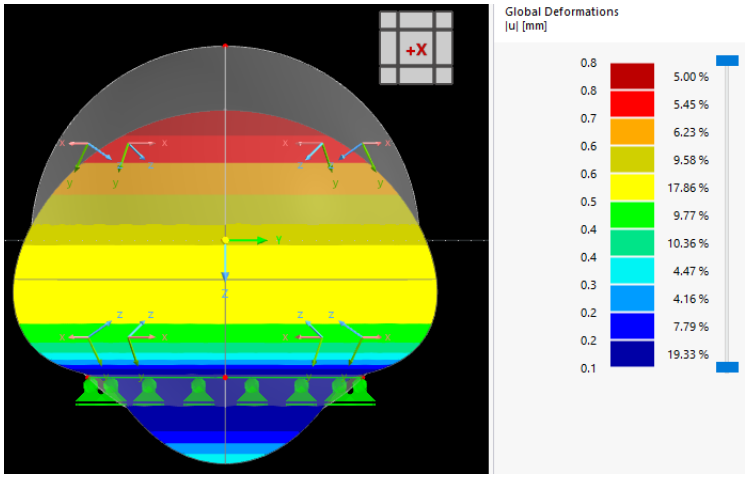

Figure H - 12 Global deformations at 100% of construction

Result of stresses in <u>local</u> x-direction at inside (left) and outside (right)

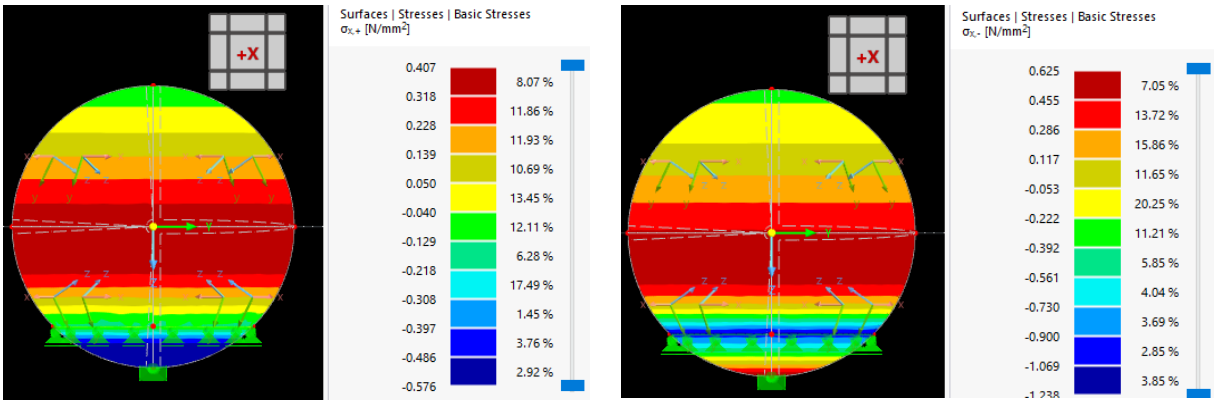

Figure H - 13 Result of stresses in local x-direction at inside (left) and outside (right).

Result of stresses in <u>local</u> y-direction at inside (left) and outside (right)

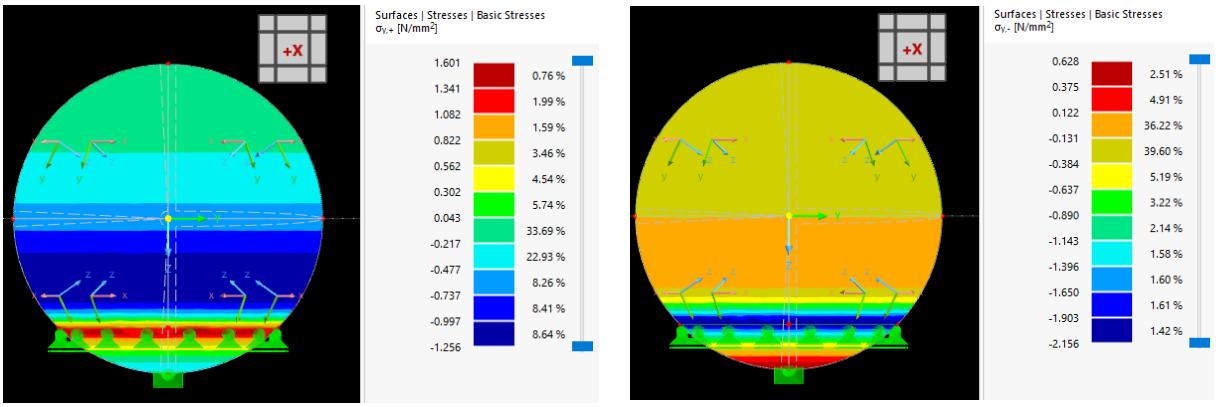

Figure H - 14 Result of stresses in local y-direction at inside (left) and outside (right).

Result of deformations and stresses for 3DCP construction method 2: submerged 3DCP + cast in place

The results are shown at 3 different stages during construction: at 50%, 75% and 100%. This is represented in Figure H - 15.

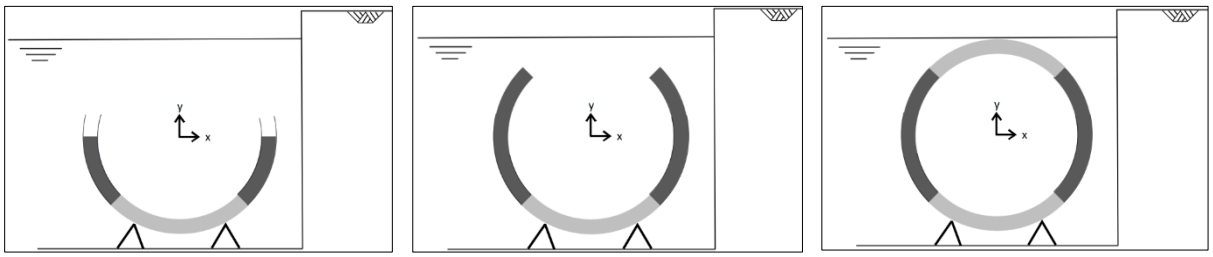

Figure H - 15 The stresses will be analysed at 3 different stages during construction: at 50%, 75% and 100%.

<u>Results at 50% of construction:</u>
Result of <u>global</u> deformations:

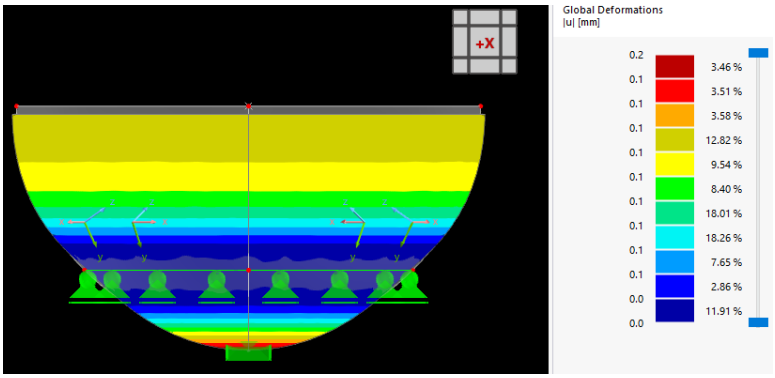

Figure H - 16 Global deformations at 50% of construction.

Result of stresses in <u>local</u> x-direction at inside (left) and outside (right)

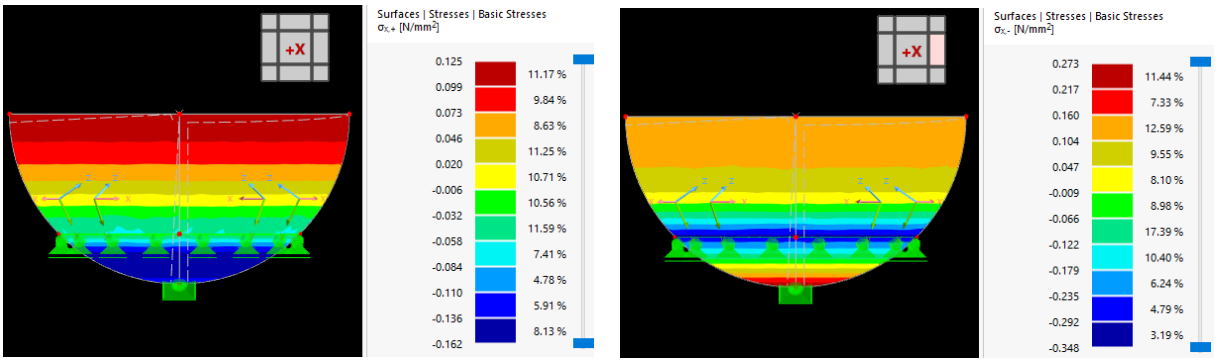

Figure H - 17 Result of stresses in local x-direction at inside (left) and outside (right).

Result of stresses in <u>local</u> y-direction at inside (left) and outside (right)

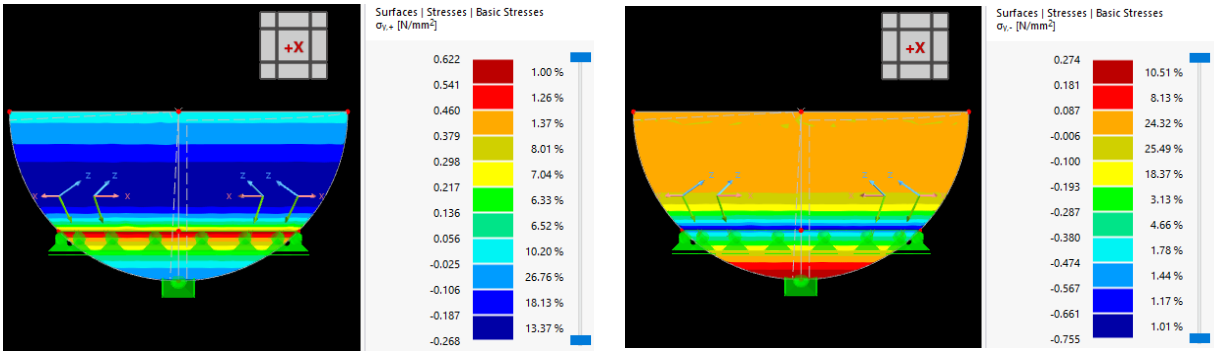

Figure H - 18 Result of stresses in local y-direction at inside (left) and outside (right).

<u>Results at 75% of construction:</u>

Result of <u>global</u> deformations:

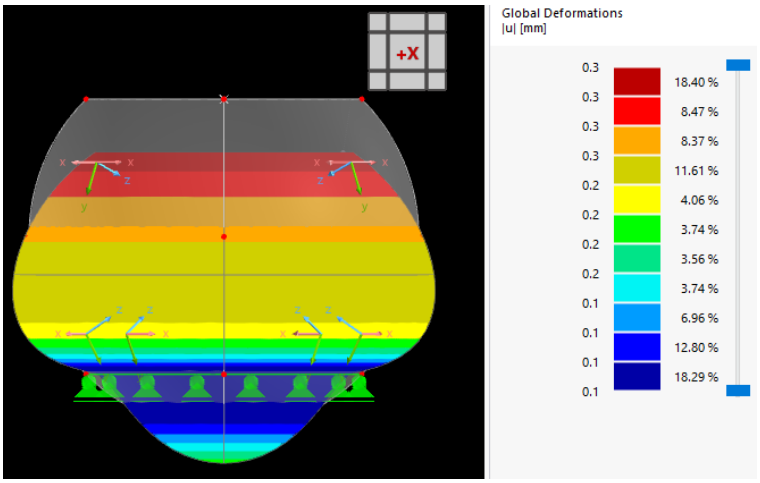

Figure H - 19 Global deformations at 75% of construction.

Result of stresses in <u>local</u> x-direction at inside (left) and outside (right)

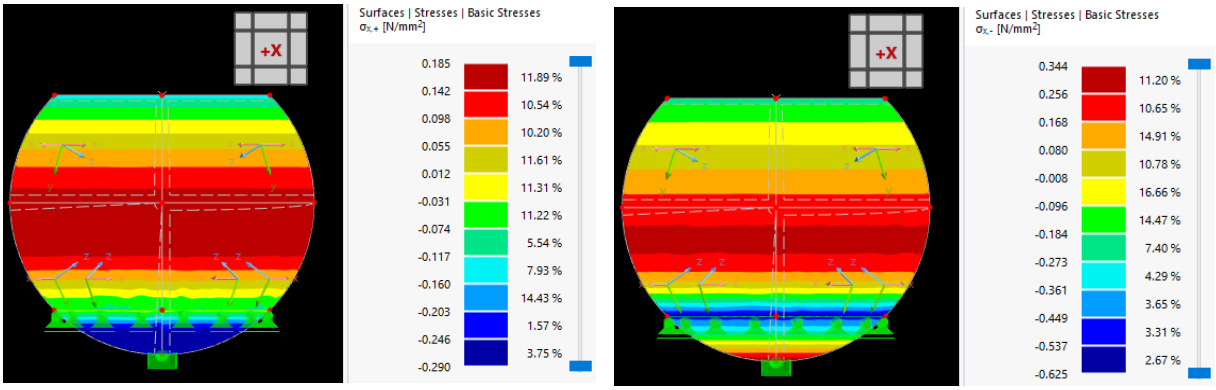

Figure H - 20 Result of stresses in local x-direction at inside (left) and outside (right).

Result of stresses in <u>local</u> y-direction at inside (left) and outside (right)

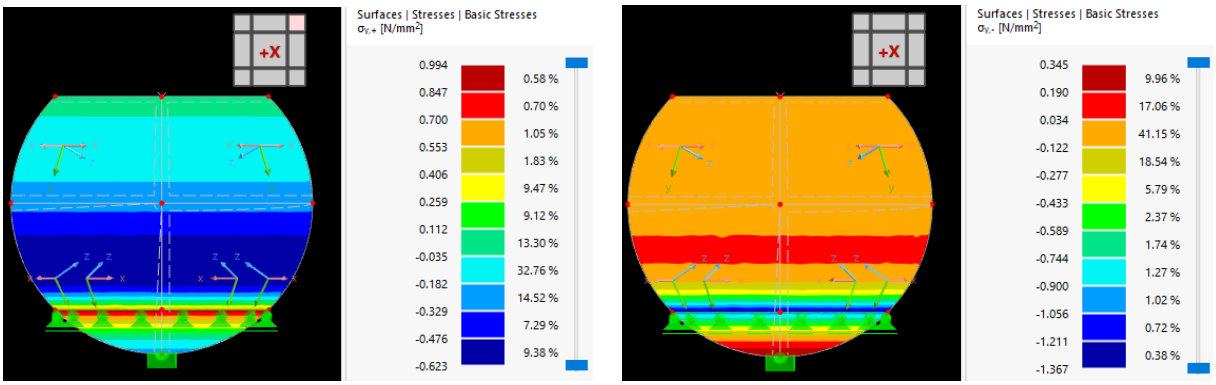

Figure H - 21 Result of stresses in local y-direction at inside (left) and outside (right).

<u>Results at 100% of construction:</u>
Result of <u>global</u> deformations:

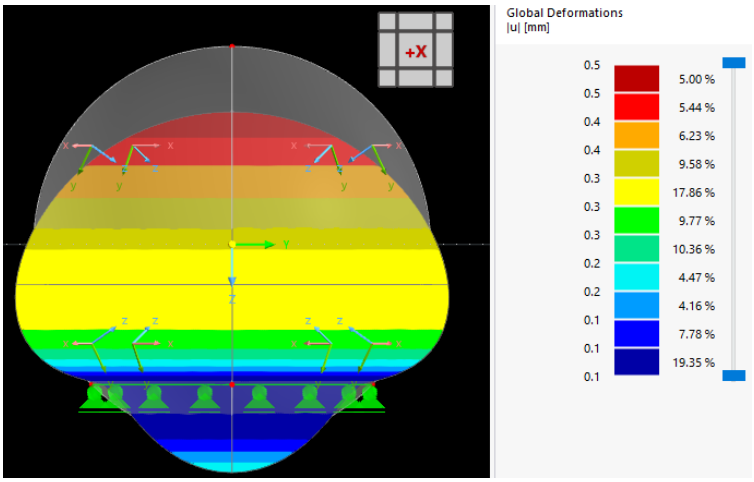

Figure H - 22 Global deformations at 100% of construction

Result of stresses in <u>local</u> x-direction at inside (left) and outside (right)

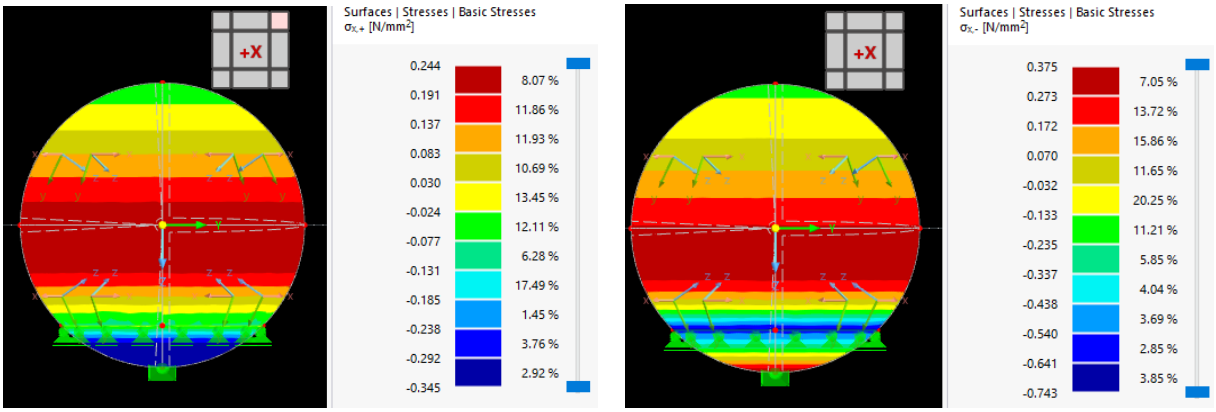

Figure H - 23 Result of stresses in local x-direction at inside (left) and outside (right).

Result of stresses in <u>local</u> y-direction at inside (left) and outside (right)

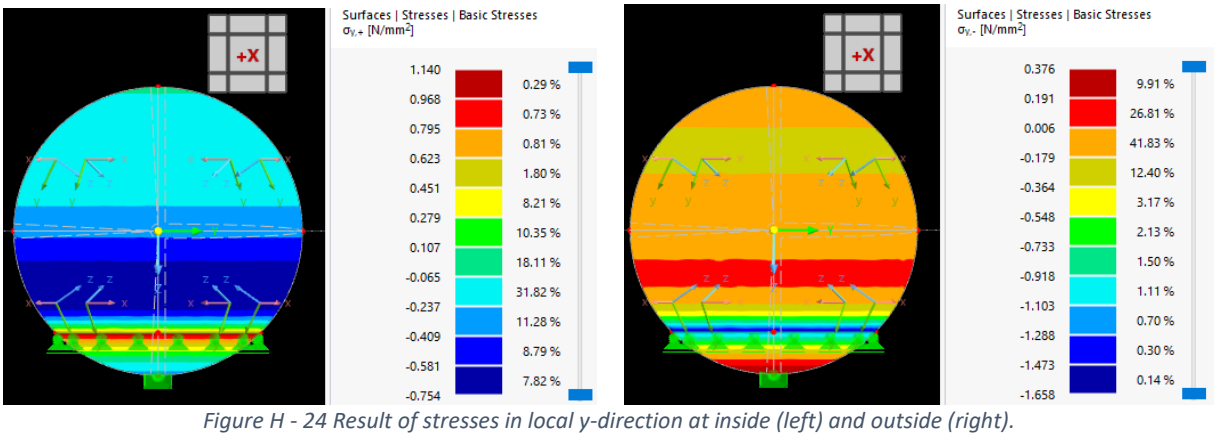

Figure H - 24 Result of stresses in local y-direction at inside (left) and outside (right).

Result of deformations and stresses for 3DCP construction method 3: 3DCP + cast in place on a pontoon

The results are shown at 3 different stages during construction: at 50%, 75% and 100%. This is represented in Figure H - 25.

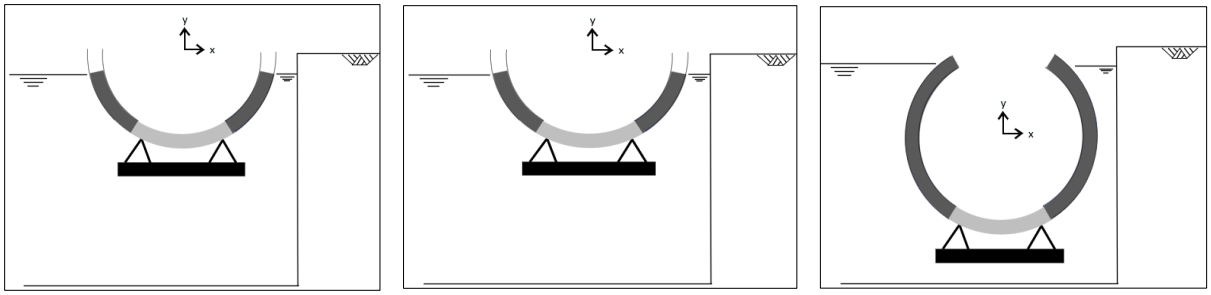

Figure H - 25 The stresses will be analysed at 3 different stages during construction: at 50%, 75% and 100%.

Results at 50% of construction:
Result of global deformations:

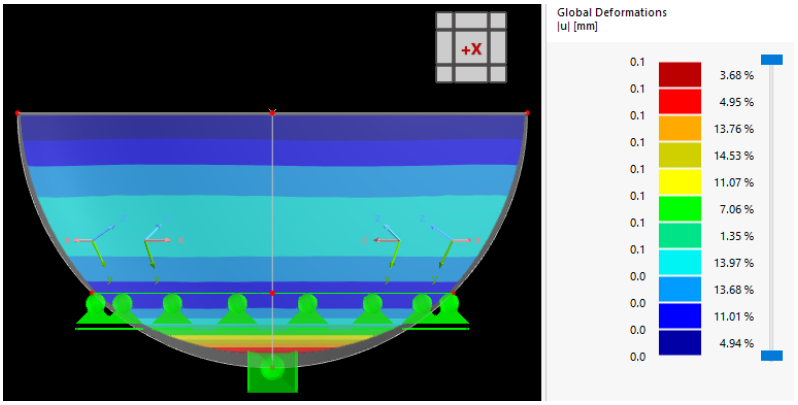

Figure H - 26 Global deformations at 50% of construction.

Result of stresses in local x-direction at inside (left) and outside (right)

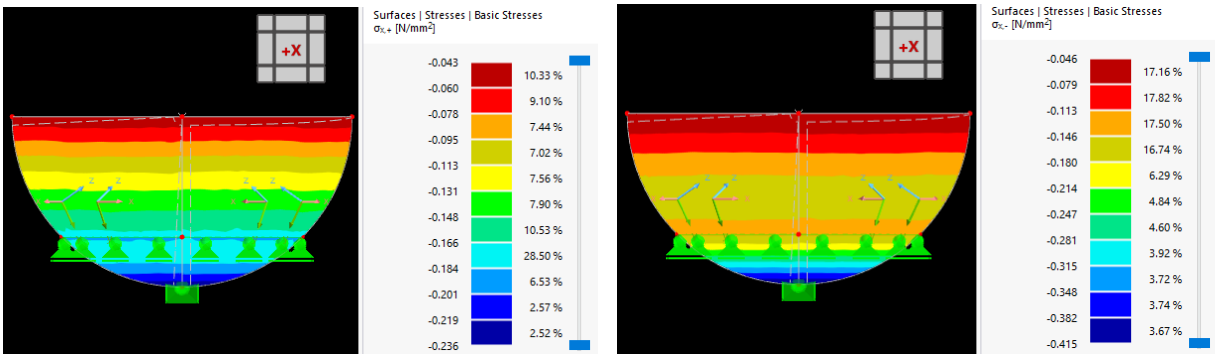

Figure H - 27 Result of stresses in local x-direction at inside (left) and outside (right).

Result of stresses in local y-direction at inside (left) and outside (right)

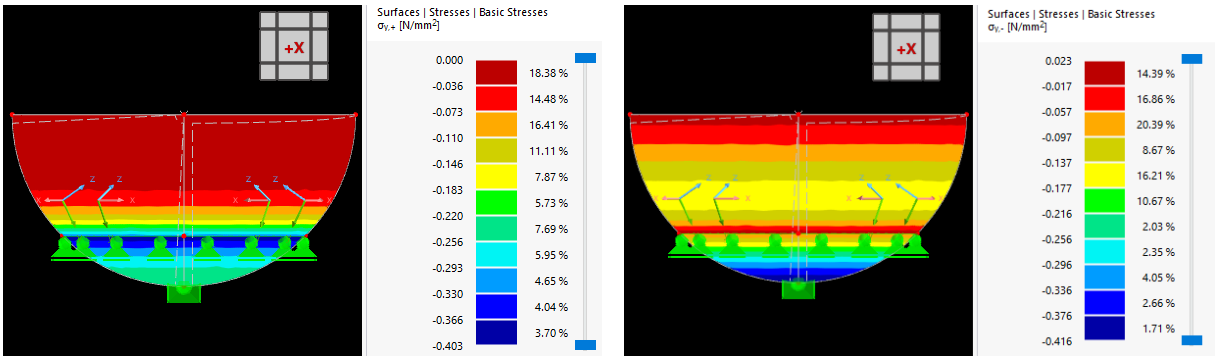

Figure H - 28 Result of stresses in local y-direction at inside (left) and outside (right).

<u>Results at 75% of construction:</u>

Result of <u>global</u> deformations:

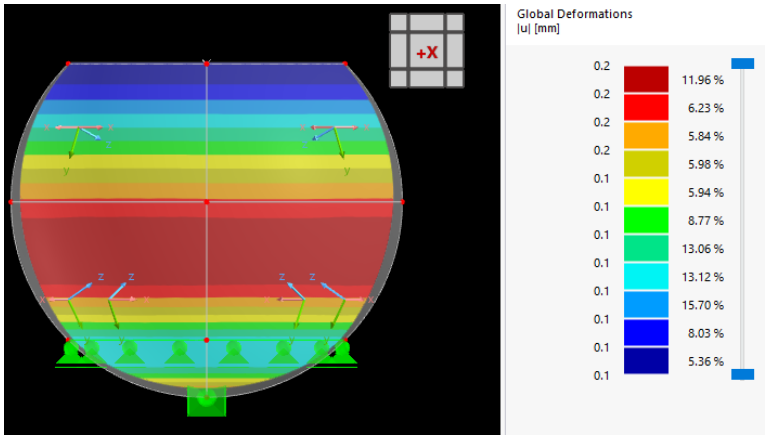

Figure H - 29 Global deformations at 75% of construction.

Result of stresses in <u>local</u> x-direction at inside (left) and outside (right)

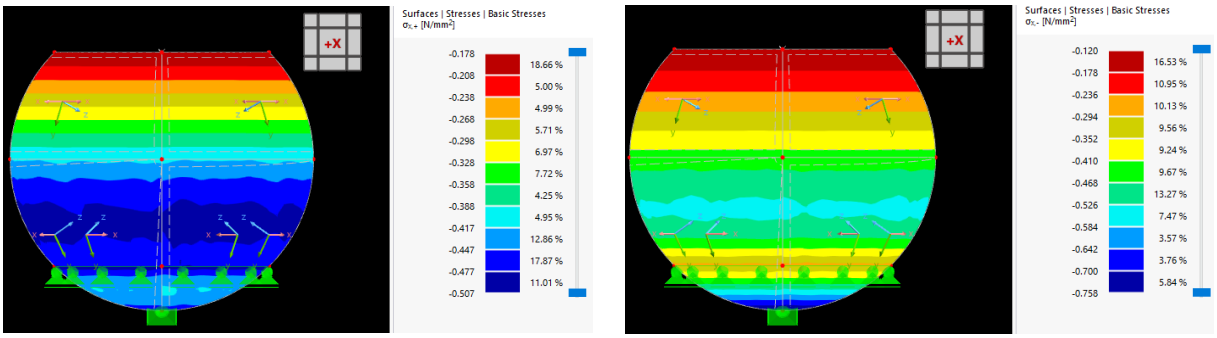

Figure H - 30 Result of stresses in local x-direction at inside (left) and outside (right).

Result of stresses in <u>local</u> y-direction at inside (left) and outside (right)

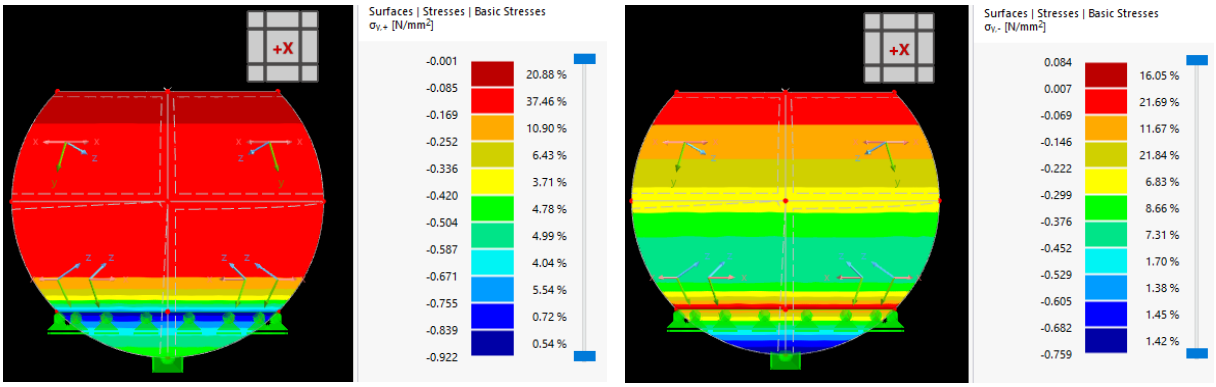

Figure H - 31 Result of stresses in local y-direction at inside (left) and outside (right).

<u>Results at 100% of construction:</u>
Result of <u>global</u> deformations:

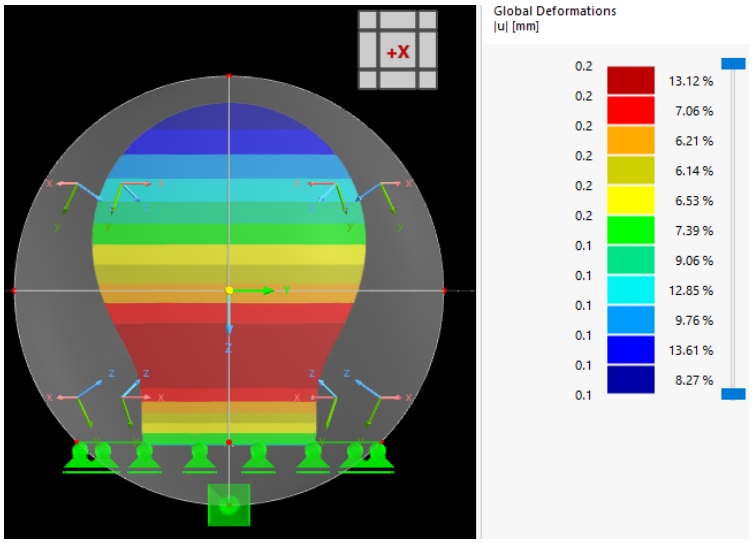

Figure H - 32 Global deformations at 100% of construction

Result of stresses in <u>local</u> x-direction at inside (left) and outside (right)

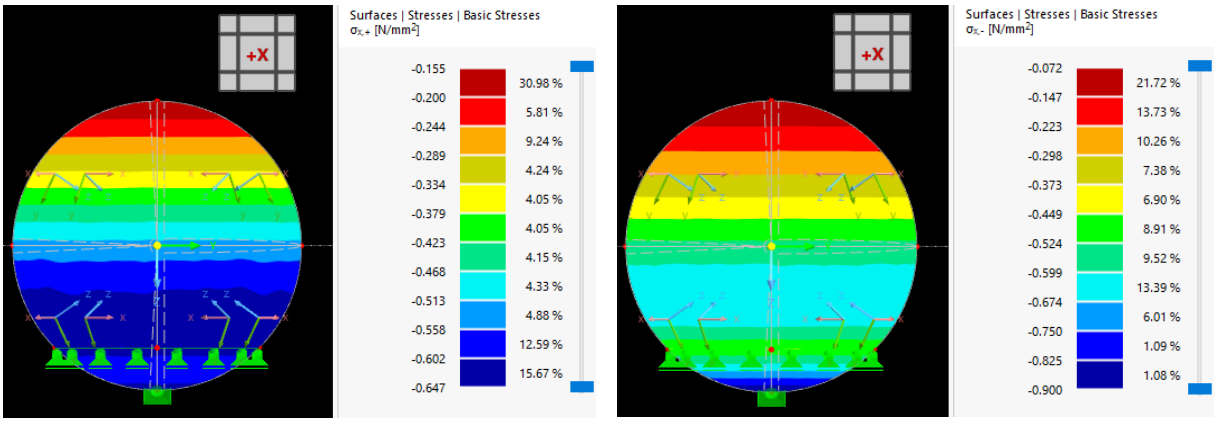

Figure H - 33 Result of stresses in local x-direction at inside (left) and outside (right).

Result of stresses in <u>local</u> y-direction at inside (left) and outside (right)

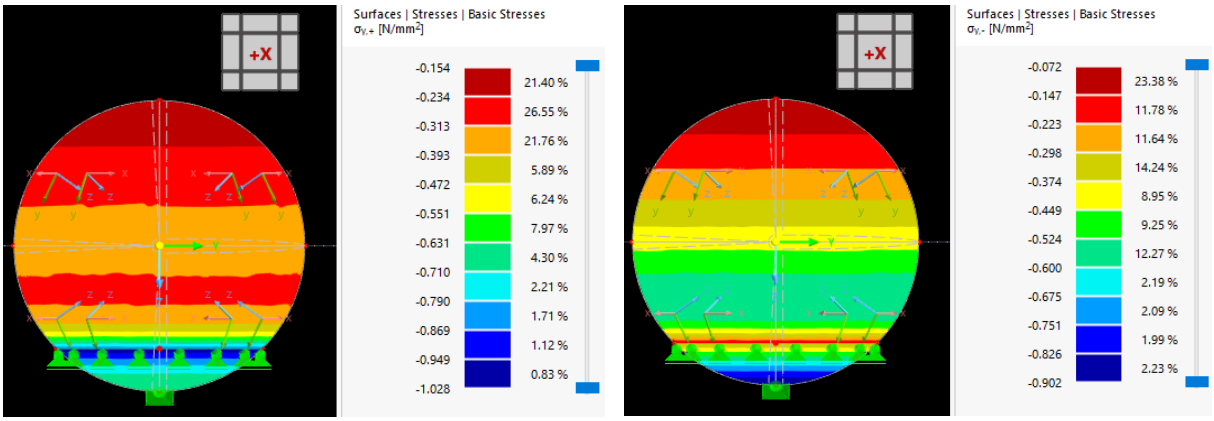

Figure H - 34 Result of stresses in local y-direction at inside (left) and outside (right).

I. Calculation of shrinkage

Because the amount of shrinkage largely determines whether the tensile strength is exceeded, the shrinkage of three most important types is calculated in this appendix. This is used in step 2.9 (the hydration heat is estimated, crack width calculations are performed and watertightness will be verified) of the design.

Thermal shrinkage

The thermal shrinkage depends on the temperature difference and the thermal expansion coefficient of concrete, which is approximately $10*10^{-6}$ / ºC.

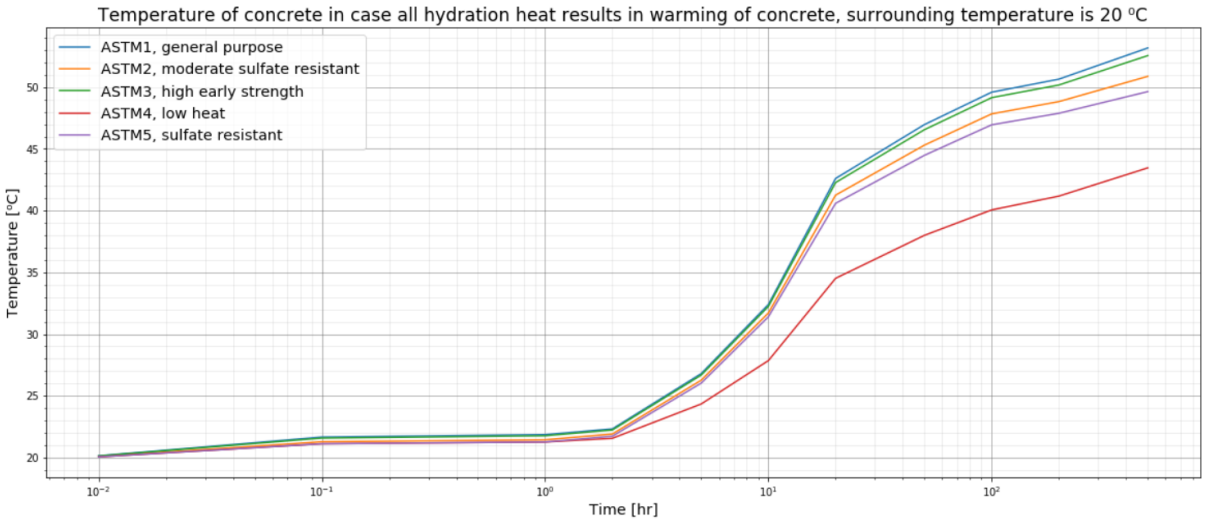

Figure I - 1 Adiabatic temperature increase of different cement types

With Figure I - 1, the shrinkage can be calculated and is given in Table I - 1.

Table I - 1 Thermal shrinkage of cement types

Cement type	**ASTM1**	**ASTM2**	**ASTM3**	**ASTM4**	**ASTM5**
Temperature	48.1	46.0	47.6	38.5	44.8
Shrinkage = α_c*ΔT	$4.81*10^{-4}$	$4.60*10^{-4}$	$4.76*10^{-4}$	$3.85*10^{-4}$	$4.48*10^{-4}$

Drying shrinkage and autogenous shrinkage

Drying shrinkage and autogenous shrinkage are both described in Eurocode 2 (EN 1992, 2011). These two components both depend on time: drying shrinkage develops slowly and ranges from days to months, whereas autogenous shrinkage is linearly linked to the hardening of the concrete, which is mostly in the first days. The total shrinkage is given in Eq. G-1 to Eq. G-4.

$$\varepsilon_{cs,\infty} = \varepsilon_{cd,\infty} + \varepsilon_{ca,\infty} \quad \text{(G-1)}$$

$$\varepsilon_{cd,\infty} = k_h \cdot \varepsilon_{cd,0} \quad \text{(G-2)}$$

Table I - 2 Value for k_h depending on the fictitious thickness of the cross-section

h_0	k_h
100	1,0
200	0,85
300	0,75
≥ 500	0,70

The initial drying shrinkage can be determined with Table I - 3. In this case, the sphere is submerged so the relative humidity is high. As starting point, relative humidity of 90% is chosen. Because the lowest required concrete class is C35/45, this is used as initial input.

Table I - 3 Value of the nominal unrestricted drying shrinkage of concrete with cement CEM and class N [in $^0/_{00}$]

$f_{ck}/f_{ck,cube}$ (MPa)	Relatieve vochtigheid ($^0/_0$)					
	20	40	60	80	90	100
20/25	0.62	0.58	0.49	0.30	0.17	0.00
40/50	0.48	0.46	0.38	0.24	0.13	0.00
60/75	0.38	0.36	0.30	0.19	0.10	0.00
80/95	0.30	0.28	0.24	0.15	0.08	0.00
90/105	0.27	0.25	0.21	0.13	0.07	0.00

Where the fictitious thickness equals:

$$h_0 = 2 \cdot \frac{A_c}{u} \tag{G-3}$$

$$\varepsilon_{ca,\infty} = 2.5 \cdot (f_{ck} - 10) \cdot 10^{-6} \tag{G-4}$$

Where:

ε_{cs}	= total shrinkage	[-]
ε_{cd}	= drying shrinkage	[-]
$\varepsilon_{cd,0}$	= initial drying shrinkage	[-]
ε_{ca}	= autogenous shrinkage	[-]
A_c	= area of the cross section	[mm^2]
u	= perimeter of the cross section	[mm]
h_0	= fictitious thickness of cross section	[mm]
f_{ck}	= characteristic compressive strength	[N/mm^2]

If 1 meter length is used, and the wall thickness is 2.5 m, the total shrinkage equals:

$$h_0 = 2 \cdot \frac{A_c}{u} = 2 \cdot \frac{2.5 \cdot 10^6}{7 \cdot 10^3} = 714 \text{ mm}$$

$$\varepsilon_{cd,\infty} = k_h \cdot \varepsilon_{cd,0} = 0.7 \cdot \ 0.13 \cdot 10^{-3} = 9.1 \cdot 10^{-5}$$

$$\varepsilon_{ca,\infty} = 2.5 \cdot (f_{ck} - 10) \cdot 10^{-6} = 2.5 \cdot (35 - 10) \cdot 10^{-6} = 6.25 \cdot 10^{-5}$$

$$\varepsilon_{cs,\infty} = \varepsilon_{cd,\infty} + \varepsilon_{ca,\infty} = 1.535 \cdot 10^{-4}$$

From this, it can be concluded that the thermal shrinkage is three times larger than the sum of the autogenous and drying shrinkage and is therefore much more important in this specific case.

J. Python scripts

In this appendix, the python scripts can be found for the calculation of stress and strength of lowest printed layer, the buckling height in case of a free wall and the adiabatic increase of temperature. This is used in step 2.7 (a quantitative verification is made for the variants) and 2.9 (the hydration heat is estimated, crack width calculations are performed and watertightness will be verified) of the design method.

Calculation of stresses in lowest printed layer (1)

```
import numpy as np
import matplotlib.pyplot as plt
%matplotlib inline

plt.figure(figsize=(13,7))
p = 0.5
Q = (p*0.5/3600)*1E+6                          # print rate [cm3/s]
r = 1500                                      #diameter is 2*r [cm]
d = 1                                         # cantilever is 'd' cm
e = [1]                                         #thickness is 'e' cm
b = 10                                        #width is 'b' cm
thau_0 = 4*10**-3
A_thix = 0.5*10**-6
g = 9.81
rho = 2200

for k in range(len(e)):
    v = Q/(b*e[k])
    print(f'printsnelheid = {v:.1f} cm/s')
    y = np.linspace(-1500,1500,int(3001/e[k]))
    x = np.zeros(len(y)-2)
    omtrek = np.zeros(len(x))
    duur = np.zeros(len(x))
    compression = np.zeros(len(x))
    tension = np.zeros(len(x))
    total_duur = np.zeros(len(x))
    total_omtrek = 0
    for i in range(len(y)-2):
        x[i] = np.sqrt(r**2-(y[i+1])**2)
        if (x[i] - x[i-1]) < -1*d:
            break
        if np.abs(x[i] - x[i-1]) > d:
            m = i
        if np.abs(x[i] - x[i-1]) < d:
            M = ((e[k]*0.01)*(b*0.01)*rho*g) * ((x[i]-x[m])*0.01)
            W = (1/6)*1*((b*0.01)**2)
            compression[i] = rho*1E-9*g*e[k]*10 + (M/W)*1E-6 + compression[i-1]
            tension[i] = rho*1E-9*g*e[k]*10 - (M/W)*1E-6 + tension[i-1]
            omtrek[i] = np.pi*2*x[i]
            duur[i] = omtrek[i]/v
            total_duur[i] = np.sum(duur)
            total_omtrek += omtrek[i]
```

Figure J - 1 Calculation of stresses and strength in lowest printed layer (1)

Calculation of stresses in lowest layer (2)

```
b = np.zeros(len(y)-2)
for i in range(len(y)-2):
    if i < int(len(y)-3):
        if np.abs(x[i+1] - x[i]) > d:
            b[i] = 0
        else:
            b[i] = e[k]

plt.subplot(1, len(e), k+1)
print(f'totale printpad = {total_omtrek:.0f} cm')
print(f'totale printtijd = {(np.max(total_duur)/(3600*24)):.1f} dagen')
layer = m

t = np.linspace(0,170000,int(np.max(total_duur)))

t_c = 1800
thau_2 = A_thix*t_c*(np.exp(t/t_c) - 1) + thau_0

plt.plot(t, -thau_2, 'o', label =f'Compressive strength development, layer 1')
plt.plot(t, 1/15*thau_2, 'o', label =f'Tensile strength development, layer 1')

plt.plot(total_duur[layer:]-total_duur[layer],-(compression[layer:]-compression[layer]), 'o',
         label =f'Compressive stress for layer 1')
plt.plot(total_duur[layer:]-total_duur[layer],-(tension[layer:]-tension[layer]), 'o', label =f'Tensile stress for layer 1')

plt.ylim(-0.015,0.015)
plt.legend(loc='upper left')
plt.title(f'printing time = {(np.max(total_duur)/(3600*24)):.1f} days, printing rate = {(Q/1000*60):.1f} l/min', fontsize=15)
plt.xlabel('time [s]')
plt.ylabel('strength and stress [N/mm^2]')
plt.xlim(0,20000)
plt.axhline(0, color='black',linewidth=5)
plt.text(12500, -0.002, 'Compression part', fontsize=20)
plt.text(12500, 0.002, 'tension part', fontsize=20)
```

Figure J - 2 Calculation of stresses and strength in lowest printed layer (2)

Calculation of elastic buckling free wall

```
import numpy as np
import matplotlib.pyplot as plt
%matplotlib inline

p = 0.5
Q = p*0.5/3600 #m^3/s
rho = 2200 #kg/m3
g = 9.81 #m/s^2
b = 0.10 #m
h = [0.01]
E_0 = 78100
poisson = 0.3
curing_E = 0.00026
r = 15
for k in range(len(h)):
    y = np.linspace(-15,15,int(30.01/h[k]))
    x = np.zeros(len(y)-2)
    omtrek = np.zeros(len(x))
    duur = np.zeros(len(x))
    buckling_height=np.zeros(len(x))
    v = Q/(b*h[k])
    for i in range(len(x)):
        x[i] = np.sqrt(r**2-(y[i+1])**2)
        omtrek[i] = np.pi*(x[i])*2
        T = omtrek[i]/v
        duur[i] = T+duur[i-1]
        i_dot = Q/(v*b*T)
        D_0 = (E_0*b**3)/(12*(1-poisson**2))
        curing_E_nor = (D_0/(rho*g*b))**(1/3)*curing_E/i_dot
        l_cr_nor = 1.98635 + 0.996*(curing_E_nor)**0.793
        buckling_height[i] = l_cr_nor/((rho*g*b)/D_0)**(1/3)
    plt.plot(y[1:439],buckling_height[0:438],color='red')
    plt.plot(y[439:-439],buckling_height[438:-438],color='green')
    plt.plot(y[-439:-1],buckling_height[-438:],color='red')
    plt.ylim(0.28,0.9)
    plt.ylabel('critical buckling height [m]')
    plt.xlabel('y [m]')
    plt.text(-9.5,0.3, f'b = {b} m, h = {h[k]} m, Q = {(Q*60*1000):.1f} l/min', fontsize='medium', color='black')
    plt.title(f'buckling height of printed concrete, depending on y')
print(f'tijd na 30 lagen printen = {(duur[488]-duur[438]):.0f} s')
plt.axvline(-np.sqrt(225/2), linestyle='dashed', color='black',linewidth=1)
plt.axvline(np.sqrt(225/2), linestyle='dashed', color='black',linewidth=1)
plt.axhline(buckling_height[438], linestyle='dashed', color='black',linewidth=1)
```

Figure J - 3 Calculation of elastic buckling height of free wall.

Calculation of adiabatic temperature increase at time t

```
import numpy as np
import matplotlib.pyplot as plt
%matplotlib inline
from IPython.display import display
from matplotlib.patches import Arrow

ASTM1 = [0.55,0.17,0.10,0.07]    #C3S, C2S, C3A, C4AF
ASTM2 = [0.55,0.20,0.06,0.10]
ASTM3 = [0.55,0.17,0.09,0.08]
ASTM4 = [0.35,0.40,0.04,0.12]
ASTM5 = [0.55,0.20,0.04,0.12]

CEM = np.array([ASTM1, ASTM2, ASTM3, ASTM4, ASTM5])

C3S = [0,0,0,1,10,21,38,43,47,48,49]
C2S = [0,0,0,0,0,0,4,9,12,16,24]
C3A = [1,9,10,10,12,15,28,37,40,42,52]
C4AF = [0,7,8,8,8,9,11,18,20,20,20]

time = [0.01, 0.1, 1, 2, 5, 10, 20, 50, 100, 200, 500]

fig = plt.figure(figsize=(20,8))
ax = fig.add_subplot(111)
ax.grid(b=True, which='major', color='#666666', linestyle='-',alpha =0.6)
ax.minorticks_on()
ax.grid(b=True, which='minor', color='#999999', linestyle='-', alpha=0.2)

hydr_heat = [500*1000, 260*1000, 865*1000, 420*1000]   #J/kg

c = 900         #J/(kg*K) = specific heat
C = 350         #kg/m3 = cement content
rho = 2300      #kg/m3 = density

temp = np.zeros((len(CEM),len(time)))

for i in range(len(time)):
    for j in range(5):
        temp[j,i] = ((0.01*C3S[i]*CEM[j,0]*hydr_heat[0] + 0.01*C2S[i]*CEM[j,1]*hydr_heat[1] + 0.01*C3A[i]*CEM[j,2]*hydr_heat[2]
                    + 0.01*C4AF[i]*CEM[j,3]*hydr_heat[3])*C)/(c*rho)

types = ['general purpose', 'moderate sulfate resistant', 'high early strength', 'low heat', 'sulfate resistant']
for i in range(5):
    ax.plot(time,temp[i,:], label='ASTM' +str(i+1)+ ', ' +str(types[i]))
    plt.xscale('log')
ax.legend(loc='best', fontsize='x-large')
plt.xlabel('Time [hr]', fontsize='x-large')
plt.ylabel('Temperature [°C]', fontsize='x-large')
plt.ylim(0,35)
plt.axvline(0.1,ymax=0.1,color='black')
plt.axhline(temp[0,1],xmax=0.24,color='black')
ax.annotate(f'temperature increase = {(temp[0,1]):.2f} °C', xy=(0.006, 2), xytext=(0.02, 6), arrowprops=dict(facecolor='black')
            ,size='large');
plt.title(f'Adiabatic temperature increase of concrete', fontsize='xx-large');
```

Figure J - 4 Calculation of adiabatic temperature increase of concrete.